AN ABSTRACT OF THE THESIS OF

MOHAN LAL GUPTA

for the Master of Science

in Chemistry

presented on May 9, 1990

Title: Fourier Transform Infrared Studies of 1:12 and 1:11 Heteropoly Tungstates

Abstract approved: 

ABSTRACT

Infrared spectroscopic features of 1:12 and 1:11 heteropoly tungstates were studied using FT - IR. Internal coordinate analysis revealed that 297 coordinates are required for the 1:12 heteropoly anions, and 303 for the 1:11 anions.

The spectra of compounds of these two families were identified and characterized using 'fingerprint' and computerized search methods. For the computer searches, four spectral libraries were created for the four different dispersive media, KBr, KCl, Nujol and CCl_4. Major bands were assigned to specific localized vibrations.

An absorbance study was performed with selected compounds using a new weighing scheme. The accuracy of this scheme was matched with the usual technique for tripalmitin in CCl_4 solution and was found to be simpler and more advantageous. An unusual absorbance vs concentration behavior was observed. This phenomenon is interpreted in terms of different vibrational nature of the anions at different concentration ranges. The absorbance study also indicated that for a given heteropoly compound in non-polar solvents, the absorption proportionality constant is also a function of concentration. Some uncertainties were observed about the stability of these compounds in the solutions with respect to time and temperature.

FOURIER TRANSFORM INFRARED STUDIES OF 1:12 AND 1:11 HETEROPOLY TUNGSTATES

A Thesis

Presented to

the Division of Physical Sciences

EMPORIA STATE UNIVERSITY

In Partial Fulfillment

of the Requirement for the Degree

Master of Science

---

by

MOHAN LAL GUPTA

May, 1990

ACKNOWLEDGMENTS

The auspicious blessings of "His Majesty Lord Shiva" made it easier for me to be successful in the completion and presentation of this thesis and research work.

This thesis has been dedicated to those whose perpetual and unconditional support, compassion, patience, enthusiasm and encouragement led me in completing it in time.

I pay my sincere gratitudes to the members of my graduate research committee who were constant beacons throughout my research and whose insights never failed in giving me structural ideas. They were extremely helpful in directing me through the difficult and complicated avenues of developing a viable research design, implementing the research procedures, and evaluating and refining the present thesis. Without their support and guidance this research project would have never reached fruition.

First, I would like to use this opportunity to thank my graduate research committee chairman and mentor, Dr. A.M. Landis, for always explaining, understanding, counseling, and constructively criticizing the subject matter throughout this research study. I greatly admire him for contributing his decisive influence, professional and logistical expertise, knowledge, enthusiasm, undying confidence, and endless support. I am especially indebted to him for his astute advice and aid in correcting and

proof-reading this thesis. In addition, I also wish to thank him for providing me a research award which supported me throughout this research.

I would like to express my gratitude to Dr. C.M. Greenlief, Chairman of the Chemistry Department and a member of the graduate research committee, for his continual efforts and advice not only for this project but also for my study at Emporia State University. His encouragement and assistance have greatly inspired me in completion of this research.

I wish to thank my another committee member, Dr. M. Jamshid, for his valuable suggestions and encouragement in presenting this thesis.

Last but not least, the most grateful thanks go to my family in extending their everlasting moral and friendly inspiration and continued love which enabled me to be successful in presenting my thesis.

Charles Grumley

Approved for the Major Division

James L. Wolfe

Approved for the Graduate Council

TABLE OF CONTENTS

Fourier Transform Infrared Studies of 1:12 and 1:11 Heteropoly Tungstates

by
MOHAN LAL GUPTA

LIST OF FIGURES

LIST OF TABLES

1.1. INSTRUMENTATION AND THEORY OF FT-IR SPECTROMETRY:

In this section instrumentation and theory of Fourier Transform Infrared (FT-IR) spectrometry including the theoretical and mathematical principles of FT-IR will be discussed. A paper by Lowenstein [*1*] is the best source of information to get a brief historical development of the field of FT-IR spectrometry. And, for brief details in general, two papers by Backer and Farrar and Griffith [*2, 3*] are the best sources. Subheadings which come under this class are: operating principle of the Michelson interferometer, advantages and disadvantages of FT-IR spectrometry and processes performed by FT-IR to produce a spectrum.

1.1.1. Operating Principle of the Michelson Interferometer:

The operating principal of FT-IR is based on the Michelson interferometer [*4 - 6*]. Basically, the Michelson interferometer is a device which divides a beam of radiation into two beams and then recombines the two beams after introducing a path difference between them. This path difference is responsible for producing the interference pattern. This path difference is also a measure of intensity variation of the beam emerging from the interferometer. The variation in the intensity of the beam passing to the detector and returning to the source gives the spectral information in the FT-IR.

In its simplest form, the Michelson interferometer

consists of two mutually perpendicular mirrors, one of which can travel in a direction perpendicular to its plane. The velocity of this mirror is controlled by a reference signal incident upon a detector which is produced by modulation of the beam from the helium-neon laser of frequency 632.8 nm [7]. The plane of these two mirrors is bisected by a beamsplitter. An ideal beamsplitter has zero absorption and 50% reflectance and transmittance each. If a collimated beam of monochromatic radiation of wavelength, L, is passed onto an ideal beamsplitter, 50% of the incident radiation will be reflected to one of the mirrors and 50% will be transmitted to the other mirror. After reflection from these two mirrors, the two beams return to the beamsplitter where they recombine and interfere. Fifty percent of the beam which was reflected from the fixed mirror is transmitted through the beamsplitter while 50% of the beam is reflected back in the direction of the source. The beam which returns in the direction of the source is known as the reflected beam and the beam which emerges from the interferometer at 90° to the input beam is called the transmitted beam. The beam which is detected by the FT-IR is the transmitted beam. For a monochromatic source of intensity, I(L), the intensity of transmitted beam, I'(x), as a function of optical path difference, x, is given as:

$$I'(x) = 0.5\ I(L) + I(x)$$

where $$I(x) = 0.5\ I(v') * \cos[44xv'/7].$$

The intensity, I(x), is characterized as modulated component of transmitted beam and is known as the interferogram. Here, v' stands for wavenumber corresponding to wavelength, L. The cosine Fourier transform I(v'), of I(x) is given as:

$$I(v') = \int_{-\infty}^{+\infty} I(x) * \cos[44xv'/7]\, dx.$$

If instead of a monochromatic source, a polychromatic source is used, then the interferogram is the sum of individual interferograms due to each wavenumber. In the form of Fourier transform, I(x) is then given as:

$$I(x) = 0.5 \int_{-\infty}^{+\infty} I(v') * \cos[44v'x/7]\, dv'.$$

1.1.2. Advantages and Disadvantages:

Some advantages and disadvantages of FT-IR spectrometry over traditional dispersive IR spectrometry are described in the following section [*2 - 6*].

1.1.2.1. Jacquinot Advantage:

The principal advantage of FT-IR spectrometry over the dispersive IR spectrometry is that the optical throughput of an interferometer, E_I, is greater than that of a dispersive instrument, E_D, operating at the same resolution. For mid-infrared FT-IR spectrometer, this advantage, known as Jacquinot advantage, is between 1 and 2 orders of magnitude. In general, the mathematical expression for this advantage at a given wavenumber, v', is given as:

$$E_I/E_D = 0.075 * (v'^2)/v'_{max}$$

where v'_{max} is maximum wavenumber in the spectrum. Jacquinot advantage is also a measure of radiation striking the detector. This advantage is important for the measurement of weak emissions and also for high resolution studies.

1.1.2.2. Fellgett's Advantage:

The other principal advantage of FT-IR instrument is known as Fellgett's advantage or the multiplex advantage. An interferometer receives information from the entire range of a given spectrum during each scan, whereas a dispersive grating spectrometer receives information from only the narrow region which lies within the exit slit of the instrument. Hence, less time is required to obtain the same information with a Fourier instrument.

Mathematically, spectra taken on instruments with equal optical throughput and efficiency at equal signal to noise ratio, SNR, and resolution using identical sources, will take M times less time on a Fourier spectrometer. Here, M is the number of resolution elements and is given as:

$$M = [\ v'_{max} - v'_{min}\ ]/\ R$$

where R is the resolution of the instrument.

For measurements taken with equal data acquisition time, the SNR taken on a Fourier spectrometer is $M^{1/2}$ times better than the SNR of the same measurement taken on a dispersive spectrometer. For a scan of the entire mid-

infrared region at a resolution of 4 cm^{-1}, the magnitude of Fellgett's advantage is equal to 30, and it increases with an increase in resolution.

For a dispersive instrument, the total active time of data acquisition, which is equal to the total time during which the sample is being irradiated, is much less than the total time involved in obtaining a spectrum. In this case the spectrum is usually plotted as the data is being recorded. But in an interferometer, the spectrum cannot be plotted until all of the interferograms have been recorded, averaged, apodized, and transformed. If only one interferogram is to be recorded then the inefficiency of interferometer negates the Fellgett's advantage. But, if several interferograms are to be recorded then the Fourier transform of previous interferograms can be averaged while the next is being collected. This improves the efficiency of interferometer and brings the total time closer to the total active time of Fellgett's advantage.

1.1.2.3. Connes' Advantage:

Connes' advantage is simply stated as the ability of interferometer to very accurately characterize the frequency. This advantage stems from the accurate measurement of the displacement of the moving mirror. Connes' advantage also allows the subtraction of background spectra.

1.1.2.4. Cooley-Tukey Algorithm Advantage:

The efficiency of interferometer is improved by the method devised by Cooley and Tukey to calculate Fourier transforms. By this algorithm, the total number of operations required to compute the Fourier transform is greatly reduced. According to this method, if sufficient zeroes are added such that the total number of data points, D, is equal to an integral power of two, then the time required for the calculation is reduced to ($D * \log_2 D$) [8].

1.1.2.5. Resolution Advantage:

Resolution advantage of interferogram deals with the precision or the resolution of the band. The resolution, R, of an interferometer is defined as the inverse of optical path difference, x, between two arms of the interferometer. Numerically, the expression for x, is given as:

$$x = 2d * \cos B$$

where, d is spatial displacement between the fixed and the movable mirror and B is the angle that the IR light source makes with the optical axis of the collimator. For a point source, value of B = 0.

The resolution can be controlled by the use of an apodizing function. Also, resolution is affected by divergence of the beam and by instability of the mirror motion in either speed or alignment. Both result in poorer resolution than expected.

1.1.2.6. Detector Performance:

One factor which is a definite disadvantage of an interferometer compared to a dispersive instrument is the performance of the detector. In the dispersive instrument, all frequencies are modulated or chopped at a constant frequency, whereas in interferometer this modulation frequency is dependent on the frequency, v, of the source radiation. This frequency is given as:

$$f(v) = 2v' * V$$

where V is the velocity of moving mirror and v' is the wavenumber corresponding to frequency, v. The FT-IR used in present study utilizes a Deuterated Tri-Glycine Sulfate (DTGS) pyroelectric detector. This detector has a Curie point equal to 49°C.

1.1.2.7. Other Advantages and Disadvantages:

A large range of wavenumbers per scan is an additional advantages of Fourier instrument over the dispersive one. Another advantage of Fourier interferometer is the measurement of complex reflection and transmission coefficients by placing the sample in one of the arm of the interferometer. This technique also helps in the calculation of amplitude and phase angle for these coefficients and complex indices of refraction.

FT-IR spectroscopy shows effects that may lead to errors in quantitative analysis [*6*]. One of the effects that is restricted to FT-IR spectrometer performance is the stability of the interferometer. Instability of the

instrument may produce frequency shift in spectra which may be due to noncoherence of coadded interferograms. This instability may induce due to mirror velocity fluctuation and mirror's non alignment. Fluctuating mirror velocity may produce a ghost peak in the spectrum. Also, mirror tilt can reduce the resolution.

Although FT-IR is more expensive than traditional IR instrument, it is capable of detecting radiations modulated in excess of 1MHz. A dispersive instrument uses a thermocouple for the same purpose and cannot detect radiation modulated in excess of 1KHz.

1.1.3. Processes Performed by FT-IR to Produce a Spectrum:

In order to produce a spectrum, FT-IR performs the following processes *[4-6]*:

1.1.3.1. Resolution:

The ultimate factor in determining the resolution of an FT-IR spectrometer is the maximum optical retardation or the maximum optical path difference. Basically two criteria are used to define the resolution. One is known as the Rayleigh criterion and the another is the full width at half height (FWHH) criterion.

Under the Rayleigh criterion, two adjacent spectral lines of equal intensity, each with $Sinc^2A$ as the instrument line shape, ILS, are considered to be just resolved when the center of one line is at the same frequency as the first zero value of the ILS of the other.

The ILS is the Fourier transform of a boxcar truncation function which is introduced into the basic Fourier integral equation for non-ideal interferometers to retain the integration limits. In general, this function has the form $Sinc^nA$, where

$$Sinc^nA = Sin^nA/A^n \quad \text{with } n = 1 \text{ or } 2.$$

If the same criterion is applied to a line having a SincA as the ILS then the two lines will not be resolved.

According to FWHH criterion, two triangularly shaped lines of equal intensity are only supposed to be resolved if the spacing between the lines is greater than the FWHH of either line.

1.1.3.2. Scanning:

Interferometers are classified according to the scan speed of the moving mirror into three types: rapid scan, step scan and slow scan interferometers. The interferometer which is useful for the mid-IR range has a rapid scanning feature. For this type, a typical mirror velocity is 0.158 cm/sec. The modulation frequencies at the extremes are:

$$f_{(4000)} = 1264 \text{ Hz}$$

$$f_{(400)} = 126.4 \text{ Hz}$$

These two modulation frequencies are also known as Fourier frequencies. Because these two frequencies lie in the audio range, they can be easily amplified without the necessity for modulating the beam with a chopper. Hence,

all the radiation is allowed to hit the detector all of the time. Ultra-high resolution obtained by a rapid scan interferometer is not more than 0.01 cm^{-1}.

1.1.3.3. Apodization:

Apodization is a mathematical process applied to the interferogram. During this process, the interferogram is multiplied by a function known as the apodizing function which removes negative sidelobes introduced into transformed spectra because of finite optical path displacement [*9*]. The main apodization function is a triangular function. It has a value equal to unity at zero path difference. This value decreases monotonically until it reaches zero near the maximum path difference. The ILS function for this triangular function is of the form $Sinc^2 A$. This ILS is basically the same function which is used for applying the Rayleigh criterion.

When an absorbing sample is placed in the beam from a continuous source, the measured interferogram is the sum of the interferogram of the source with no sample present and of the interferogram due to sample. Because energy is being absorbed by the sample, these two interferograms are 180° out of phase. At this stage, the effect of apodization is considered important for the background spectrum. At high retardation the background spectrum contains negligible informations.

1.1.3.4. Phase Correction:

To get the actual measured interferogram, an additional term is added to the phase angle, (44v'x/7). This correction to the phase angle arises due to optical, electronic, and sampling effects. Theory assumes that the interferogram is symmetrical at x = 0. But actually, the first data is sampled at x = $-p_1$ before the zero optical path difference. Thus the new phase angle is given as [44v'(x-p_1)/7].

Electronic filters, which are designed to remove high frequency noise from the interferogram, also have the effect of putting a wavenumber dependent phase lag (p_2) on each cosinusoidal component of the interferogram. Thus the resultant phase due to this correction becomes [(44v'(x-p_2)/7].

After using these phase corrections and the orthogonal properties of sine, cosine, and transcendental exponential functions, the total computed components can be divided into two parts. A real part due to cosine Fourier transform and an imaginary part due to sine Fourier transform. As the shape of ILS is intermediate between a truncated sine wave of the cosine Fourier transform and Sinc function resulting from the cosine transform of the truncated cosine wave, the process of removing these two sine components from an interferogram is known as phase correction.

1.2. HETEROPOLY COMPOUNDS:

1.2.1. Definition of Heteropoly Compounds:

Heteropoly compounds usually are defined as the compounds containing heteropoly anions. Heteropoly anion HPA(s), are the anions which contain two or more different kinds of positive valent atoms in addition to oxygen [*10*]. Of these two or more atoms, one type of atom is known as the central hetero atom, X. A second type of atom is known as the peripheral hetero atom, Y. And a third type of atom is known as the addendum atom, Z. In their most general form, the anions of 12-tungsto-heteropolies can be represented as:

$$[X_a(Y[1])_bZ_{(12-b)}O_{(40-b)}]^{e-}$$

with a = 1
b = 0, 1 or 2
and e = net charge

In most of the compounds, Z is usually Mo, W, or V in its highest oxidation state, Y may be Co or Cr or another first row transition metal, and 1 is the terminal ligand on Y hetero atom [*13*]. In the case of Co and Cr, these two atoms may be present in either the +2 and/or +3 oxidation states. X, the central hetero atom may be Si, P, B, Zn, Ga, Ge, and dihydrogen. A total of 67 different elements of periodic table can act as either central or peripheral hetero atoms [*11*]. This variety of hetero atoms which may also be in different oxidation states together with the basically complex nature of heteropoly chemistry has lead to a proliferation of heteropoly anions which at first

sight is somewhat confusing [*12*].

The hetero atom, X may be a non-metal of moderate electronegativity or a metal especially transition metals. The elements that can function as the addenda atoms, Z, appear to be limited to those with both a favorable combination of ionic radius, charge, and the ability to form coordination bond. There is no such restriction on hetero atoms [*13*].

The basic difference between the conventional coordination compounds and heteropoly compounds can be stated in terms of their coordination linkage and average charge density. Size of addenda atoms, and their dpi electron acceptor properties also make them different from the coordination compounds [*10*]. For heteropoly compounds, no discrete ligands are coordinated to the central hetero atom; instead, the structure coordinated to the X atom is interconnected. Also the dissociated fragments do not coincide with any discrete ligand. Secondly, because of the large size of these anions, the average charge density on the surface of heteropoly anions is very low as compared to that for more typical coordination compounds.

1.2.2. Historical Background:

The first heteropoly was discovered in 1826 when Berzelius noted the yellow precipitate of 12-molybdophosphate when he added ammonium molybdate solution to phosphoric acid [*11*]. Analytical study of this compound

was done in 1848 by Svanberg and Struve who postulated the compounds of this type as double salts. A more precise study of composition of 12-tungstosilicate was performed by Marignac in 1862.

In 1908, Miolati made the first systematic study to understand the nature of heteropoly compounds. He suggested the structure of these compounds on the basis of ionic theory and Werner's coordination theory. He also developed a theory which was later modified by Rosenheim and became known as the Miolati-Rosenheim theory [*11*]. According to this theory, heteropoly acids are based on six coordinate hetero atoms with ZO_4^{2-} or $Z_2O_7^{2-}$ anions as ligands or bridging groups coordinated to the central atom. Formulae produced by this theory suggest a different basicity than expected from the modern theory. However, these formulae are still used to interpret their structure [*12*].

Early structure characterization of heteropoly compounds came in 1929 when Pauling attempted to propose a structure for the heteropoly compound having the ratio of number of central atoms to the addenda atoms as 1:12 [*14*]. According to Pauling's explanation, a stable 12-tungstosilicate heteropoly complex ion can be formed by arranging ZO_6 octahedra in such a way that they share corners with each other but not edges and faces. Complete detail of this structure was derived by Keggin in 1933

using powder X-ray crystallography using 12-tungstophosphate [*15 - 17*]. The structures of Pauling and Keggin although essentially based on the same sharing of octahedra are not identical. Pauling's structure has been found in one of the paratungstates. Whereas Keggin's structure forms the basis of a large class of heteropolies. The Keggin structure was later confirmed by Bradley and Illingworth in 1936.

After nearly twelve years in 1948, Evans using X-ray crystallography reported the next new structure of a polyanion, $[TeMo_6O_{24}]^{6-}$. This shows that until 1950, X-ray was the best known tool for researchers in this field. But now in addition to this technique, many other advanced techniques such as electronic spectroscopy, vibrational spectroscopy, NMR, EMF methods, polarography and voltammetry, salt cryoscopy, diffusion and dialysis, ultracentrifugation, ESR, and EPR are widely used to explore the indepth details of this less commonly known field [*11*].

The earlier literature in this field, according to Tsigdinos [*12*], should be used carefully and interpreted in the light of recent findings because analyses reported in the earlier literature are often inaccurate due to the high molecular weights of the heteropoly compounds.

1.2.3. General Classification and Formulation:

The heteropoly anions which are well characterized

structurally can be conveniently classified into five broad classes depending upon the ratio of the number, a, of central hetero atom, X, to the number, c [this is also equal to (12-b)] of addenda atoms, Z [*12, 18, 19*]. This classification also depends upon coordination number of the central hetero atoms. Compounds with the same number of atoms in the anions are usually isomorphous and have similar chemical properties. The heteropoly anions of molybdenum and tungsten containing non-transition elements as central hetero atoms have more structural analogues than those containing transition elements as the central hetero atom [*18*].

Group A: Heteropoly anions having the ratio of (a:c) as 1:12 and 1:11 and containing a tetrahedrally coordinated hetero atom, X, belong to this group. Related heteropoly anions containing more than one hetero atom, Z also represent this group.

Group B: This group includes the heteropoly compounds with the ratio (a:c) as 2:18 and 2:17 and containing the tetrahedrally coordinated hetero atom, X. These compound are structurally related to group A. Related anions having more than one hetero atom, Z again come under this group.

Group C: The heteropoly compounds with the ratio (a:c) as 1:6 and having octahedrally coordinated central hetero atom represent this group.

Group D: This group contains the heteropoly compounds with the ratio of (a:c) as 1:9 and having octahedrally coordinated central hetero atom. These compounds are unrelated to 2:18 anions of group B.

Group E: This group includes the compounds having the ratio of (a:c) as 1:12 but contain an icosahedrally coordinated metal atom and in which the parent octahedra share faces and corners with each other compared with the edge sharing of corners plus edge sharing of the first four group.

1.2.4. General Properties of Heteropoly Compounds:

Some general properties of heteropoly compounds are included in this section but more emphasis is given to 1:12 heteropoly compounds of tungsten [*10 - 13, 18, 19*].

1. Heteropoly tungstates are more stable in acidic than in neutral solutions. All heteropoly compounds are decomposed in concentrated basic solution.

2. When heated, heteropoly tungstates do not start losing water molecules until 150°C. Complete decomposition occurs at about 500°C.

3. The lesser the charge on heteropoly anions, the higher the stability. This stability also depends on the size of the hetero atom, X. Heteropoly tungstates are hydrolytically more stable than the corresponding molybdenum compounds.

4. Salt formation between heteropoly anions and

polycations is often not a case of simple ionic bonding. Although even this electrostatic attraction may be unusually important due to the high negative charge generally associated with the polyanions. Strong ion pairing is expected in solution.

5. The color of heteropoly compounds is highly dependent on nature of the central, X, and/or peripheral, Z, hetero atoms. In general, the 1:12 heteropoly compounds of tungsten are colorless.

6. Heteropoly acids show very strong affinity toward other oxygen donor ligands.

7. The determination of ionic weight by light scattering in aqueous and organic solvents and determination of size from ultracentrifugation, viscosity, and density measurements show that 1:12 heteropoly acids are monomeric in nature.

8. Typically, polyoxoanions are air stable species of large size (0.60 - 2.50 nm) and high ionic weight (1000-10,000). For $[SiW_{12}O_{40}]^{4-}$ the ionic weight is 2876.

9. The free acids and many of their salts are very soluble in water. This high solubility combined with their high molecular weights produce very dense solutions. Some metal salts are relatively insoluble. Usually the larger the size of cation, higher soluble is its ealt with a given heteropoly anion. Solubility of heteropoly compounds in water is attributed to very low lattice energy and energy

of solvation of anions.

10. The free 1:12 heteropoly acids are insoluble in non-oxygenated solvents such as benzene, chloroform etc.

11. Crystalline heteropoly acids and salts are highly hydrated with up to 50 molecules of water per anion. Much of this water is zeolytic in nature. Also, the hydrated acids usually are isostructural.

12. Some heteropoly compounds are strong oxidizing agents and can be readily changed to fairly stable reduced compounds of very intense color. These compounds of mixed valance are known as heteropoly blues. The reduced compound can in turn act as reducing agents. The original color of the compound is restored on oxidation.

1.2.5. Some Important Uses of Heteropoly Compounds:

Applications of heteropoly compounds mainly lie in their catalytic properties. High charges, ionic weights, solubilities, solvolytic behavior in both aqueous and organic media, thermal stabilities, and redox properties are of particular interest in characterizing heteropoly compounds for their various usee [*11, 12*].

1.2.5.1. Catalysis:

In a number of reactions, heteropoly compounds are successfully used as the heterogeneous catalyst. For example, 12-tungstophosphoric acid and 12-tungstosilicic acid have been reported as the most effective catalysts for the dehydration of castor oil to unsaturated oils. Also,

12-tungstophosphoric catalyses the hydroxylation of alkyl alcohol to glycerol using hydrogen peroxide. The catalytic oxidation of lower olefins to unsaturated aldehydes and subsequent conversion into unsaturated in the presence of various heteropoly compounds has also been studied [*11*]. Heteropoly compounds have been used as catalysts for the vapor-phase partial oxidation of naphthelene and vapor-phase hydration of ethylene. Recently, solid heteropoly acids have been reported to be efficient catalysts for the polycondensation of benzyl alcohol. Catalytic processes involving heteropoly anions in homogeneous solution is also a broad field to study.

1.2.5.2. Chemical Analysis:

Phosphate, silicate, arsenate, and germenate ions may be determined gravimetrically or by means of colorometric analytical methods involving reduction to heteropoly blue solutions. By these methods, it can be determined whether these ions occur separately or together in solution. It can be done by forming the corresponding heteropoly complexes and selectively extracting complexes using organic solvents at the suitable pH.

1.2.5.3. As Ion-Exchangers:

Crystalline heteropoly compounds with porous structure are used as ion-exchangers. The ions are able to move freely through this type of structure so that ion-exchange takes place throughout the entire crystal lattice

and not only on the surface of the crystals.

1.2.5.4. Biochemical Applicatione:

Phosphotungstic acid is a good analytical reagent for proteins, alkaloide, and purines. Also, it acts as a good precipitant for proteins. Phosphotungstic acid can aleo be used as a non-specific dense strain for electron microscopy. The latter two applications are based upon coulombic interaction between the polyanion and cationic sites on the biomolecules. Only phosphomolybdatee are found to be selective inhibitors of certain acid phosphotases.

1.2.5.5. Corrosion Inhibition:

Heteropoly compounds have been used as conversion coatings in steel and aluminum and as organic coatings on steel with anticorroeion properties. This application of heteropoly compounds must be approached carefully because some heteropoly compounds undergo hydrolytic degradation in very dilute solutions.

1.2.5.6. Flame Retardant:

Molybdenum compounds can act as a flame retardant for wood and textiles and as smoke suppressants in textiles and plastics.

1.2.5.7. General Uses:

Heteropoly acids are excellent protonic conductors and are electrochromic in the solid state as a result of the formation of heteropoly blues. These heteropoly blues

are also used to detect several organic radicals generated by radiolysis of aqueous solutions.

1.3. Statement of the Objectives:

The primary objective of this research was to identify heteropoly compounde using infrared techniques. Though the field of heteropoly compounds is nearly 150 years old, not much work has been done in the area of their infrared spectra [*11*]. The available literature concerning the infrared spectra of these compounds is not very consistent [*19*]. Moreover, most of this information is given for 1:12 class of heteropoly compounds [*19*]. Also, studies reported only have used the dispersive type of infrared instruments. Therefore, the field related to infrared spectra study of 1:11 class of heteropoly family using FT-IR methods needs to be explored. Keeping this fact in mind, the research was concentrated on identification of unknown heteropoly compounds using 'fingerprint' and computerized methods. Computing capabilities now allow for the identification of compounds using spectral search libraries. Therefore a part of this objective was to set up spectral libraries of heteropoly compounds.

A second objective of this study was to assign the bands of the infrared spectrum of a given heteropoly compound, and hence to characterize the spectrum. As mentioned earlier (section 1.2.1.), heteropoly compounds of a family and addenda atom differ from each other only

because of the presence of central hetero atom and peripheral hetero atom. Therefore, the infrared spectra of these compounds should be almost the same with the exception of certain peaks due to the nature of different hetero atoms.

A third objective of this study was to observe the absorbance behavior of some heteropoly compounds in non-polar solvents such as CCl_4 and CS_2.

Another objective of this research was to develop FT-IR quantitative methods for using heteropoly compounds as a catalytic agent (section 1.2.5.1.).

2. STRUCTURAL AND VIBRATIONAL SPECTROSCOPY OF HETEROPOLY COMPOUNDS:

2.1. Principle Basis of IR Spectroscopy:

Infrared spectroscopy for the mid-IR region is mainly concerned with the absorption of energy by a molecule or with the study of emission of IR radiation by the concerned species in the excited state. In this region absorption occurs somewhere between 4000 - 400 cm^{-1}. For heteropoly compounds this region of interest lies in the 'fingerprint region' of 1100 - 350 cm^{-1} [*7, 20*]. The occurrence of a vibrational spectrum is dependent upon an overall change in electrical dipole moment of the ion or molecule. The electrical dipole moment is defined as the product of the charge produced and the displacement produced during a

particular vibrational motion. Hence, the intensity of an IR absorption band is dependent on the magnitude of the dipole moment change. The interaction of radiation with the vibration in the molecule is responsible for producing the absorption band in the IR spectrum.

An IR absorption spsctrum of a molecule is one of its unique physical properties because no two molecules having different structures can show the same IR spectra. The study of these spectral properties for a given compound can differentiate it from others without doing any chemical analysis.

The spectral comparison of two compounds can be done by using two methods: one is by visual comparison of standard spectra and the other is by computerized comparison of standard spectra. The first method is often called the 'fingerprint method'. In this method a spectrum of an unknown compound is visually compared with standard spectra until a match is found. The second method uses digitized spectra rather than the more common analog graphical spectra and a computer program performs the comparisons.

In the first or fingerprint method, spectra of known compounds are recorded in the normal or analog form and stored in notebooks. Then the spectrum of an unknown compound is recorded. The major bands in the unknown spectrum are used to aid in manually searching the standard

spectra in the notebooks to find similar spectra. These similar spectra are then compared until a match is found. Since similar compounds have some bands which are similar, the standard spectra of classes of compounds are usually stored in adjacent sections in the notebooks.

For the second or computer method, spectra of known compounds are digitized and stored in a file called a library. Then the spectrum of an unknown compound is obtained in an identical digitized form. Each of the spectra in the library are compared to the unknown spectrum and a numerical value assigned to represent the closeness of the match. A list of the spectra which most closely match is then displayed. The computer operator then makes a visual verification.

An important requirement for using either of these two methods is that all the spectra must be taken under the identical conditions of resolution and number of scans and should also have been dispersed in the same medium [*21*]. The former method is very time consuming and depends upon highly trained personnel. The latter method is much faster since a computer can operate at much higher speeds. Also since the latter method can search all the spectral files, a lower probability exists of missing the correct standard spectrum. Computer searches, however, are highly dependent upon the algorithm used to perform the match or search.

2.2. Structural Arrangement of Atoms in Heteropoly Anions:

The simple HPA $[SiW_{12}O_{40}]^{4-}$ results if, in the general formula, b = 0, X = Si, and Z = W. This HPA has the idealized Keggin structure [*15 - 17*]. In a simple diagram of Keggin etructure, the silicon atom can be considered to be placed at the center of the regular cube. This silicon atom when combined with a group of four oxygen atoms forms a regular tetrahedron at the center of regular cube. These oxygen atoms are arranged with their centers at the corners of this regular undistorted tetrahedron. Each of the twelve tungsten atom is placed at the center of each edge of this regular cube and forms its own distorted octahedron which has six oxygens at the corners (*Figure 1*). These tungsten atoms are moved off the center towards the exterior of their octahedra. These twelve octahedra are arranged in four units, W_3O_{13}, of three octehdra each. In each unit of W_3O_{13}, each octahedron sharee three oxygen atoms with the other two octahedra in the group (Figure 2). Two adjacent equatorial oxygen atoms are shared: one with each octahedron in the group. Hence, three oxygen atoms form an equilateral triangle. The third oxygen atom, from each octahedron which is shared within the group, is the interior axial atom. This oxygen atom ie shared with all three octahedra in the unit and the tetrahedron. Besides sharing three oxygen atoms with the other octahedra in the same unit, the two remaining adjacent equatorial oxygen atoms are shared with two octahedra in two of the other

units of W_3O_{13} (Figure 3).

Hence, in a complete structure, each WO_6 octahedron consists of one oxygen atom shared between a unit of three WO_6 octahedra, W_3O_{13}, and one SiO_4 tetrahedron, two oxygen atoms shared with two other octahedra of the same unit, two oxygen atoms shared with two other units containing three octahedra each and one oxygen atom remain unshared. Within each unit of three octahedra, two edges of each WO_6 octahedron are shared with edges of the two other octahedra (Figure 4). Between units of three octahedra, only corners are shared. In HPC(s), there is no direct linkage between the individual molecules, but instead, it is the hydrogen bonding through some molecules of water of hydration. These water molecules are also responsible for packed unit structure in the crystal [*12, 22*]. In the overall structure, all HPA are arranged in spiral which surrounds a relatively large space. This space accommodates the cations and water molecules present in the HPC [*10*].

The main reason that the octahedra are distorted by the W atom being displaced towards its exterior appears to be due to coulombic electrostatic repulsion between the positively charged central Si atom and the W addendum atom [*10*]. In addition, the peripheral, unshared oxygen atom is polarized toward the W addendum atom and the interior of the complex. This polarization results in a very high ion-induced dipole interaction with the tungsten atom and can

account for the observed distortion of the octahedron.

Interior oxygen atoms have positive valent atoms near them on several sides and, therefore, cannot be polarized so intensively in any one direction [*10*]. The exterior oxygen atoms, being heavily polarized inwards, suck the tungsten atoms outwards. The two dimensional spatial arrangement of atoms of this simple HPA is shown in [*23*].

For other HPA(s) on which this research is concentrated, e.g. $[Si^{4+}Co^{2+}(H_2O)W_{11}O_{39}]^{8-}$, one tungsten atom and its terminal oxygen atom are replaced from the simple HPA by a peripheral hetero atom, Co, and a ligand molecule, H_2O. This type of anion has a 'defective' or 'pseudo' Keggin structure [*24*]. A very detailed account of the historical development of these compounds is mentioned in [*20, 25*].

2.3. Schoenfliess Point Group of the Heteropoly Anions:

For the HPA(s) having the ideal Keggin structure, it is observed after applying symmetry operations such as E, C_3, C_2, S_4 and σ_d that this type of anion possess T_d as the point group with 24 as the point group order, h. Here, σ_d mentioned refers to symmetry operation corresponding to reflection through a dihedral mirror plane. For the HPA(s) having defective Keggin structures, the assigned point group is C_s with the symmetry elements E and σ_h. Thus, the point group order for this symmetry group is two. Here, σ_h refers to symmetry operation corresponding to reflection

through horizontal mirror plane.

2.4. IR Active Modes of $[SiW_{12}O_{40}]^{4-}$ Anion:

The infrared active modes of the HPA $[SiW_{12}O_{40}]_4$- having T_d as the point group is determined by first constructing a reducible representation for the dipole moment which is denoted as G(dm) [*26*]. The characters of this reducible representation for proper rotations, that is the E, C_3 and C_2 symmetry operations, is given as [1 + 2cosQ], where Q, is the angle of rotation due to each of these symmetry operations. The value of the characters for improper rotations, S_4 and s_d, is equal to [-1 + 2cosQ]. Thus, the reducible representation of the dipole moment for T_d is given as:

h=24	E	C_3	C_2	S_4	s_d
Q	0	120	180	90	0
r	1	8	3	6	6
G(dm)	3	0	-1	-1	1
$G(F_2)$	3	0	-1	-1	1

where r represents the repetitive number of each operation that can be performed to give the molecule its original position, and $G(F_2)$ represents the irreducible representation corresponding to F_2 mode of vibration.

By comparing the values of G(dm) and $G(F_2)$ for each symmetry operation, one can justify the conclusion that the

F_2 mode is the only IR active vibrational mode for this HPA.

2.5. Total Number of Bande Belonging to Each Normal Mode for $[SiW_{12}O_{40}]^{4-}$ Anion:

A normal mode of vibration is one during which each atom of a molecule executes simple harmonic motion. In a normal mode of vibration, all the atoms move with the same frequency and are in phase. Therefore, the center of gravity of the molecule remains unaltered.

The number of bands belonging to F_2 band, which is the only IR active mode, is determined by first calculating character, G(v) of the reducible representation for the vibratory motion of the atoms in this HPA [*26*]. This can be done by calculating G(m), the character of the reducible repreeentation for all types of motion shown by all atoms in the HPA and then subtracting from this representation the characters of the reducible representations of the translational motion and of the rotatory motion. The character G(m) for the proper rotations is given as [N(1+2cosQ)] and for the improper rotations is given as [N(-1+2cosQ)]. In these expressions, N denotes the total number of atoms that remained unshifted under each symmetry operation [*26*].

If the characters of each symmetry operation for the reducible representation for translational motion are designated as G(t), the characters of each symmetry

operation for rotatory motion, G(v), can be calculated from the expression:

$$G(v) = G(m) - 2G(t)$$

The value of G(v) can be placed in the following relation to calculate the total number of bands, $B(F_2)$, corresponding to an F_2 eymmetric vibration:

$$B(F_2) = (1/h) \sum_{F_2} r\ G(F_2) * G(v)$$

Work related to the determination of N was not done because of insufficient time, but according to the literature the value of $B(F_2)$ should be 22 [*19, 20*].

2.6. Internal Coordinate Analysis of Heteropoly Anions of the Type 1:12 and 1:1:11:

The normal coordinates of a vibrating system expreas all the individual independent displacements of the atoms involved in the vibratory motion, i.e. a normal mode of vibration. A HPA having a 1:12 ratio of hetero atoms to the addenda atoma, has 53 atoms which gives it 159 total degrees of freedom, d.f. Because this type of anion is non-linear in structure, only 153 d.f. correspond to the vibrational motion.

When this anion undergoes vibratory motion, internal variations take place within the anion in the form of changes in bond angles and bond lengths. These changes in the anion can be described in terms of four internal coordinates s, m, n, and p [*27*]. The symbol s refers to bond stretching, m to bond angle deformation, n to out of

plane bending, and p to torsion produced during vibration. The number of coordinates required to completely specify these changes in internal structure are N_s, N_a, N_n, and N_p respectively. These coordinates are directly related to number of atoms, N_a; number of bonds, N_b; the number of atoms in the anion which participate only in one bond, A_1; and to the bond multiplicity of the atoms, M_1 [*27*]. The bond multiplicity ie defined here as the number of coplanar bonds (i.e. three or more) which meet at that atom.

$$N_a = N_b$$

$$N_a = 4N_b - 3N_s + A_1 - M_1 + 2$$

$$N_n = M_1 - 2$$

$$N_p = N_b - A_1$$

For the ideal Keggin structure in which all the octahedra in the anion are undietorted, which is not a real case, $N_a = 53$, $N_b = 76$, $A_1 = 12$. And for each octahedron $M_1 = 4$. Thus,

$$N_s = 76; \quad N_a = 133; \quad N_n = 24; \quad N_p = 64$$

For the anion having all distorted octahedra, for example HPA $[SiW_{12}O_{40}]^{4-}$, $N_a = 53$, $N_b = 76$, $A_1 = 12$, and $M_1 = 0$. Thus,

$$N_s = 76; \quad N_a = 157; \quad N_n = 0; \quad N_p = 64$$

Hence, the total number of internal coordinates required to specify the changes in internal structure for this anion is 297. As this anion has 153 d.f. for vibration, some redundancies are present. The presence of redundancies can

be checked by using the characters of the reducible representation for internal coordinates, G(int). This reducible representation can be derived by observing the unshifted nature of each internal coordinate under all symmetry operations of the T_d group. And then, subtraction of G(v) from G(int) will provide the characters G(red) of reducible repreeentation corresponding to redundancies [*26*]. The work related to this part was not completed because of insufficient time.

The 1:11:11 type of HPA, $[Si^{4+}Co^{2+}(H_2O)W_{11}O_{39}]^{6-}$ for example, has 55 atoms. The total number of vibrational degrees of freedom for this anion is 159. An analysis of the structure of this anion reveals that N_a = 55, N_b = 78, and A_1 = 13 and, hence:

$$N_a = 55,\ Nb = 78,\ A_1 = 13,\ \text{and}\ M_1 = 0.$$

Thus, the number of coordinates required to completely specify these changes in internal structure, N_a, N_a, N_n, and N_p are:

$$N_a = 78;\quad N_a = 160;\quad N_n = 0;\quad N_p = 65$$

Thus, the total number of internal coordinates required to completely specify the vibratory motion is 303.

To do further study in the field of normal coordinate analysis of 1:12 type of anions, a paper by Yurchenco [*28*] is the best source of information.

3. EQUIPMENT AND EXPERIMENTAL TECHNIQUES:

3.1. Equipment:

A Bomem MB-100 FT-IR interfaced to a NEC APC IV personal computer and IBM color plotter was used to obtain all spectra. "Spectra Calc" software from Galactic Industries Corporation was used to obtain the spectra and to perform data treatment. The NEC computer could also be connected to an AT&T network. However the memory requirements during the collection of the interferograms precluded connection to the network during data collection. All other calculations and data treatment were performed using Quattro, spreadsheet.

Standard KBr windows from Wilmad Glass Company were used as the window material for the sample cell. Demountable cells from McCarthy were used to place the KBr windows in the path of light of FT-IR. Teflon spacers of thickness 55×10^{-6} - 45×10^{-6} m were used for obtaining solution spectra. The sample cells without spacers were used to obtain the Nujol spectra.

All samples were ground in an agate mortar and pestle. All masses were determined using a Gram-amatic analytical balance (Fisher Scientific Company). The sensitivity of this balance is given as 0.01 mg.

Other standard general laboratory apparatus and glassware were used as needed.

3.2. Chemicals:

The heteropoly compounds were provided by Dr. A.

Landis. All other chemicals were ACS reagent grade or HPLC Spectral grade unless otherwise noted. All heteropoly compounds and other chemicals were used without further purification. The chemicals used for this study were:

Potassium bromide

Potassium chloride

Carbon tetrachloride

Carbon disulfide

Heavy mineral oil (Nujol)

Cyclohexane

Tripalmitin (provided by Prof. Ericson)

18 heteropoly compounds, detail of which is given in section 3.2.1.

3.2.1. IUPAC Nomenclature, Formulae, and Abbreviated Notations for Heteropoly Compounds:

According to IUPAC system, the central hetero atom in the formula of a heteropoly compound should be placed first in the formula and placed last in the name along with ite oxidation state [*29*]. The peripheral hetero atom is to be placed along with its ligand after the central hetero atom in the formula. But in the name, the peripheral atom is to be placed at the beginning of the anionic part. The number of addenda atoms also is to be stated in the name to justify the ratio of number of central atoms to the number of addenda atoms.

In this thesis, a 'general formula' devised to

designate the oxidation state of each hetero atom is given in addition to the IUPAC formula. The total number of water molecules is given at the end of these formulae for all compounds except those for which tetra-n-heptylammonium is the cation. The compounds with tetra-n-heptylammonium as the cation were prepared from their corresponding K^+ or Na^+ cations using 'liquid ion exchange phase transfer' method [*30*]. The number of water molecules attached to each heteropoly compound is taken from [*12*, *20*].

An abbreviated notation is used for convenience in this thesis. The first symbol is the cation. Next is the peripheral hetero atom with its oxidation state. Then the central atom is given. The symbol, Am, is used for tetra-n-heptylammonium cation. For 1:12 HPA, W^{6+} is used to rsplace the Co^{2+}. For example, KCo3+B is the abbreviated notation for potassium aquocobalto(III)-11-tungstoborate(III) or $K_6[BCo(H_2O)W_{11}O_{39}] * 16.8\ H_2O$.

For convenience in this thesis, the heteropoly compounds are arranged, reported, and discussed in the same order throughout. All those HPC with the same central hetero atom are placed together. The order used is based on increasing order of atomic weight with the exception of phosphorous hetero atom which is placed before boron atom, i.e. H_2, P, B, Si, Zn, Ga and Ge. For a given central hetero atom, the 1:12 compound is placed first, then the 1:11 analogs in the order of increasing oxidation state

(i.e. Co^{2+} before Co^{3+}). For a given central hetero atom and peripheral atom (ie. a specific anion), the order is based upon the counter cation- first hydrogen, then sodium, potassium, and lastly tetra-n-heptylammonium.

All of the HPC used in this investigation are listed below. The IUPAC name and formula, the general formula, and the abbreviated notation are given for each. The order is the same as that to be used in the thesis.

a. Sodium 12-tungstodihydrogenate

IUPAC: $Na_6[H_2W_{12}O_{40}] * x H_2O$

Formula: $Na_6[H_2W_{12}O_{40}] * x H_2O$

Notation: NaW6+H2

b. Potassium aquocobalto(III)-11- tungstodihydrogenate

IUPAC: $K_7[H_2Co(H_2O)W_{11}O_{39}] * 14.3 H_2O$

Formula: $K_7[H_2Co^{3+}(H_2O)W_{11}O_{39}] * 14.3 H_2O$

Notation: KCo3+H2

c. 12-tungstophosphoric(V) acid

IUPAC: $H_3[PW_{12}O_{40}]* 29H_2O$

Formula: $H_3[P^{5+}W_{12}O_{40}]* 29H_2O$

Notation: HW6+P

d. Potassium aquocobalto(II)-11-tungstophosphate(V)

IUPAC: $K_5[PCo(H_2O)W_{11}O_{39}]* 16.9H_2O$

Formula: $K_5[P^{3+}Co^{2+}(H_2O)W_{11}O_{39}]* 16.9H_2O$

Notation: KCo2+P

e. Potassium aquocobalto(II)-11-tungstoborate(III)

IUPAC: $K_7[BCo(H_2O)W_{11}O_{39}]$ * 13.7 H_2O

Formula: $K_7[B^{3+}Co^{2+}(H_2O)W_{11}O_{39}]$ * 13.7 H_2O

Notation: KCo2+B

f. Potassium aquocobalto(III)-11-tungstoborate(III)

IUPAC: $K_6[BCo(H_2O)W_{11}O_{39}]$* 16.8$H_2O$

Formula: $K_6[B^{3+}Co^{3+}(H_2O)W_{11}O_{39}]$* 16.8$H_2O$

Notation: KCo3+B

g. Tetra-n-heptylammonium aquocobalto(III)-11-tungstoborate(III)

IUPAC: $[N(C_7H_{15})_4]_6[BCo(H_2O)W_{11}O_{39}]$

Formula: $[N(C_7H_{15})_4]_6[B^{3+}Co^{3+}(H_2O)W_{11}O_{39}]$

Notation: AmCo3+B

h. Potassium aquocobalto(II)-11-tungstosilicate(IV)

IUPAC: $K_6[SiCo(H_2O)W_{11}O_{39}]$* 15.2$H_2O$

Formula: $K_6[Si^{4+}Co^{2+}(H_2O)W_{11}O_{39}]$* 15.2$H_2O$

Notation: KCo2+Si

i. Tetra-n-heptylammonium aquocobalto(II)-11-tungstosilicate(IV)

IUPAC: $[N(C_7H_{15})_4]_6[SiCo(H_2O)W_{11}O_{39}]$

Formula: $[N(C_7H_{15})_4]_6[Si^{4+}Co^{2+}(H_2O)W_{11}O_{39}]$

Notation: AmCo2+Si

j. Potassium aquocobalto(III)-11-tungstosilicate(IV)

IUPAC: $K_5[SiCo(H_2O)W_{11}O_{39}]$* 15.7$H_2O$

Formula: $K_5[Si^{4+}Co^{3+}(H_2O)W_{11}O_{39}]$* 15.7$H_2O$

Notation: KCo3+Si

k. Potassium aquocobalto(II)-11-tungstozincate(II)

IUPAC: $K_8[ZnCo(H_2O)W_{11}O_{39}]* 13.6H_2O$

Formula: $K_8[Zn^{2+}Co^{2+}(H_2O)W_{11}O_{39}]* 13.6H_2O$

Notation: KCo2+Zn

l. Potassium aquocobalto(III)-11-tungstozincate(II)

IUPAC: $K_7[ZnCo(H_2O)W_{11}O_{39}]* 16H_2O$

Formula: $K_7[Zn^{2+}Co^{3+}(H_2O)W_{11}O_{39}]* 16H_2O$

Notation: KCo3+Zn

m. Tetra-n-heptylammonium aquocobalto(III)-11-tungstozincate(II)

IUPAC: $[N(C_7H_{15})_4]_6[ZnCo(H_2O)W_{11}O_{39}]$

Formula: $[N(C_7H_{15})_4]_6[Zn^{2+}Co^{3+}(H_2O)W_{11}O_{39}]$

Notation: AmCo3+Zn

n. Potaesium aquocobalto(II)-11-tungstogallate(III)

IUPAC: $K_7[GaCo(H_2O)W_{11}O_{39}]* 13.1H_2O$

Formula: $K_7[Ga^{3+}Co^{2+}(H_2O)W_{11}O_{39}]* 13.1H_2O$

Notation: KCo2+Ga

o. Sodium aquocobalto(III)-11-tungstogallate(III)

IUPAC: $Na_6[GaCo(H_2O)W_{11}O_{39}]* 17.4H_2O$

Formula: $Na_6[Ga^{3+}Co^{3+}(H_2O)W_{11}O_{39}]* 17.4H_2O$

Notation: NaCo3+Ga

p. Tetra-n-heptylammonium aquocobalto(III)-11-tungstogallate(III)

IUPAC: $[N(C_7H_{15})_4]_6[GaCo(H_2O)W_{11}O_{39}]$

Formula: $[N(C_7H_{15})_4]_6[Ga^{3+}Co^{3+}(H_2O)W_{11}O_{39}]$

Notation: AmCo3+Ga

q. Potassium aquocobalto(II)-11-tungstogermanate(IV)

IUPAC: $K_8[GeCo(H_2O)W_{11}O_{39}]* 14.3H_2O$

Formula: $K_8[Ge^{4+}Co^{2+}(H_2O)W_{11}O_{39}]* 14.3H_2O$

Notation: KCo2+Ge

r. Tetra-n-heptylammonium aquocobalto(II)-11-tungstogermanate(IV)

IUPAC: $[N(C_7H_{15})_4]_6[GeCo(H_2O)W_{11}O_{39}]$

Formula: $[N(C_7H_{15})_4]_6[Ge^{4+}Co^{2+}(H_2O)W_{11}O_{39}]$

Notation: AmCo2+Ge

3.3. Techniques:

Depending upon the nature of spectral analysis to be done for heteropoly compounds and also on nature of HPC(s) itself, three different experimental techniques were used for taking the IR spectra. Though the exact value of characteristic frequency of a particular vibrating set of atoms depends on the environment of nearby vibrations, but this frequency is partly dependent on the preparative technique for taking the IR spectra [*19*, *21*, *31*]. Hence, IR spectra of some of HPC(s) were taken by using two or more techniques. The physical state of HPC(s) and their relative solubility behavior in non-polar solvents put some restrictions in taking the IR spectrum of each of compounds using all the three techniques described below. Comparison of IR spectra of a compound with the previously taken spectrum of the same compound also forces the use of these three different techniques.

3.3.1. Classification of Heteropoly Compounds:

IR spectra of the 18 HPC(s), which were available for this research, can be claasified into three classes according to different IR spectra taking techniques as:

a. IR spectra of only four HPC(s) with Na^+ or K^+ as cation NaCo3+Ga, KCo3+B, KCo2+Ge, and KCo2+Ge were taken by pellet making technique.
b. IR spectra of thirteen HPC(s) with K^+ or Na^+ as cation were taken by Nujol mull technique.
c. IR spectra of five HPC(s) with $[N(C_7H_{15})_4]^+$ as a cation i.e. AmCo3+Ga, AmCo3+B, AmCo3+Zn, AmCo2+Ge, and AmCo2+Si were taken by using liquid cell technique.

3.3.2. Pellet Making Technique:

Pellet making technique is supposed to be the best IR technique for both qualitative and quantitative analysis of a given compound if the pressure applied in forming the pellet and the particle eize of the sample are the same [*21, 31 - 33*]. The bands in the IR spectrum of HPC(s) in KCl and KBr are free from interfering bands because of the good transmittance range of KCl and KBr. Also, this technique allows for excellent control on the use of the sample concentration and on the thickness of the pellet formed. Assuming that KCl pellets give better results than that given by KBr pellets because of ite less hygroscopic nature, IR spectra of all the four HPC(s) of class (c) were taken by using both alkali halides [*21*]. Main disadvantage of this technique with respect to HPC(s) is

that the particle size of sample is never reproducible.

A general method used for taking the IR spectra by this technique is given as: First of all both a sample and KBr are dried in a oven at 110°C and 105°C respectively. And then, both are ground to a very small particle size separately keeping in mind the principal of Christiansen effect [*34*]. According to this effect the particle size of the sample must be less or equal to the order of wavelength of IR radiation; otherwise, some of the radiation incident on the pellet will be scattered out of the sample beam and hence, the detector will give a false zero level on the distorted spectrum. This effect also arises because of appreciable difference in refractive indices of sample and surrounding medium. This effect develops because the refractive index ie a function of frequency that has a discontinuity in the frequency region of a strong band [*34*]. To make the grinding process easier, parts of the sample was ground with 5 - 10 drops of cyclohexane which, because of its non-polar nature, has no chemical effect on the sample [*21*]. This process of adding liquid and then grinding was repeated until good particle size was achieved. After grinding by this process, the sample was kept for sufficient time for complete evaporation of the liquid. After the grinding process, both sample and KBr were weighed out in the ratio of approximately 1:100 and then, KBr was added in small quantities to obtain a

omogeneous mixture. Each addition of KBr was just equal o that of the sample. Mixing of both was then almost done ithout grinding to prevent the absorption of water by KBr. fter the complete mixing of sample with KBr, the mixture as placed in a die and then the die was pressed to a sufficient pressure to get a good pellet. Before taking a absorbance spectrum for the mixture, a reference spectrum of air, absorbance spectrum of KBr and reference spectrum of KBr were collected. The same process was repeated for other samples and for KCl pellets. Resolution of 4 cm^{-1} and number of scans equal to 16 for all the spectra were kept constant. Spectra of all HPC(s) of class (a) were taken by this technique. All the spectra were scanned from 5000 - 200 cm^{-1}. Another concentration ratio of sample to KBr as 1:25 was also used for taking the spectra of these HPC(s).

3.3.3. Nujol Mull Technique:

Only heavy Nujol, high boiling fraction from petroleum and a mixture of alkane in the range C_{20} - C_{30} with some olefinic aromatic hydrocarbon, was used for mull technique because it does not show the highly interferable bands in the spectral region which is of the importance for HPC(s) [*34*]. IR spectrum of Nujol shows strong absorption near 3000 cm^{-1} due to C-H stretching vibration and near 1400 cm^{-1} due to C-H bending vibration [*34*]. From Nujol mull technique it is not possible to get reliable intensity

values since there is no simple control on the sample thickness nor on the sample concentration [*32, 33*]. For this technique, a demountable cell with KBr windows was used. A demountable cell has the advantage that it can be disassembled for filling and cleaning. A special handling care was given to KBr windows because the hygroscopic and the easily damaged nature of a crystal increase with increase in IR transmission range. The same method of drying and grinding the eample was used as was employed in the case of pellet making technique. About 1 mg of well ground sample was mixed with a drop of Nujol with the help of mortar and pestle. Special care also was given to proper ratio of sample to Nujol. After homogeneously mixing the sample with Nujol, it was placed gently on KBr window with the end of pestle and then it was evenly distributed by rotatory motion of the windowe. Resolution of 4 cm^{-1} and number of scans equal to 25 for all the spectra were kept conetant. Ae in previous case, first reference spectrum of air, absorbance spectrum of Nujol and then reference spectrum of Nujol were taken before taking the absorbance spectrum of the Nujol mull. All the spectra were scanned from 5000 -200 cm^{-1}. IR spectra of all compounds coming under class (b) were taken by using this technique.

3.3.4. Solution Technique:

For best quantitative analysis of IR spectra, a

solution technique is considered as the most reliable one [*21, 32, 33*]. This is because spectra taken by this technique are very reproducible if the same unopened cell is used. The major advantages that can be gained by employing this technique include the ease of sample preparation, uniformity of dispersion of solute and the ease in fixing both the concentration and layer thickness [*32, 33*]. For this technique sealed demountable cells were used which have the advantages of filling and cleaning without changing the path length. For this technique only HPC(s) with $[N(C_7H_{15})_4]^+$ as cation were used because these compounds were found to be soluble in non-polar solvents like CS_2 and CCl_4 [*30*]. Selection of these solvents is governed by two facts: Firstly, these solvents do not exhibit strong absorption in the spectral range which is of the importance for HPC(s); secondly, these solvents do not appreciably interact with the concerned HPC(s) because of their homogeneous dielectric field and also because of their non-polar nature [*7, 31 - 34*]. Because of their volatile nature, the number of scans was reduced to nine while the resolution was kept unchanged at 4 cm^{-1}. For solution techniques, the spacer of approximate thickness of (55 - 45x10^{-6} m) was used because with a greater thickness, these solvents are not sufficiently transparent to IR radiation [*34*].

Because of the nature and physical appearance of the

HPC, this technique does not require the grinding of the sample. But, all these HPC(s) were dissolved and then evaporated 2 - 3 times with the solvent to free them from the methylene chloride in which they were prepared [*30*]. As in previous cases, first the reference spectrum of air, absorbance spectrum of solvent and the reference spectrum of solvent were taken before taking the absorbance spectrum of the solution. In between two consecutive spectra, the cells were thoroughly washed with the relevant solvent. IR spectra of one HPC were taken for 10 - 13 different concentrations at a given path length for a particular liquid. All the spectra were scanned from 5000 - 200 cm^{-1}. The spectra of all compounds representing the clase (c) were taken by this technique.

3.3.4.1. Details of New Weighing Scheme:

Assuming that the solution of HPC(s) with any of the above mentioned solvents is homogeneous and the rate of evaporation of solvent is negligible as compared to total weight of solution, a new weighing scheme was devised to improve the accuracy of the result and to reduce the excessive use of the HPC(s). This scheme has reduced the total number of weighing necessary for taking the spectra. For example, to take ten spectra if the general weighing scheme is used then number of times the weighing should be done will be 30 and use of this current scheme has reduced the number of weighings to 21. Briefly this scheme is

iven as:

irst weighing : Let weight of sample = x_1 g

econd weighing: Let weight of solvent = y_1 g

ence, total weight of solution formed = (x_1+y_1) grams, in which ratio of solute to solvent is $x_1:y_1$. The concentration of this solution is calculated in grams of solute/ liter of solvent, g/L. The volume of the solvent is calculated by dividing its total weight by its density at a given temperature. The temperature dependence of densities for CCl_4 and CS_2 were taken from [*35*]. If z_1 grams of this solution is used for first spectrum then:

Third weighing : Weight of solution after first spectrum

$= (x_1+y_1-z_1)$ g

$(x_1+y_1-z_1)$ grams of solution still has the ratio of solute to sample as $x_1:y_1$. Now, if w_1 grams of solvent is added to the solution then:

Fourth weighing: Total weight of solution before second spectrum $= (x_1+y_1-z_1+w_1)$ g

Now, in this solution ratio of solute to solvent will be $x_2:y_2$, where the value of x_2 and y_2 will be calculated using simple mathematics. Now, if z_2 grams of solution is used for the second spectrum then weight of solution after second spectrum will be:

Fifth weighing : Total weight of solution after second spectrum $= (x_1+y_1-z_1+w_1-z_2)$ g

In this solution, the ratio of solute to solvent will be

$x_3 : y_3$. Up to this point, this shows that for two spectra the number of weighing to be done is five, whereas for general weighing procedure this number would be six.

3.3.5. Spectral Peak Table:

Peak tables of all spectra were created using the Spectra Calc software. Normally, for producing a peak table a sensitivity factor of 10 is recommended but for the present study its value was kept at 20. Actually, the latter value of the sensitivity factor causes the eoftware to identify more peaks. The peak tables originally created contained four columns: one for the peak position, one for the corresponding absorbance values and two columns for the estimated left and right edges of the peaks. These peak tables were then modified using the Quattro spreadsheet. Each modified peak table has three columns: one for peak positions, one for the corresponding absorbances, and one for relative abeorbances of all peaks normalized with respect to the highest absorbance in that table.

3.3.6. Spectral Search Library:

Four different libraries were created using Spectra Calc for the spectra taken in four different dispersing media as Nujol, KBr, KCl, and CCl_4. The features of these libraries are controlled by two factors: one is matching resolution, Res, of two spectra and another is number of data points, N_{dp}, used to match a unknown spectrum against the spectra stored in each library. These two factors are

related by the following relation:

$$N_{dp} = (\nu'_{max} - \nu'_{min})/Res$$

If ν'_{max} = 1095 cm^{-1} and ν'_{min} = 356.44 cm^{-1}, then for Res of 2.556 cm^{-1} the total number of data points which are to be matched will be 289. All the spectra stored in one particular library were taken under identical conditions of dispersing media, number of scans, and resolution for collecting a spectrum. Also, the spectra, which were identified using a particular library, were taken under similar conditions. Each standard library matches a spectrum by giving its 'hit quality index', HQI, against each spectrum stored in the library. If the value of HQI is 0.000 then it means the match is perfect. And, if this value is greater than 1.414 then it shows the worst match. All the spectra in the eearch result are arranged in the increasing order of HQI values. In Nujol search library 14 spectra were stored. In KBr, KCl and CCl_4 libraries, the number of spectra stored is 5.

4. RESULTS:

This section is divided into two parts: qualitative analysis and quantitative analysis.

4.1. Qualitative Analysis:

Qualitative analysis of the spectrum of a given unknown compound is generally related to its identification without doing any chemical analysis. The identification of

a spectrum was performed in two ways: using the 'fingerprint' method and using a computerized search library. Therefore, this section is further divided into two parts.

4.1.1. Fingerprint Method:

In presenting the results of this section, the spectra of compounds will be given in the order mentioned in section 3.2.1. except that, for ease of presentation, the phosphorous compounds are placed before the boron compounds. In other words, the compounds are arranged on the basis of increasing atomic weight of their central hetero atoms except for the phosphorous hetero atom, i.e. in the order of H_2, P, B, Si, Zn, Ga, and Ge. This order was chosen to simplify the corresponding discussion. For the same central hetero atom, the order of peripheral hetero atom of W^{6+}, Co^{2+}, and Co^{3+} is followed. For the same central and peripheral hetero atoms, the cation order of K^+, Na^+, and $[N(C_7H_{15})_4]^+$ is used. For each compound, the spectrum in KBr is placed first and then spectra taken in KCl, Nujol, CCl_4, and CS_2. The results of HPC(s) containing dihydrogen or phosphorous as their hetero atom are given under the same section because both 1:12 HPC(s) have either of W^{6+} or Co^{2+} hetero atoms.

4.1.1.1. Dihydrogen and Phosphorous Compounds:

The compounds having dihydrogen or phosphorous as their hetero atom are NaW6+H2, KCo3+H2, HW6+P, and KCo2+P.

The spectra of all four of these compounds were taken in Nujol. The spectra of first two compounds are shown in Figure 5. And their corresponding peak tables containing peak positions, absorbances, and relative absorbances are given in Tables I and II. Similarly, for the two latter compounds, the spectra are shown in Figure 6 and corresponding peak tables are given in Tables III and IV.

4.1.1.2. Boron Compounds:

The compounds representing this hetero atom are KCo2+B, KCo3+B and AmCo3+B. The spectrum of KCo2+B was taken in Nujol. Three spectra of KCo3+B were collected in KBr, KCl, and Nujol. Spectra of AmCo3+B were taken in CCl_4 at different concentrations. As an example, the spectra of KCo3+B in KBr and Nujol and of AmCo3+B in CCl_4 are shown in Figure 7. The concentration for the solution chosen is given as 39.34 g/L. The peak tables of these spectra are summarized in Tables V - VII.

4.1.1.3. Silicon Compounds:

The compounds with silicon as central hetero atom are KCo2+Si, AmCo2+Si, and KCo3+Si. The spectra of KCo2+Si were taken in three dispersive media, KBr, KCl and Nujol. Spectra of AmCo3+Si were taken in CCl_4 at several different concentrations. Also, the only spectrum of KCo3+Si was collected in Nujol. To show the effect of dispersive media on the spectra, three spectra of KCo2+Si are shown in Figure 8. The peak tables for all these spectra are given

n Tables VIII - X.

4.1.1.4. Zinc Compounds:

Three compounds which have Zn as central hetero atom are KCo2+Zn, KCo3+Zn and AmCo3+Zn. The spectra of the first two compounds were taken in Nujol. Spectra of AmCo3+Zn were taken in CCl_4 at different concentrations. Only two spectra of KCo2+Zn and of AmCo3+Zn, are shown in Figure 9. The concentration of the solution is given as 14.55 g/L. The corresponding peak tables of these spectra are given in Tables XI and XII.

4.1.1.5. Gallium Compounds:

The compounds with Ga are KCo2+Ga, NaCo3+Ga, and AmCo3+Ga. The only spectrum of KCo2+Ga was collected in Nujol. Three spectra of NaCo3+Ga were taken in KBr, KCl, and Nujol. The spectra of AmCo3+Ga were taken in CCl_4 and CS_2 at different concentrations. Three spectra of Ga compounds are shown in Figure 10. These spectra include: a spectrum of NaCo3+Ga in KBr, a spectrum of AmCo3+Ga in CCl_4 at concentration of 52.09 g/L and a spectrum of AmCo3+Ga in CS_2 at concentration of 61.11 g/L. The peak tables of these spectra are given in Tables XIII - XV.

4.1.1.6. Germanium Compounds:

The compounds with Ge as central atom include KCo2+Ge and AmCo2+Ge. The spectra of KCo2+Si were taken in KBr, KCl and Nujol. Spectra of AmCo2+Ge were collected in CCl_4 at different concentrations. Two representative

ectra of these two compounds are shown in Figure 11 and their peak tables are summarized in Tables XVI and XVII. The concentration chosen for the germanium solution in CCl_4 is 13.91 g/L.

3.1.2. Search Libraries:

All heteropoly compounds containing K^+ and Na^+ as their cations were identified by using the Nujol search library. The four compounds of the "a" class of section 3.3.1. were also identified by the KBr and KCl search libraries. All these spectra were searched within 1095 - 356.44 cm^{-1}. All compounds containing $[N(C_7H_{15})_4]^+$ were identified by using the CCl_4 library. But in this case, the compounds were searched between 1095 - 810 cm^{-1} and 740 - 356.44cm^{-1}. Total number of searched data points and matching resolution for these libraries are 289 and 2.561 cm^{-1} respectively.

The working accuracy of the Nujol library is checked by matching a known spectrum of KCo2+Si against the spectra stored in the library. The hit quality index 'HQI' of the KCo2+Si spectrum, stored in the library, was observed as 0.000 (Table XVIII). This match verified the working of the Nujol library in identifying a given spectrum.

Two typical search results of the unknown compounds KCo2+P and KCo2+Si in Nujol are shown in Figure 12 - 15. In case of KCo2+P, the HQI for the first hit is found to be 0.138 against the known spectrum of KCo2+P (Figure 12,

Table XIX). For the second hit, the hit quality index is equal to 0.393 against the known spectrum of HW6+P (Figure 13). In case of KCo2+Si, the HQI of the first hit is found to be 0.232 against the known spectrum of KCo2+Si (Figure 14, Table XX). For the second hit, the hit quality index is equal to 0.371 for the known spectrum of KCo3+Si (Figure 15).

4.2. Quantitative Analysis:

The study of absorbance variation with concentration at two different wavenumbers was carried out for all five compounds containing $[N(C_7H_{15})_4]^+$ as the cation. The absorbance plots verses concentration are given in the same order as before, i.e. in the increasing order of atomic weight of central hetero atoms, i.e. first plot is of B and then Si, Zn, Ga, and Ge respectively. For the same central hetero atom, the order of solvent chosen is CCl_4 and CS_2. All the plots were drawn within the same limits of concantration, 0 - 70.00 g/L and absorbence, 0 - 0.16. Here, this absorbance behavior with concentration is described only for AmCo3+B in CCl4 and for AmCo3+Ga in CCl_4 and CS_2.

4.2.1. Boron Compound:

For AmCo3+B solution in CCl_4, two graphs of absorbance verses concentration (given in grams of solute/ liter of solvent, g/L) were drawn at 949 cm^{-1} and 901 cm^{-1} (Figure 16). For both plots, the absorbance was observed

in increasing order with concentration within the range of 8.223 - 28.37 g/L. In this concentration range the absorbance proportionality constant, K, is given as 0.0031 L/g and 0.0039 L/g at 949 cm^{-1} and 901 cm^{-1} respectively. After that it suddenly dropped at 31.71 g/L and then again started to increase up to the concentration of 39.34 g/L. The lines in the figure are the best fit lines through these two concentration ranges. The first regression analysis is for the lower concentration data set. The second regression is for the highest three concentration points. Data for these two graphs are summarized in Tables XXI and XXII.

4.2.2. Silicon Compound:

For a solution of AmCo2+Si in CCl_4, two graphs were drawn at 901 cm^{-1} and 909 cm^{-1} within the concentration range of 2.381 - 10.63 g/L. These two graphs are shown in Figure 17 and their corresponding data are tabulated in Tables XXIII and XXIV. The lines drawn in the graphs are the best fit lines through all the data points. The regression analysis for these data points is also shown in these tables.

4.2.3. Zinc Compound:

For a solution of AmCo3+Zn in CCl_4, two graphs drawn at 939 cm-1 and 876 cm-1 are shown in Figure 18. The concentration range for these two graphs is 2.381 - 10.63 g/L. The absorbance and concentration data for these two

raphs are aummarized in Tablea XXV and XXVI. The linea rawn in the graphs are the beat fit linea through all the ata pointa. The regreaaion analyaia for theae data pointa e alao ahown in theae tablea.

4.2.4. Gallium Compound:

For a aolution of AmCo3+Ga in CCl_4, two abaorbance plota were drawn at 947 cm^{-1} and 883 cm^{-1} (Figure 19). The concentration range for theae two graphs ia 7.449 - 52.09 g/L (Tablea XXVII and XXVIII). Overall, the abaorbance waa found to be in incraaaing ordar with the concentration except at the concentration of 36.66 g/L. Thia overall increaaing trend of abaorbance with concentration waa not linear. But whan data pointa were broken into three aegmenta of concentration range 7.449 -29.85 g/L, 29.86 - 45.62 g/L and 45.62 - 52.09 g/L, then abaorbance waa found to be linaarly increaaing with concentration except at the above atated concantration of 36.66 g/L. At 947 cm^{-1}, for the firat two aegmenta, the abaorbance proportionality conatanta, K, are given aa: 0.0010 L/g and 0.0003 L/g. At 883 cm^{-1}, the valuaa of K are given aa and 0.0007 L/g and 0.0013 L/g raapectively. The baat fit linea through theaa thraa aegmenta are ahown in the figure. Alao, regreaaion analyaia of theae data pointa ia aummarizad in the tablea.

For AmCo3+Ga in CS_2, two plota were drawn at 949 cm^{-1} and 882 cm^{-1} (Figure 20). Theae two graphs were plotted within the concentration range of 1.665 - 61.11 g/L

Tables XXIX and XXX). At both wavenumbers, at low concentration region of 1.665 - 7.971 g/L a very random behavior of absorbance was observed. From 7.971 - 54.77 g/L the absorbance was found to be increasing with concentration except at 42.40 g/L for 882 cm^{-1}. From 54.77 - 81.61 g/L, the absorbance was found in decreasing order. As in the previous case, within two segments of concentration range of 18.59 - 42.40 g/L and 42.40 -54.77 g/L, the absorbance was observed in linear increasing order. At 949 cm^{-1}, the absorbance proportionality constants, K, for these two segments are 0.0003 L/g and 0.0028 L/g respectively. At 882 cm^{-1}, the values of proportionality constants for these two ranges are 0.0006 L/g and 0.0033 L/g respectively. The solid lines in the graph represent the best fit lines through the different sets of data points. The regression analysis of these three segments of data points are shown in the tables.

4.2.5. Germanium Compound:

For a solution of $AmCo_2$+Ge in CCl_4, two graphs drawn at 957 cm^{-1} and 985 cm^{-1} are shown in Figure 21. The concentration range for these graphs is 2.994 - 13.91 g/L (Table XXXI and XXXII). The lines drawn in the graphs are the best fit lines through all the data points. The regression analysis for these data points is also shown in these tables.

DISCUSSION:

The infrared spectroscopic study was performed on eighteen heteropoly compounds of 1:12 and 1:11 Keggin family. A general formula was devised for clearly specifying the anions (section 1.2.1.). Later, this formula was found to have been reported by Pope [*13*]. In addition to explicitly defining the number of addenda atom and hetero atoms, this formula also specifies the position of any ligand such as H_2O in the anion.

A study of the structural arrangement of atoms in heteropoly anions of 1:12 class showed that they have a tetrahedral Keggin structure with T_d as the Schoenfliese point group. Whereas the anions of 1:11 class have 'pseudo Keggin' structure with C_s as the Schoenfliess point group. The application of group theory to the T_d point group proved that for the anions of 1:12 family, F_2 is the only active mode. This fact is also reported by others [*19, 20, 28*]. In going further in this field, a method is suggested to find the total number of bands belonging to the T_d point group. Some authors [*19, 20, 28*] have reported this number to be 22. Internal coordinate analysis of HPA of 1:11 and 1:12 class showed that the anion of 1:12 needs a total of 297 internal coordinates to completely specify its vibratory motion. Of these 297 coordinates, 76 belong to stretches, 133 to bond angle deformations and 64 to torsions. No internal coordinate is reported for out of

plane bending because there is no more than one bond which is coplanner with others. In case of HPA of 1:11 compounds, a total of 303 internal coordinates are required to designate its vibratory motion. Of these 303 coordinates, 78 belong to stretches, 160 to bond angle deformations and 65 to torsions. In both cases, the number of coordinates corresponding to stretches directly refers to the number of total bonds in the anions.

The identification of the eighteen heteropoly compounds was performed on the basis of a few different peaks in their spectra. These different peaks are observed because of the different nature of central and peripheral hetero atoms. Most of the peaks in each spectrum of these compounds are observed to be the same because all these HPA(s) have similar tungstan addenda atoms. Also, the similarities of the spectra of the HPC(s) strongly indicate that they have identical structures [*11*]. The characterization of all spectra obtained in this study were assigned by comparisons using 'fingerprint' methods. According to Kazanskii, "on account of the complexity of the structure of HPA(s) in which various types of metal-oxygen bonds are realized, the assignments of the absorption bands in the infrared spectra presents great difficulties and causes numerous contradictory judgements" [*36*]. Hence, the assignment of the bands is performed somewhat arbitrarily. Kazanskii, also indicated that the

Vibration analysis of HPA(s) can be performed on the assumption of group vibrations. But, according to Weakley [19], there may be a possibility of intercoupling vibration. In intercoupling vibration, two sets of vibration can produce their peaks at the same wavenumber. In the present study, this coupling vibration may be between addenda atom and oxygen vibration and hetero atom and oxygen vibration. Hence, HPA(s) do not fulfil the requirement for the appearance of group frequencies in the spectrum.

Generally, infrared spectra of the compounds were scanned from 5000 - 200 cm^{-1} at a resolution of 4 cm^{-1}. Pope [11] has reported that the only region of interest for HPA(s) lies between 1000 - 400 cm^{-1}. Sharpless and Munday [37] suggested that this region lies between 1200 - 650 cm^{-1}. Whereas Weakley [19] stated that the higher wavenumber region may be informative for some other types of HPC(s). Study of the spectra obtained in this investigation indicated that this region actually depends upon the nature of vibration between hetero atom and oxygen atom. This fact is supported by the explanation given by Kazanskii [36]. Detailed study of the spectra obtained reveals that for the vibration of hetero atom and oxygen, the region of interest lies between 1100 - 900 cm^{-1} and 650 - 460 cm^{-1}. For the spectra of the eight different hetero atoms used in the present study, this region starts near

400 cm^{-1} because the phosphorous and oxygen stretching band occurs near 1050 cm^{-1} [*36 - 39*]. The other end of the spectral range is restricted to approximately 350 cm^{-1}. because below this value, interfering bands were observed due to the dispersive media.

For four compounds, KCo3+B, KCo2+Si, NaCo3+Ge and KCo2+Ge, the spectra were collected using three dispersive media, KBr, KCl, and Nujol. For a given compound, nearly identical spectra were observed in these different media. In different media for one compound, some of the positions are observed to be significantly shifted. In case of KCo2+Si spectra, for most of the bands the band positions were found to be shifted within plus or minus 4 cm^{-1}. But for some other bands, this shifting was found to be more than 4 cm^{-1} (Figure 8, Table VIII - X). This observation suggests an affect of the dispersive media on the position of the peaks. Weakley [*19*] stated that the difference in observed peak positions may be due to differences in the cations.

For the spectra of one particular compound, more bands were observed in one dispersive medium e.g. Nujol as compared to that observed in another medium e.g. KBr (Figure 8, Table VIII - X). Kazanskii [*36*] also reported this phenomenon. This observation can be explained in terms of how well the sample is dispersed in a medium, the preferential orientation of the molecules, and the particle

e of the sample. The intenaity of a particular band in given medium may account for this phenomenon. Also, an purity in the compounds may be a reaponaible for some of e extre peaks.

Similarly, the spectra of the HPC(a) look identical ether they were taken using pellet, mull or aolution chnique e.g. the apectra of KCo3+B in KBr, Nujol, and Cl4 (Figure 7, Table V - VII). This atrongly suggeats hat the atructure of HPA(a) in the solution is the esme aa hat obaerved in the crystal form. This observation is lso reported by Pope and Yurchenko [*11, 40*].

For purposes of diecuaaion, the apectral region of intereat is limited to 1100 - 350 cm^{-1} and peaks teblea were obtained using the peak aanaitivity factor of 20. The most common bande obaerved in all apectra are because of tungeten and oxygen vibratione. Some common bands obaerved in 1100 - 900 cm^{-1} are attributed to W=O atretching [*19, 24, 38*]. Here, thle oxygen atom ia the terminal oxygen atom in a octahedron aa explained in aection 2.2. Weakley [*19*] reported that there should be two bande corresponding to thia vibration in the region 1000 - 900 cm^{-1}. Hence, aa in caae of the apectrum of KCo3+B in Nujol, (Figure 7), where a peak ia obaerved at 916 cm^{-1} thia peak may be assigned to W=O vibration. Thia obaervation of Weakley ia alao aupported by the atudy of Deltcheff and Thouvenot and Tsigdinoa [*12, 24*]. But, Kazanakii [*36*] obaerved only one

d due to W=O vibration in the region 1000 -900 cm^{-1}. er common bands observed in 900 - 350 cm^{-1} are assigned W-O bending [*24, 35, 38*]. As for a specific example of spectrum of NaW0+H2 in Nujol, (Figure 5, Table I), the st common bands in 1100 - 900 cm^{-1} are at 1055 cm^{-1} and cm^{-1}. And for 900 - 350 cm^{-1}, most common bands are at 0, 775, 721, 663, 669, 656, 457, 424, 401, 384, and 374 cm^{-1}. The Nujol absorbance spectrum also has a band at 721 cm^{-1}. But the intensity of this band observed in case of PC(s) shows that this band also has some contribution due to W-O-W vibrations. This band is also reported by Deltcheff and Thouvenot [*24*]. They also noted that for 1:12 anions, this band occurs at 740 cm^{-1}. They interpreted this lowering of frequency in terms of lowering of W-O-W angle. The band observed at 669 cm^{-1} also appears in ambient carbon dioxide [*41*]. But again because of its greater absorbance in the heteropoly compounds spectra, this band also might be due to a W-O vibration. According to Brown [*38*] the relatively high number of W-O peaks shown by HPA(s) is due to the lower symmetry of distorted WO_6 octahedra. Also, depending upon the sharing of the oxygen atoms in a octahedron with its neighboring octahedra, each anion has three different type of W-O bonds. In general, these are given as: Z-O, Z-O-X, and Z-O-Z, where X stands for central hetero atom and Z stands for addenda atom. For 1:12 anions, Brown indicated that the band near 800 cm^{-1} is

ue to Z-O-X bonding. Hence, this position is highly ffected by the particular hetero atom. In most of the pectra, this band was obeerved between 800 ~ 820 cm^{-1}. imilerly, he stated that for 1:12 anions, the band at 740 cm^{-1} dapends upon the nature of central hetero atom. In the present study, thia band is always noted between 725 - 719 cm^{-1}, which is not a significant shift when compared to the resolution of the spectra.

But Deltcheff and Thouvenot [*24*] explained that the band between 800 - 620 cm^{-1} band for 1:11 lacaunary HPA is due to an antieymmetrical valance vibration of Z-O-Z. Here, thia oxygen atom is one which is shared equally between the two octahedra of in the group containing a set of three octahedra (Figure 2). They also geve a explanation for the band near 721 cm^{-1}. Similarly, the bands near 880 cm^{-1} and 374 cm^{-1} are assigned due to Z-O-Z bonding. For these two bands, the oxygen atom is now shared by each octahedron from a sets of two groups conteining three octahedra (Figure 3). For 1:12 anions, Kazanskii [*36*] assigned the band near 370 cm^{-1} due to deformation vibration of both W=O and of the vibration of entire anion. For 1:12 HPA(s), Kazanskii reported that the intensity of band near 889 cm^{-1} is less than that et 600 cm^{-1}. In the preeent study, this is not always the case.

For the same central hetero atom, the spectra of 1:12 compounds, i.e. NaW6+H2 and HW6+P in Nujol (Figure 5 and 6;

bles I and III), and 1:11 compounds, KCo3+H2 and KCo2+P in Nujol (Figure 5 and 6; Tablee II and IV) were differentiated. All sixteen HPC(s) of 1:11 family used in this etudy have Co as the peripheral hetero atom in its +2 or +3 oxidation state. All of the 1:11 compounds show a peak between 613 - 619 cm^{-1}, but this band was not observed in the spectra of the two compounds of 1:12 family. This suggests that this paak is most probably due to a Co-O vibration. A peak near this range is also reported in the spectra of cobalt acetate and beta-carbonato(trien)cobalt(III) perchlorate [*42*] and in the spectrum of sodium hexanitrocobaltate (III) [*43*]. All three of these compounds have Co-O bonding in their structures. Brown [*39*] reported a band a near 453 cm^{-1} due to Co-O vibration, but the band at this position is also observed for both compounds of 1:12 family and hence, it is assigned due to W-O vibretion.

For the same peripheral hetero atom, the spectra of both 1:12 HPC(s) and the spectra of 1:11 family were also differentiated. For W^{6+} as peripheral hetero atom in case of HW6+P (Figure 6, Teble III), three bands at 1080, 596, and 523 cm^{-1} were observed. These three bands are not obaarved in the spectrum of NaW6+H2 (Figure 5, Table I). Also in addition to three bands at nearly the same positions, one more band at 1057 cm^{-1} is uniquely noted in the spectrum of KCo2+P (Figure 6, Table IV). This

servation suggests that these bands are most probably due P-O stretches and/or bends. A band near 1080 cm^{-1} is also reported by several authors [*36-40, 44 - 46*]. All these authors have assigned this band to P-O stretching. A band at 1057 cm^{-1} is also observed in the spectra of other compounds. But the intensity of this band indicates that it also has some contribution due to W-O and P-O vibrations, a case of intercoupling vibration as mention before. For a lacunary anion of 1:11 heteropoly anion containing P as hetero atom, Deltcheff and Thouvenot [*24*] observed the two bands of P-O vibration at 1085 and 1040 cm^{-1}. A band at 1040 cm^{-1} was not observed for 1:12 anion. They interpreted this phenomenon in terms of splitting of the bands because of lowering of symmetry from T_d to C_s for 1:11 HPA(s). The bands at 598 cm^{-1} and 523 cm^{-1} are assigned due to a bending vibration of the P-O bonds [*12, 19, 36, 39, 44*]. For the *HW6+P* spectrum, nearly all major bands around the same positions are also reported by Thouvanot et al. [*46*] and Kazanskii [*36*].

The peak due to O-H vibration in NaW6+H2 and KCo3+H2 is not observed in the range of 1100 - 350 cm^{-1} (Figure 5, Tables I and IT). This peak has a high probability of occurring near the same positions as shown by atmospheric water molecules in the region of 3550 - 3200 cm^{-1} and also around 1600 cm^{-1} [*12*]. Hence, no additional attempts were made to assign its band. But for the same anion of

W6+H2, Deltcheff et al. [44] reported peaks assigned to H at 960 cm^{-1} and 430 cm^{-1}. For the spectrum of NaW6+H2, nly two bands were observed in the present study from 1100 900 cm^{-1} at 1055 and 941 cm^{-1} whereas, for this anion azanskii [38] reported three bands at 975, 957, and 940 cm^{-1}. This observation can be interpreted in terms of fewer number of observed bands because of their low intensities as mentioned earlier.

In case of the spectra of boron compounds, in addition to all other peaks due to W-O and Co-O vibrations, two more unique peaks are observed (Figure 7 and Table V -VII). The peak at 991 cm^{-1} is due to stretching and another peak between 500 ~ 511 cm^{-1} due is due to bending. For 1:12 compounds, several authors have also reported these two peaks between 978 - 990 cm^{-1} and 530 - 540 cm^{-1} respectively [38, 39, 43]. For the spectrum of KCo3+B in Nujol, a peak at 916 cm^{-1} which seems to be due to intercoupling vibration is also assigned to B-O vibration (Figure 7, Table VI). This peak is also reported by Deltcheff et al. [44]. For this spectrum, a peak between 978 - 990 cm^{-1} was not observed which may be due to low intensity.

In general, the spectra of silicon compounds showed the peaks due to W-O and Co-O vibrations as explained earlier. But two characteristic peaks are observed due to Si-O bonding between 1001 - 997 cm^{-1} and 525 - 529 cm^{-1} (Figure

and Tables VIII - X). The first band is due to Si-O stretching and second is due to the corresponding bending. For 1:12 HPA(s), some authors also reported two peaks due to Si-O vibration near these two wavenumbers [*12, 19, 38-39, 44 -47*]. For the lacaunary anion of the 1:11 anion of silicon. these two pesks at nearly the same wavenumbers have been reported by Deltcheff and Thouvenot [*24*]. They have also reported a peak at 985 cm^{-1} due to stretching of Si-O bond. For the spectrum of KCo3+Si in Nujol, a peak at 918 cm^{-1} is also observed. Weakley [*19*] also reported a peak near 919 cm^{-1} due to Si-O vibration for 1:12 compounds. This again looks to be a case of intercoupling vibration.

In case of the zinc compounds, only one characteristic peak between 461 - 457 cm^{-1} is obeerved due to Zn-O bonding (Figure 9, Tables XI and XII). Brown [*38*] and Tsigdinos [*12*] have reported this band for 1:12 compounds conteining zinc. They heve reported another band due to Zn-O vibration at 248 cm^{-1}. This could not be confirmed in this work becauee the instrumentation limits the spectral range to 350 cm^{-1}. No other characteristic band in the range 1100 - 900 cm^{-1} is noted for this bonding.

For the spectra of the Ga compounds, in addition to bands due to W-O and Co-O bondinge, only one peak at 534 cm^{-1} seems to be due to Ga-O vibration (Figure 10 and Tables XIII - XV). This band at 535 cm^{-1} is very

reasonable in relation to the bands of Si-O, P-O, and B-O vibrations at nearly the same wavenumber. No other characteristic band in the range 1100 - 900 cm^{-1} is noted for this bonding.

For the Ge compound spectra, the peak near 525 cm^{-1} is due to Ge-O vibrations (Figure 11, Tables XVI and XVII). The peak at 460 cm^{-1} is also reported by two authors [39, 44]. They have also reported one more peak due to Ge-O stretching near 815 cm^{-1}. A peak at this position is also noted and has already been assigned to W-O bonding. So, if this is true then these two peaks seem to result from intercoupling vibration.

Identification of all the eighteen compounds was also performed using search libraries. As mentioned in the results section, four different libraries were created depending upon the nature of dispersive media, namely KBr, KCl, Nujol, and CCl_4. These libraries have been used to identify unknown spectra in the spectral region 1095 - 356.44 cm^{-1}. The compounds with $[N(C_7H_{15})_4]^+$ as a cation were only identified using CCl_4 library, because only these compounds were found soluble in solvents such as CCl_4 [29]. While four compounds, KCo3+B, KCo2+Si, NaCo3+Ga and KCo2+Ge were identified using the KBr, KCl and Nujol libraries. In case of the CCl_4 library, the searching was performed only in the spectral region 1095 - 810 cm^{-1} and 740 - 356.44 cm^{-1}

This is because a strong band was obaerved in 810 -740 cm^{-1} in the absorbance spectrum of CCl_4.

The working characteriatics of each library was found be dependent upon two factors: one ia the total number data pointe aearched and another ia the matching eolution of two epectra. Theae two factors are related each other by a formula given in aection 3.3.6. After ing many triala, the beat spectral range for aearching he epectra was found to be 1095 - 356.44 cm^{-1}. For xample, two Nujol libraries were created. The firat Nujol ibrary ueed the range 1095 - 355 cm^{-1}. The aecond library eaed the range 1095 - 356.44 cm^{-1}. Using the firat ibrary, only 12 spectra out of 14 could be correctly identified aa the firat choice. The epectra of KCo2+B and KCo2+Ga were not identified uaing thie library. Whereaa uaing the aecond library, all epectra except the epectrum of KCo2+Ga could be identified. For a total of 289 data pointa, the matching reaolution of firat library ia given aa 2.561 cm^{-1}, whereaa for the aecond library thia reaolution ia given aa 2.556 cm^{-1}. But for the firat library, when the spectra were aearched within 1095 -356.44 cm^{-1} with the aame matching reaolution then all fourteen spectra were identified.

To check the working accuracy of the Nujol library, the known spectrum of KCo2+Si was aearched againat the aame spectrum atored in the library. The 'hit quality index'

HQI of 0.000 was found for this spectrum (Table XVIII). Hence, this correct matching of the spectrum established the exact working of all created libraries.

When the unknown spectrum of KCo2+P was searched against the Nujol search library within the above stated working limit, then the first hit number was given to the known spectrum of KCo2+P with HQI, of 0.138 (Figure 12, Table XIX). The second hit number was given to HW6+P, (Figure 13), with HQI of 0.393 because only these two compounds have the same central hetero atom, P. The only difference in these compounds is the peripheral hetaro atom. In first case the peripheral hetero atom is Co^{2+} while in the second case W^{6+} is the peripheral hetero atom.

Use of the Nujol library resulted in accurate differentiation of the compounds having the same central hetero atom and nearly the same peripharal hatero atom. When the unknown spectrum of KCo2+Si was searched against the nujol library then the first hit number was found for the known spectrum of KCo2+Si atored in the library with HQI, of 0.232 (Figure 14, Table XX). The second hit number was found for KCo3+Si with HQI of 0.371 (Figure 16). This searching looks to be obvious because out of all the spectra in the library, only these two known spectra have the same Si as central hetero atom. Moreover, both these compounds have same peripheral hetero stom, Co, but in different oxidation states.

In both search results, very close values of HQT's for known spectra stored in the library show how closely their structures resemble each other (Tables XVIII -XX).

The heteropoly compounds show a very unusual absorbance behavior with the change in concentration at a given wavelength and pathlength. These absorbance measurements were performed only on the five compounds containing $[M(C_7H_{15})_4]^+$ as a cation. As described earlier these compounds were found to be soluble in non-polar solvents like CCl_4 and CS_2.

The absorbance study was performed using a new weighing scheme which may be known as the 'Method of Continuous Dilutions'. The working details of this scheme are given in section 3.3.4.1. Two major assumptions were used for the use of this scheme. First, the rate of evaporation of the solvent throughout the duration of experiment is negligible as compared to the total weight of the solution. Second, the solution is assumed to be uniform during the course of the experiment. This scheme has three main advantages over the 'traditional weighing method'. First, this scheme reduces the total number of weighings for collecting the given number of spectra. For example, if the general weighing scheme is used to collect ten spectra then the number of weighings will be 30. This new scheme has reduced this number to 21. Thus in addition to reducing the sources of error due to weighings, this new

eme has the additional advantage of saving the erimental time. Finally, this new scheme has nificantly reduced the amount of sample used. Because high cost this advantage is very notable for tungsten C(s).

To justify this new scheme, two methods were employed a tripalmitin system which was known to obey Beer's law 6]. Two graphs of absorbance versus concentration were rawn for tripalmitin solution in CCl_4 at 1746 cm^{-1} (Figure 2, Tables XXXIII and XXXIV). One graph is drawn using the traditional weighing technique and another is drawn using this newly devised scheme. At 1746 cm^{-1}, the infrared spectrum of tripalmitin shows a characteristic peak due to carbonyl group. Griffith [6] has mentioned that at 1737 cm^{-1} tripalmitin shows a linear increase of absorbance with increasing concentration when dissolved in chloroform. Within the experimental concantration range 1.490 - 9.492 g/L, both graphs show the linear increase of absorbance with an increase in concentration. The slopes of these plots were not the same. This difference in slope is probably due to change in pathlength because the cells were opened in between two experiments. This shows that the results from the new scheme are in good agreement with those obtained using the traditional weighing scheme.

As mentioned in results section, the five compounds for which the absorbance study was performed are: AmCo3+B,

Co2+Si, AmCo3+Zn, AmCo3+Ga, and AmCo2+Ge. All compounds were dissolved in CCl_4. In addition, AmCo3+Ga was also dissolved in C_6H_6. For each sample, two plots were drawn at two different wavenumbers (Figures 16 - 21, Tables XXI - XXII). The bands at these two wavenumbers, as described earlier, are due to W-O vibrations and are free from any other interfering band of the spectrum. In case of Si, Zn, and Ge, concentrations were varied within the range 2.361 - 14.55 g/L. While for B and Ga compounds, this concentration was varied between 1.665 - 61.00 g/L. These concentration ranges were arbitrarily chosen.

At low concentrations, all compounds except AmCo3+B, (Figure 16), showed a significant deviations from the normal behavior of absorbance with increasing concentrations i.e. from the Beer's Law in that concentration region. This 'scattering' may be due to changes in chemical and vibrational behavior of the HPA(s).

For plots of AmCo3+B at 949 and 901 cm^{-1}, the absorbance linearly increased within the concentration range of 8.223 - 28.37 g/L (Figure 16, Tables XXI and XXII). From 31.71 - 39.34 g/L, another increasing trend was observed but with a different absorption proportional constant, K. For a given HPC at a given wavelength and pathlength, these different values of K indicate that the proportionality constant is also changing with the concentration. Similarly, all other plots show any

ticular linear increasing trend of absorbance with the al experimental concantration range. But, when thie creasing trend of absorbance is divided into parts then thin each part, the abeorbance doea increase linearly. is phenomenon is much more pronounced in the caee of Co3+Ga when diseolved in CS_2 (Figure XX, Tablea XXIX and X). In thie eolvent, for the concentration range was 665 - 54.77 g/L three beet fit linea were drawn in three ncentration ranges of 1.665 -16.59, 16.59 - 42.40, and 2.40 - 54.77 g/L. The first beat fit line ehowe the scattered' behavior of abeorbance. But the later two beet it lines clearly ehow the above etated abeorbance henomenon.

In deriving the abeorbance - concentration relation i.e. Beer's Law:

$$A = K * C$$

it is aeeumed that the abeorbance proportionality conetent, K, is only a function of wavelength of incident radiation. However, in caee of heteropoly compounds the different K valuea at differant concentrationa euggeat that this constant alao depends upon the concentration. In other words, for heteropoly compounde the Beer's Law can be written aa:

$$A = K(C) * C$$

To illustrate that different vibrations behave differently at variouo concentratione, a plot wae drawn for

o3+Ga in CS_2 between peak positions and concentration igure 23, Table XXXV). Here, peak positions refer to the venumber corresponding to the second highest relative sorbance when the original absorbance at different ncentrations for all wavenumbers is normalized with spect to the absorbance at 882 cm^{-1}. This graph shows at these peak positions varied in nearly the same fashion the original absorbances have shown with concentration Figure 20, Tables XXIX and XXX). If this compound is to ey Beer' Law then these peak positions must be observed t the same wavenumber. This is because the absorbances of ll peaks should change in one particular order. This xplanation clearly indicates the different behavior of various vibrations in the solution at different concentrations.

In case of AmCo3+8 in CCl4, the peak positions of second highest relative absorbences were observed at the same wavenumber, 901 cm^{-1} when the original absorbances were normalized with respect to the absorbance at 831 cm-1 (Figure 23, Table XXXVI). This observation indicates that there is some other phenomena like solute-solute interaction, solute-solvent interaction, chemical association, and/or chemical dissociation taking place in the solution at different concentrations.

For all absorbance verses concentration plots, the non-zero intercepts on Y-axis may be due to different values of

absorbance proportionality constant, K, at different concentrations. Also, nonequivalent measurement conditions for taking the refsrence and solution spectra may account for these non-zero intercepts. These nonequivalent measurement conditions are due to the concentration valuss of solvent in the referencs and solution spectra. As stated in section 3.3.4., before taking a solution spectrum a reference spectrum of the dispersive medium was collected. In both cases, if the amount of solvent is different then different absorbance values will be recorded than expected. This difference in the expected and the observed absorbance valuss may account for non-zero intercept.

At the highest experimental concentrations of 61.11 g/L, (or 11.62×10^{-3} M, if there is no any water of hydration preeent in the compound), in case of AmCo3+Ga in CS_2 (Figure XX) and 13.91 g/L, (or 2.687×10^{-3} M, if there is no any water of hydretion present in the compound), in case of AmCo2+Ge in CCl_4 (Figure XXI), an unexpected sudden drop in absorbance was observed. Without having some more points beyond these concentrations, nothing should be concluded. But, this peculiar behavior of absorbance has raised some uncertainties about the chemical nature of these two compounds. A possible explanation for this observation is given by Ingle and Crouch [41]. According to them, at higher concentrations a significant portion of

incident radiation is absorbed. A fraction of this absorbed radiation is converted to fluorescence and observed by the detector. Thus, the observed radiant power of the sample is higher than expected. This change in sample radiance power causes the lower measurement of absorbance.

For a sample to obey Beer's Law, the peak for which the absorbance - concentration plot is drawn, must always occur at the same wavenumber i.e. there should not be any peak shifting. But for AmCo3+Ga in CS_2, at low concentrations the peak at 949 cm^{-1} is found to be shifted to either side by 2 cm^{-1} (Table XXXVII). The resolution of the spectra is 4 cm^{-1} but this shifting can be a possible cause of the observed scattering of the absorbance at low concentration and of the deviation from Beer's Law in general. Griffith [8] mentioned that this type of shifting of peaks may be due to instrumental error. This type of instrumental error in FT-IR may occur if the velocity of movable mirror in Michelson optics is not uniform. According to him, for the spectra obtained from FT-IR in addition to stray radiation, insufficient resolution may be a possible cause of observed deviation from Beer's Law. But the peak shift in case of AmCo3+B in CCl_4 is not observed (Table XXXVIII). Hence, this observation has ruled out the first possibility due to instrumental error. As mentioned earlier, the spectra were collected at 4 cm^{-1}

resolution. Therefore, to justify Griffith's explanation of inefficient resolution, further study needs to be done at the maximum resolution, of 1 cm^{-1}.

Multiple reflections of the infrared radiation at the wall of the windows may explain the unusual high absorbance for $AmCo^{3+}Zn$ in CCl_4 for both wavelengths at 9.658 g/L (Figure XVIII). Because about 4% of the radiations reaching the rear cell wall - air interface is reflected back into the cell and passes through the solution. Most of this reflected radiation passes out of the cell; however, about 4% of the radiant is reflected off the front cell wall - air interface and then passes back through the solution. In this way, the reflected ray experiances a pathlength of three times of the spacer thickness and correesponds to 0.16% of the direct transmitted beam. Hence, the net result of multiple reflections causes the higher value of this observed absorbance than expected because part of the monitored radiation is absorbed more strohgly due to the enhanced pathlength.

The variability in the pathlength travereed by the rays of the incident beam can also cause the deviation from Beer's Law. Thickness measurement of Teflon spacer which was used for collecting the spectra indicated that it is not uniform at all points. The thickness of the spacer was found to lie between 55×10^{-6} - 45×10^{-6} m.

The infrared spectra of $AmCo^{2+}Si$ collected at three

fferent times raised some uncertaintities about its bility with respect to time and perhaps, with respect to mperature (Figure XXIV). Three infrared spectra of this mpound taken in CCl_4 at approximately one month intervals owed the appearance and/or the disappearance of some aks. These spectra were collected for nearly the same ncentration, 10.65 g/L. This unique behavior probably dicates that during this time interval there was some composition occurred which resulted in the appearance and disappearance of the peaks. This behavior also suggests hat to justify thie explanation some more studies need to e done with other compounds at different intervals of time nd at different concentrations.

One way to give some more supporting evidences to this observed peculiar absorbance behavior is to measure the refractive index, n, of the solution at different concentrations. If some inconsistency is observed in the changing behavior of refractive index, which is generally due to the reflection loss at the cell wall and solution interface, with concentration then the proportionality constant, K, must be modified in terms of K' as given below:

$$K' = K * \{n/(n^2 + 2)^2\}$$

The changes in refractive index can also cause the change in position, size, and solid angle of the ray transmitted to the detector [41].

Second suggested way is to do the conductometric measurement of the solution at different concentrations. The necessary requirement for a compound to give its infrared spectrum is that there should be a change in the dipole moment during the molecular vibration. If some changes in conduction measurement are observed then that may be a possible cause for the shifting of peaks. Any change in conduction measurements will definitely change the dipole moment in some unexpected way because dipole moment is the vector product of charge and the displacement.

The heteropoly compounds are stable in moderately acidic solution but unstable in basic solution (section 1.2.4.); therefore, another suggested way is to measure the acidity of the solution at different concentrations. If the acidity of the solution is found to be significently changed, then this may be a possible explanation for the observed deviation from Beer's Law, and for the appearance and/or disappearance of some peaks as observed in case of AmCo2+Si spectra in CCl_4 collected at three different times.

BIBLIOGRAPHY

1. Lowenstein, E.V. *Appl. Phys.* 1966, *5*, 845.

2. Becker, E.; T. Farrar *Science* 1972, *178*, 381.

3. Griffith, P.R. *Science* 1983, *222*, 297.

4. Bell, R.J. *Introductory Fourier Transform Spectroscopy*; Academic: New York, 1972.

5. Durig, J.R., Ed., *Analytical Applications of FT-IR to Molecular and Biological Systems*; D. Reidal: MA, 1980.

6. Griffith, P.R.; J.A. deHaseth *Chemical Infrared Fourier Transform Spectroscopy*; Willey: New York, 1986.

7. Willard, H.H. *et al.*, Eds., *Instrumental Methods of Analysis*; 7th ed., Wadsworth: CA, 1988.

8. Forman, M.L. *J. Opt. Soc. Am.* 1966, *56*, 978.

9. Filler, A.S. *J. Opt. Soc. Am.* 1964, *54*, 762.

10. Baker, L.C.W. "Advances in the Chemistry of Heteropoly Electrolytes and Their Pertinence for Coordination Chemistry", in *Advances in the Chemistry of the Coordination Compounds*; Kirschner, S., Ed., 604, Mac Millan: NY, 1961.

11. Pope, M.T. *Heteropoly and Isopoly Oxometallates*; Springer-Verlag: Berlin. 1983.

12. Tsigdinos, G.A. "Heteropoly Compounds of Molybdenum and Tungsten", in *Topics in Current Chemistry- Aspects of Mo and related chemistry*; Dewar, M.J.S., Eds., Vol. 76, 4, Springer-Verlag: Berlin, 1978.

13. Pope, M.T. "Isopolyanions and Heteropolyanions", in *Comprehensive Coordination Chemistry- the syntheses, reaction, properties, and applications of coordination compounds*; Wilkinson, G., Ed., 1st ed., Vol. 3, 1023, Pergamon: Oxford, 1987.

14. Pauling, L.C. *J. Am. Chem. Soc.*, 1929, *51*, 2868.

15. Keggin, J.F., *Nature*, 1933, *131*, 908.

16. Keggin, J.F. *Proc. Roy. Soc. (London)*, 1934, *A144*, 75.

17. Illingworth, J.W.; J.F. Keggin *J. Chem. Soc.*, 1935, 575.

18. Kepert, D.L. "Isopolyanions and Heteropolyanions", in *Comprehensive Inorganic Chemistry*; J.C. Bailars, Jr., et al., Eds., Vol,4, 607, Pergamon: NY, 1973.

19. Weakley, T.J.R. "Some Aspects of the Heteropolytungstates and Heteropolymolybdates", in *Structure and Bonding- Large Molecules;* J.D. Dunitz et al., Eds., Vol. 18, 131, Springer-Verlag: Berlin, 1974.

20. Landis, A.M. Doctoral Dissertation, Georgetown University, 1977.

21. Alpert, N.L. et al. *IR Theory and Practice of Infrared Spectroscopy*; 2nd ed., Plenum: NY, 1970.

22. Spitsyn, V.I. et al. *Soviet Scientific Rev. B. Chemistry.*, 1981, *3*, 111.

23. Backer, P.A.; L.V. Natarajan *J. Chem. Ed.*, 1979, *56*, 642.

24. Rocchiccioli-Deltcheff, C.; M.R. Thouvenot *J. Chem. Res. (S)* 1977, 46.

25. Figgis, J.S.F. Doctoral Dissertation, Georgetown University, 1970.

26. Ross, S.D. *Inorganic Infrared and Raman Spectra*; McGraw: London, 1972.

27. Decius, J.C. *J. Chem. Phys.*, 1948, *16*, 1025.

28. Yurchenko, E.N. *J. Mol. Struct.* 1980, *60*, 325.

29. Nomenclature in inorganic chemistry, in: *J. Am. Chem. Soc.*, 1980, *82 (Part. 4)*, 5523.

30. Zaidi, S.H.K. M.S. Thesis, Emporia State University, 1989.

31. Smith, A.L. "Infrared Spectroscopy", Chapter 5, *Treatise on Analytical Chemistry*; 2nd ed., P.J. Elving, E.J. Meehan and I.M. Kolthoff, Eds., Part 1, Vol. 7, Willey: NY, 1981.

32. Conley, R.T. *Infrared Spectroscopy*; 2nd ed., Allyn & Bacon: MA, 1972.

33. Croea, A.D. *Practical Infrared Spectroscopy*; 2nd ed., Butterworthe: London, 1964.

34. Potts, J.R. *Chemical Spectroscopy*; Vol. 1, Willey: NY, 1963.

35. Washburn, E.W. et al., Eds., *International Critical Tables of Numerical Data, Physics, Chemistry and Technology*, Vol. 3, 27, Mc Graw: NY, 1928.

36. Kazanskii, L.P. *Bull. Acad. Sci., USSR, Div. Chem. Sci.* 1975, 432.

37. Sharplese, N.E.; J.S. Hundey *Anal. Chem.*, 1957, *29*, 1619.

38. Brown, D.H. *Spectrochim. Acta* 1963, *19*, 585.

39. Lenge, G. et al. *Z. Naturforsch., B:* 1969, *24*, 1498.

40. Yurchenko, E.N.; V.I. Bugaev *J. Mol. Struct.* 1984, *115*, 71.

41. Ingle, J.D. Jr.; S.P. Crouch *Spectrochemical Analysis*; Prentice-Hall: NJ, 1988.

42. Pouchert, C.J., *Ed.*, *The Aldrich Library of Infrared Spectra*, 3rd ed., Vol. 2, Aldrich Chemical Company, Milwaukee, WI, 1985.

43. Nyquist, R.A.; R.O. Kagel *Infrared Spectra of Inorganic Compounds*; Academic: NY, 1971.

44. Rocchiccioli-Deltcheff, C. et al. *Spectrochim Acta* 1976 *32A*, 587.

45. Rocchiccioli-Deltcheff, C.; M.R. Thouvenot *Spectrosc. Letters*, 1979, *12(2)*, 127.

46. Thouvenot, M.R. et al. *C.R. Acad. Sc. Paris, t. 278 C*, 455.

47. Rocchiccioli-Deltcheff, C.; M.R. Thouvenot *C.R. Acad. Sc. Paris, t. 278 C*, 1974, 857.

APPENDIX A - FIGURES

FIGURE 1.

Structural Arrangement

of

Silicon and Tungsten Atoms

in

Keggin Structure

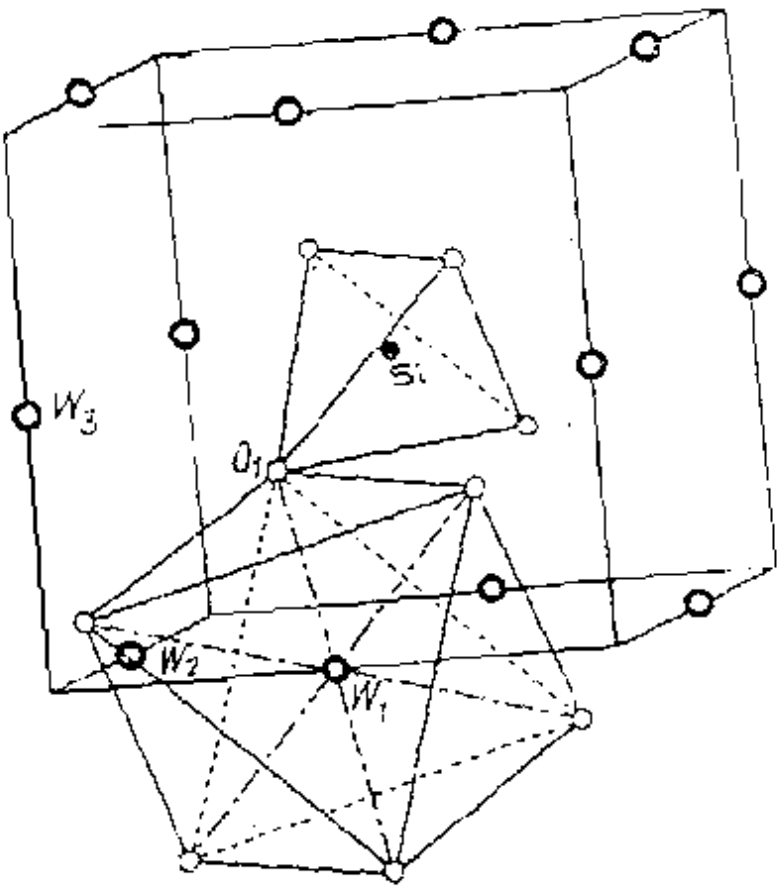
W3
O1
Si
W2
W1

FIGURE 2.

Relative Position

of

One WaO_3 Unit

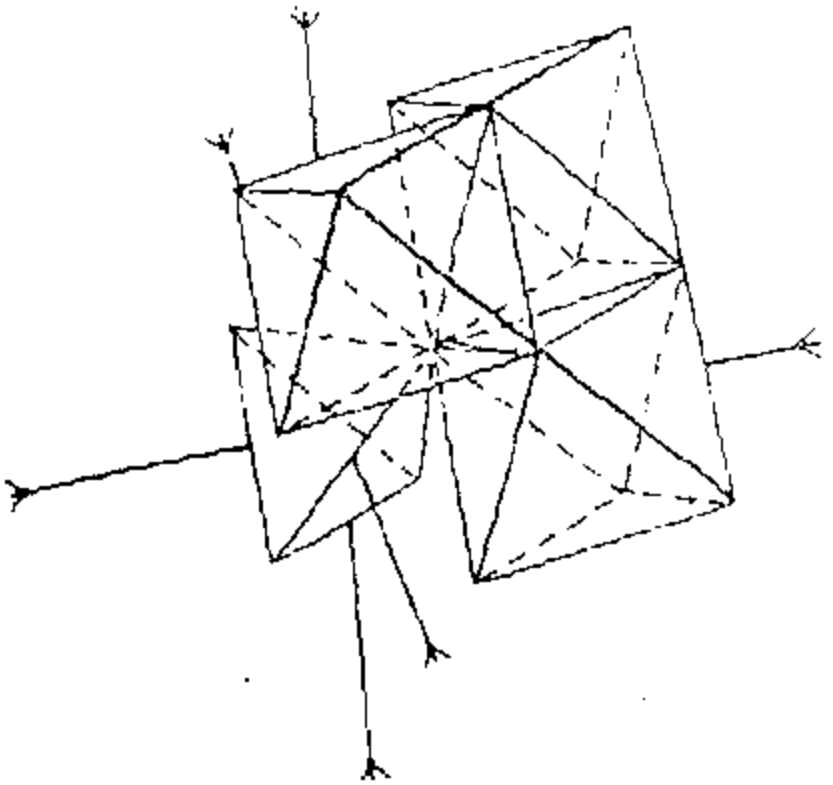

FIGURE 3.

Relative Position

of

Two WO_3 Units

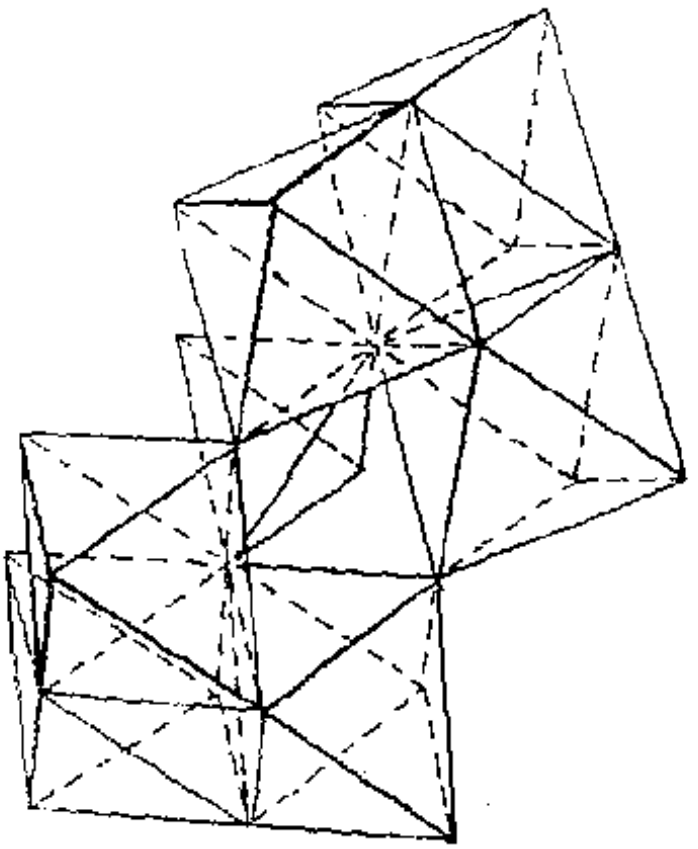

FIGURE 4.

Complete Keggin Structure

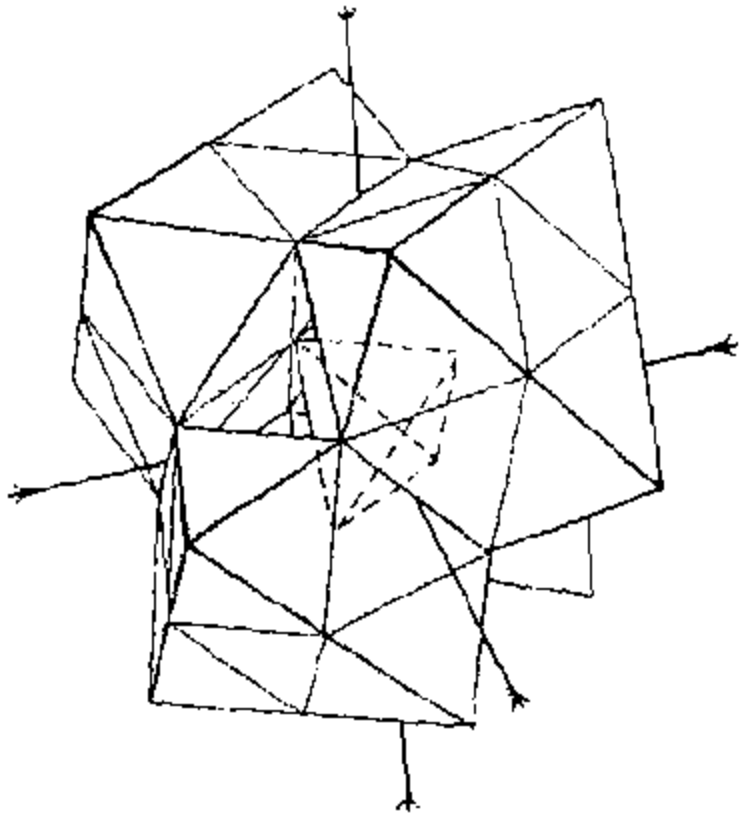

FIGURE 5.

Two Spectra

of

Dihydrogen Compounds

NaW6+H2 and KCo3+H2

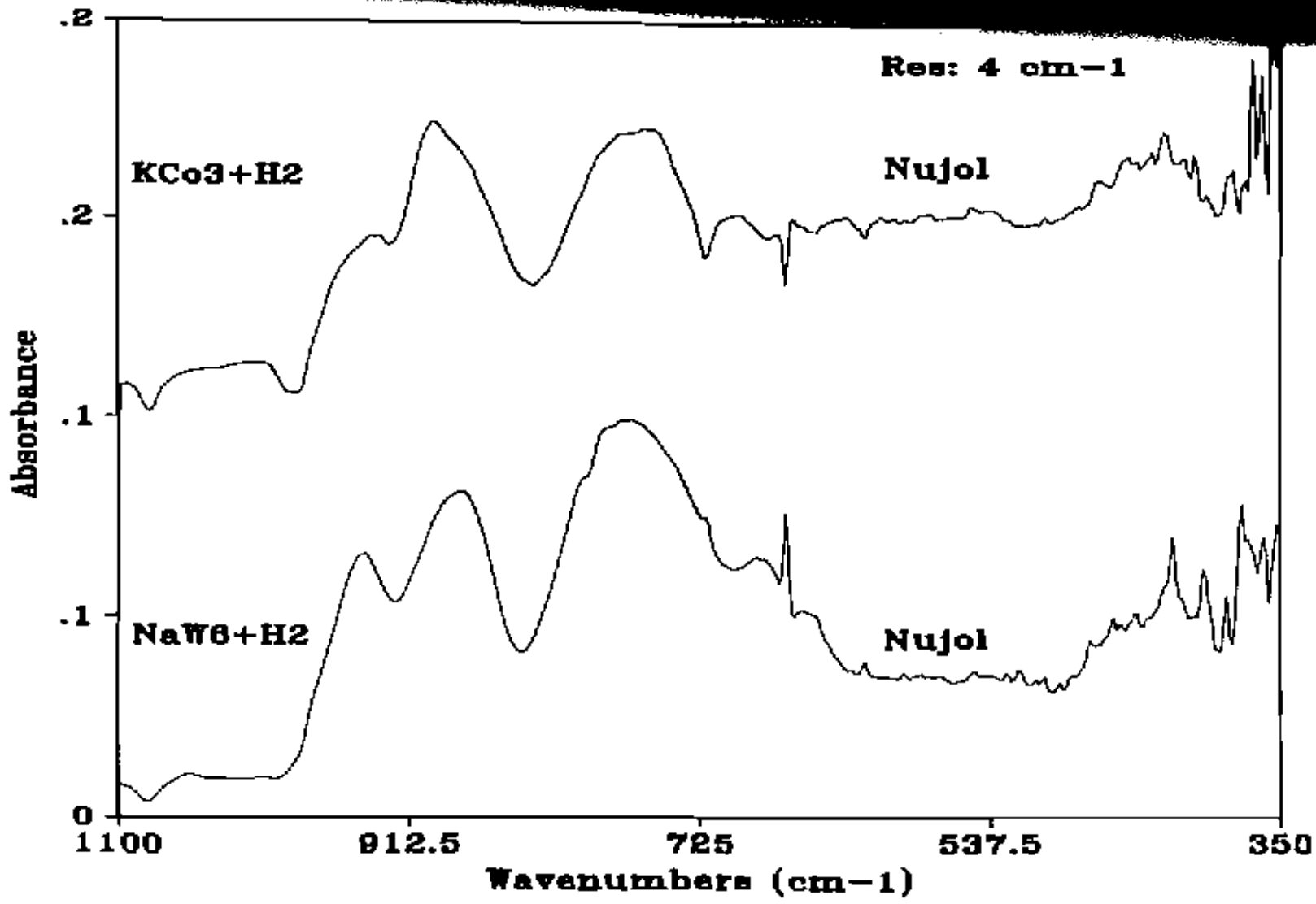
.2
.2
.1
.1
0
Absorbance
Res: 4 cm-1
KCo3+H2
Nujol
NaW6+H2
Nujol
1100
912.5
725
537.5
350
Wavenumbers (cm-1)

FIGURE 6.

Two Spectra

of

Phosphorous Compounds

HW6+P and KCo2+P

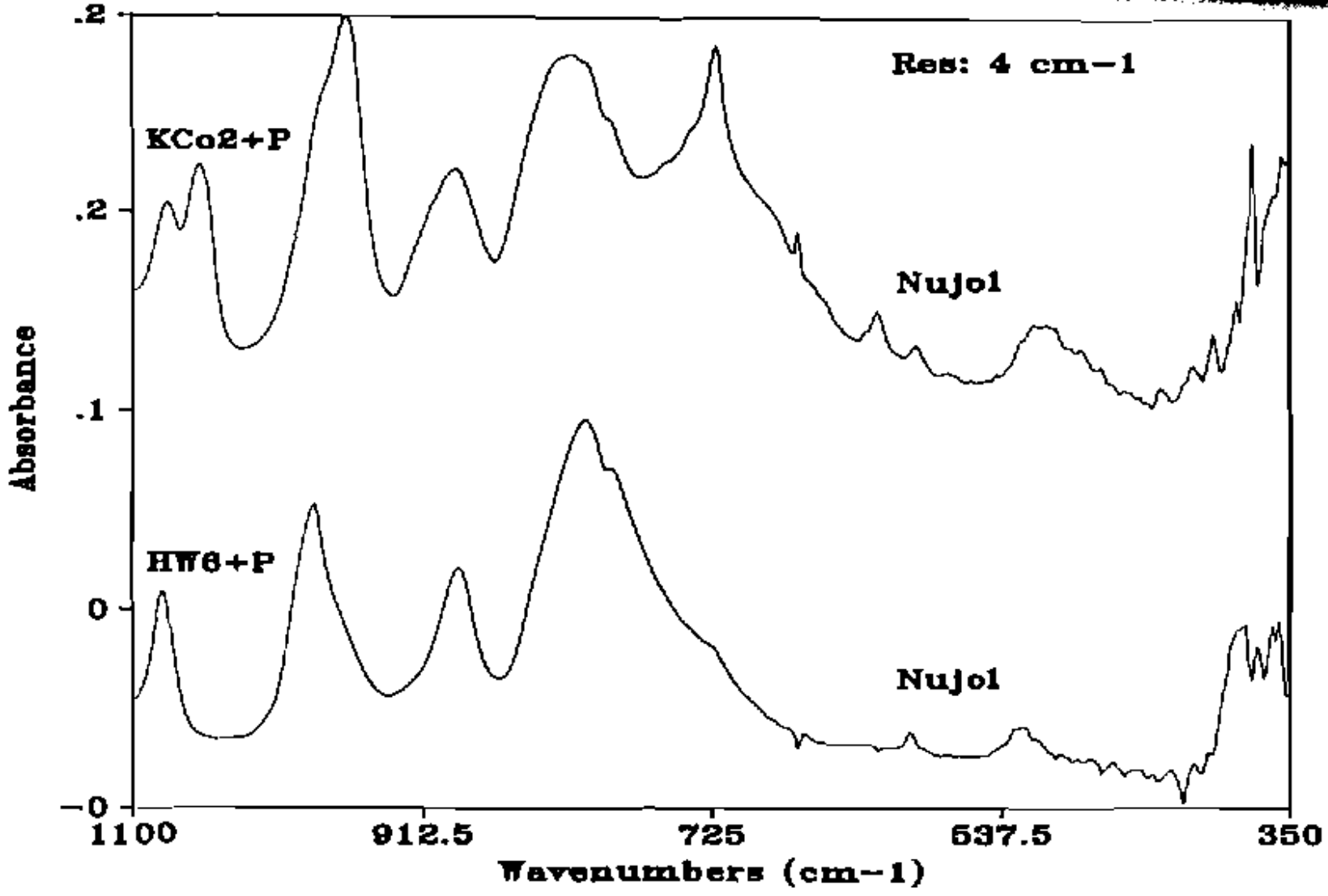
.2
.2
.1
0
−0
Absorbance
KCo2+P
Res: 4 cm−1
Nujol
HW6+P
Nujol
1100
912.5
725
537.5
350
Wavenumbers (cm−1)

FIGURE 7.

Three Spectra

of

Boron Compounds

KCo3+B and AmCo3+B

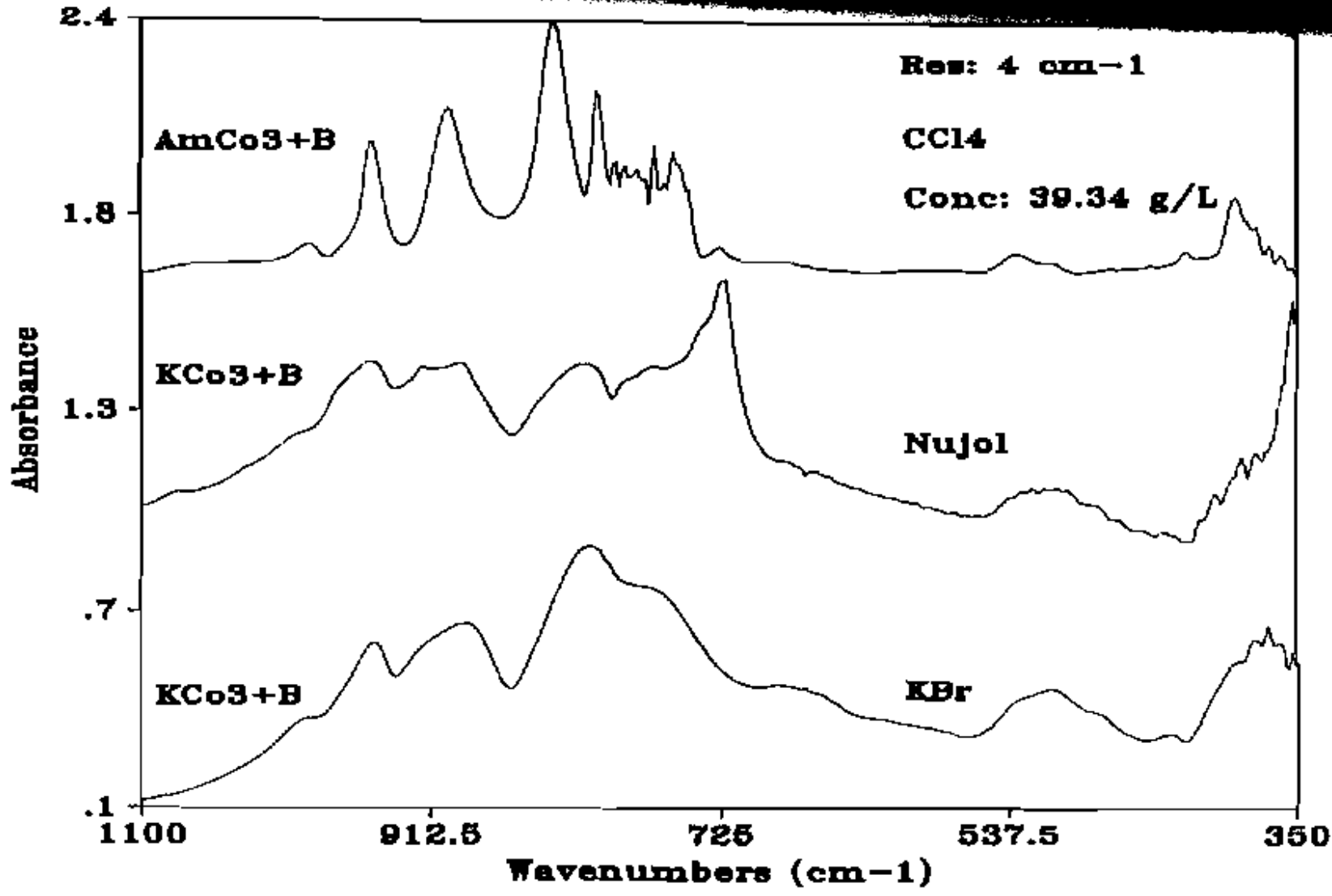
2.4
1.8
1.3
.7
.1
Absorbance
AmCo3+B
KCo3+B
KCo3+B
Res: 4 cm-1
CCl4
Conc: 39.34 g/L
Nujol
KBr
1100
912.5
725
537.5
350
Wavenumbers (cm-1)

FIGURE 8.

Three Spectra

of

KCo2+Si

in

Different Dispersive Media

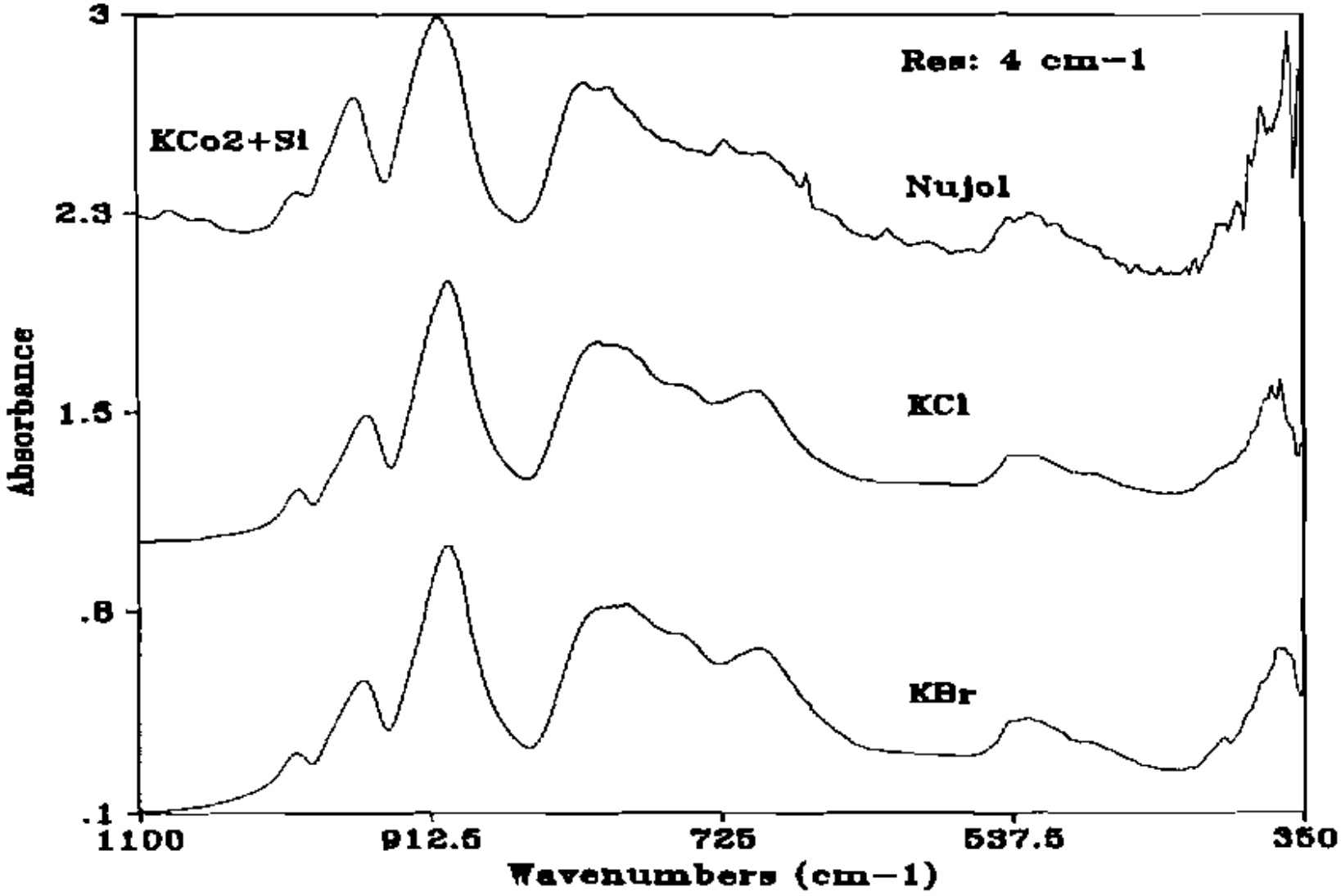
Res: 4 cm-1
KCo2+Si
Nujol
KCl
KBr
Absorbance
3
2.3
1.5
.8
.1
1100
912.5
725
537.5
350
Wavenumbers (cm-1)

FIGURE 9.

Two Spectra

of

Zinc Compounds

KCo2+Zn and AmCo3+Zn

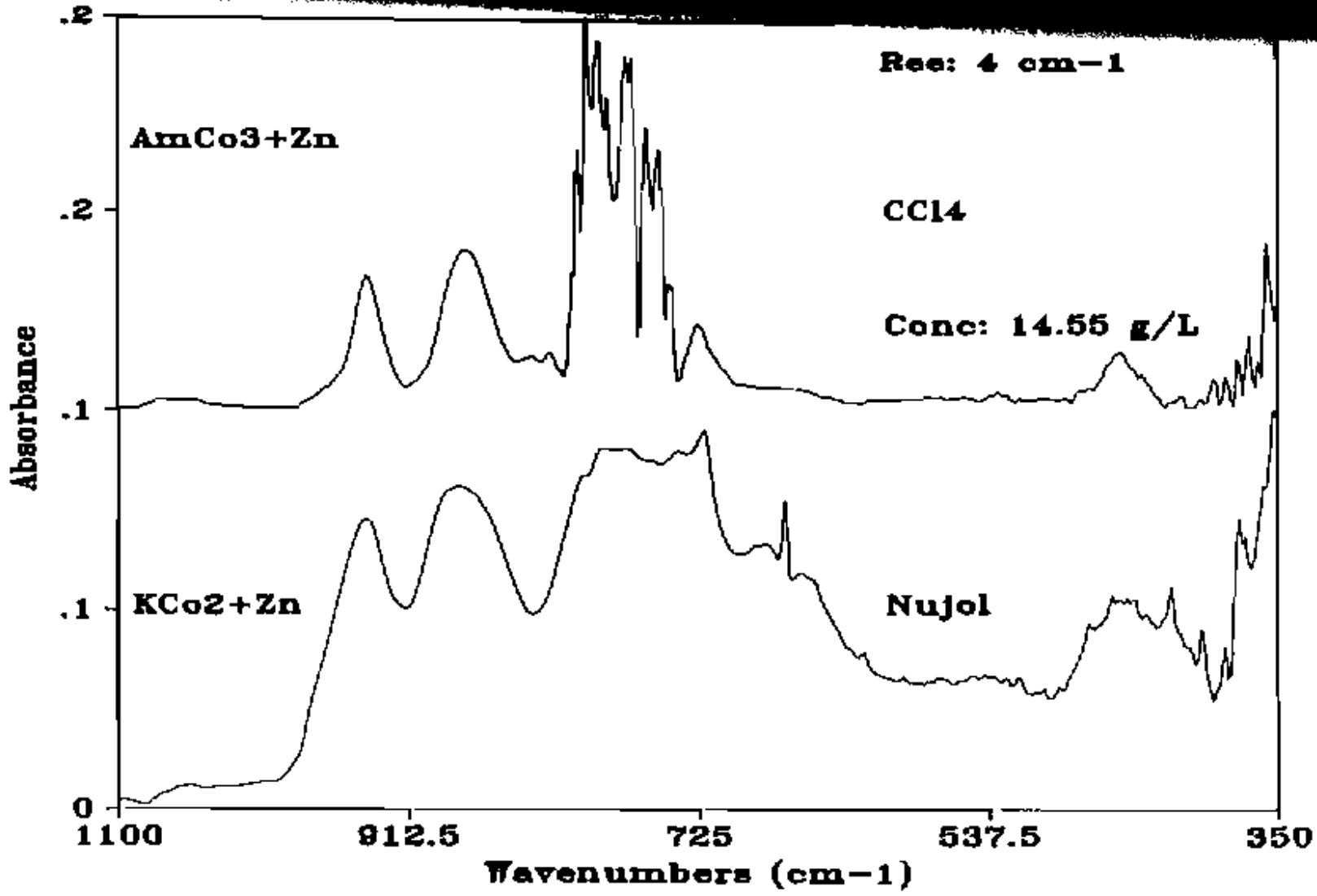
.2
.2
.1
.1
0
Absorbance
AmCo3+Zn
KCo2+Zn
Res: 4 cm-1
CCl4
Conc: 14.55 g/L
Nujol
1100
912.5
725
537.5
350
Wavenumbers (cm-1)

FIGURE 10.

Three spectra

of

Gallium Compounds

$NaCo_3+Ga$ and $AmCo_3+Ga$

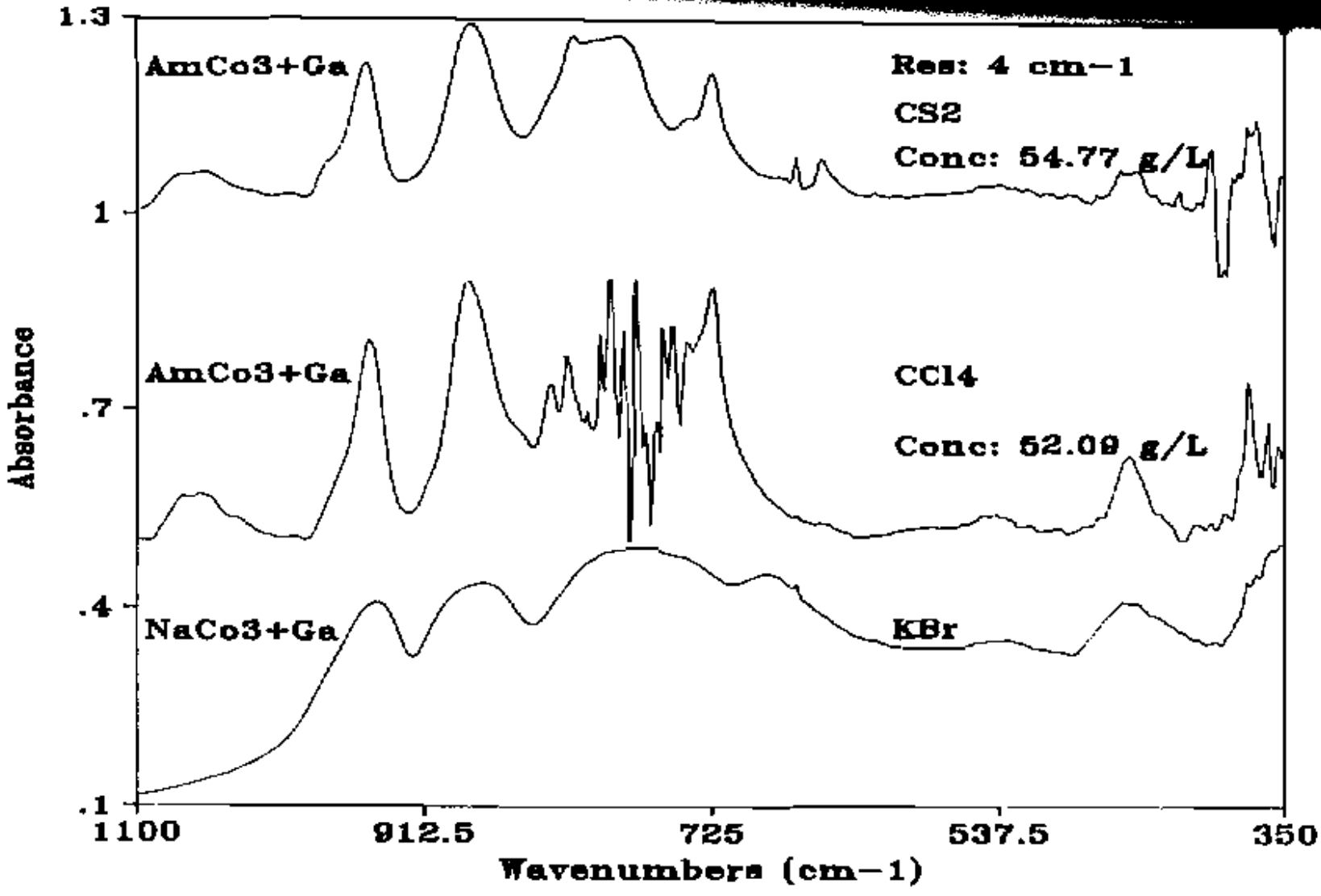
1.3
1
.7
.4
.1
Absorbance
AmCo3+Ga
Res: 4 cm-1
CS2
Conc: 54.77 g/L
AmCo3+Ga
CCl4
Conc: 52.09 g/L
NaCo3+Ga
KBr
1100
912.5
725
537.5
350
Wavenumbers (cm-1)

FIGURE 11.

Two Spectra

of

Germanium Compounds

KCo_2Ge and $AmCo_2Ge$

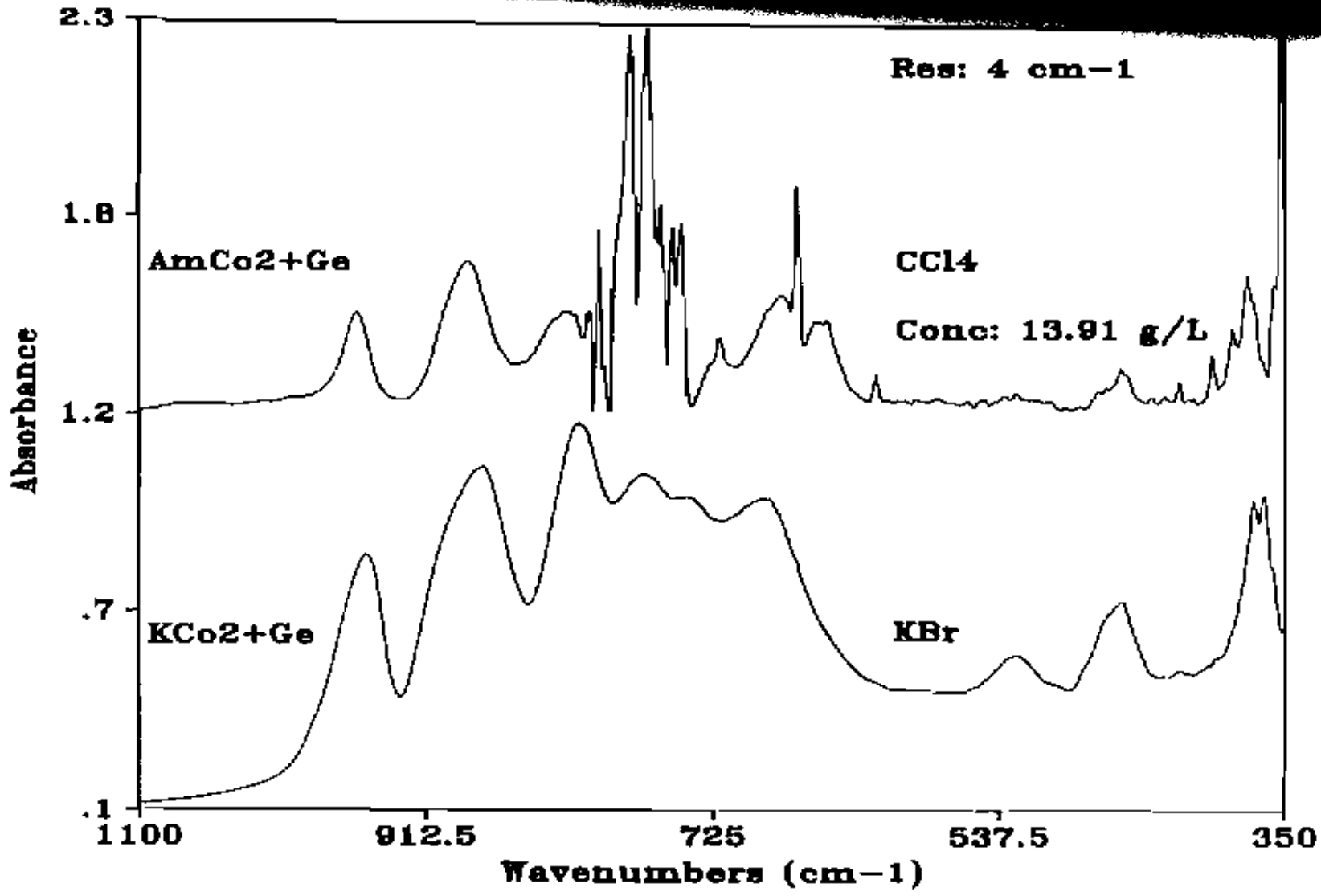
2.3
1.8
1.2
.7
.1
Absorbance
Res: 4 cm-1
AmCo2+Ge
CCl4
Conc: 13.91 g/L
KCo2+Ge
KBr
1100
912.5
725
537.5
350
Wavenumbers (cm-1)

FIGURE 12.

Two Spectra

of

Known KCo2+P and Unknown KCo2+P

Matched Using

Nujol Search Library

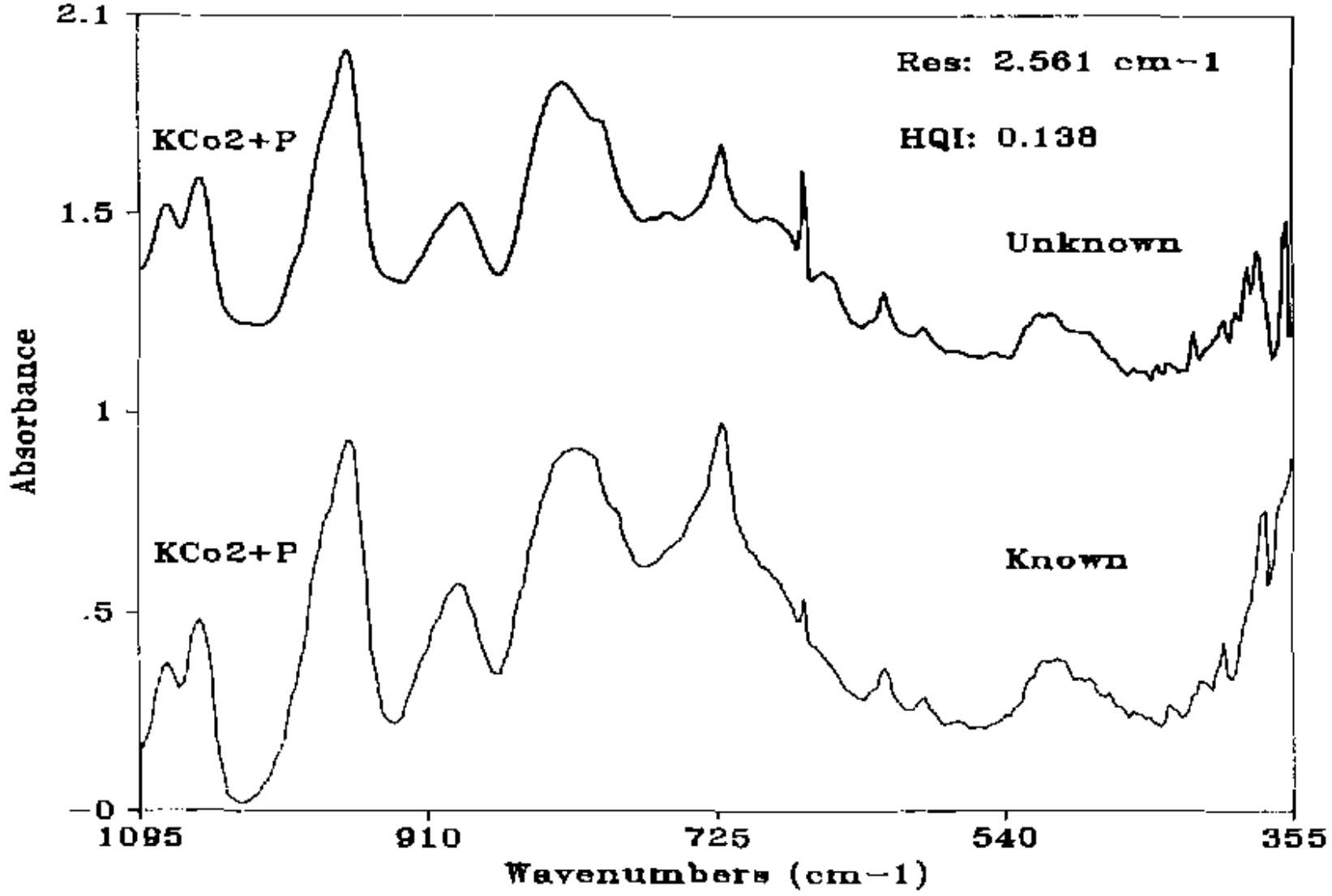
2.1
1.5
1
.5
0
Absorbance
KCo2+P
Res: 2.561 cm-1
HQI: 0.138
Unknown
KCo2+P
Known
1095
910
725
540
355
Wavenumbers (cm-1)

FIGURE 13.

Two Spectra

of

Known HW6+P and Unknown KCo2+P

Matched Using

Nujol Search Library

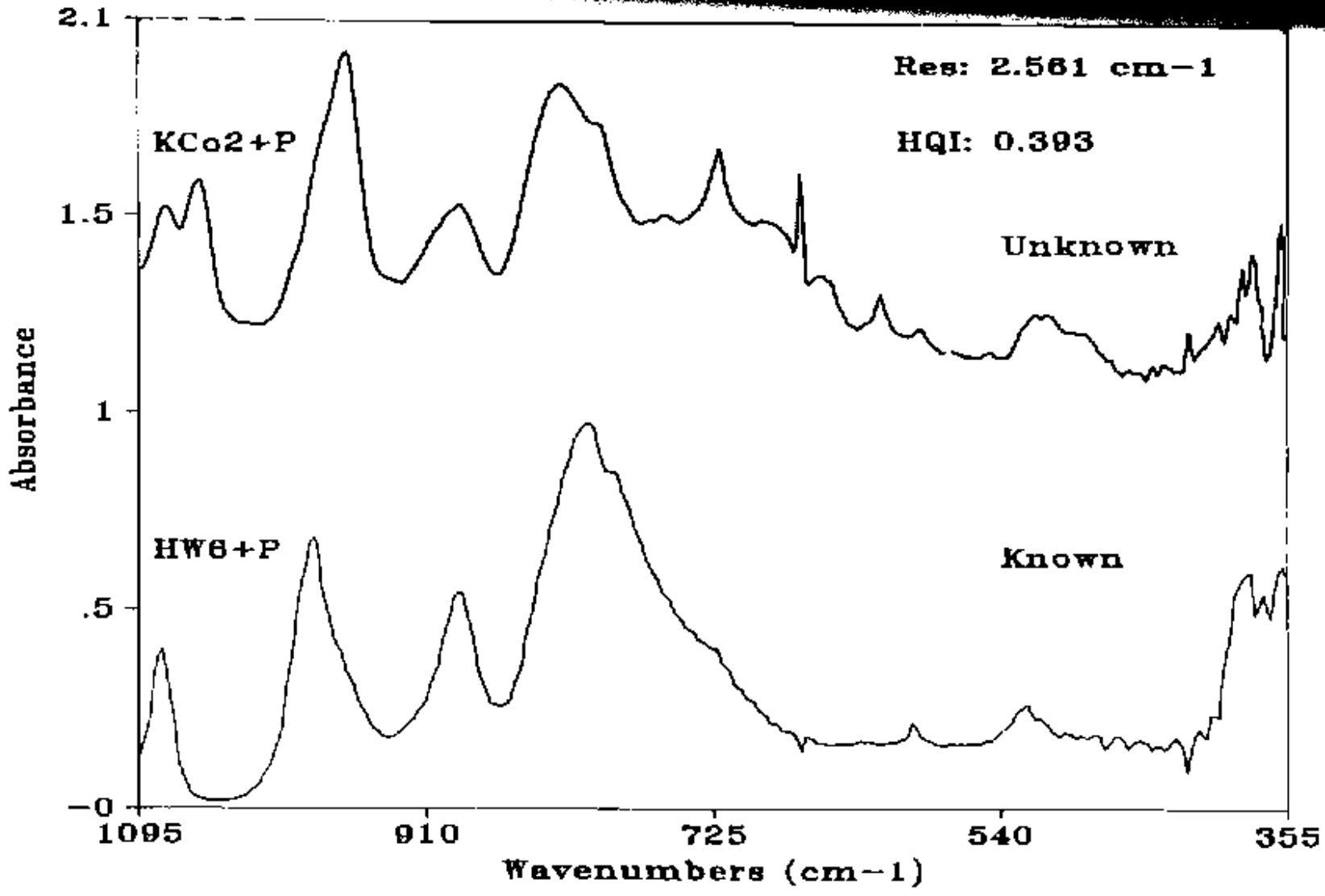
Res: 2.561 cm-1
HQI: 0.393
KCo2+P
Unknown
HW6+P
Known
Absorbance
2.1
1.5
1
.5
-0
1095
910
725
540
355
Wavenumbers (cm-1)

FIGURE 14.

Two Spectra

of

Known KCo2+Si and Unknown KCo2+Si

Matched Using

Nujol Search Library

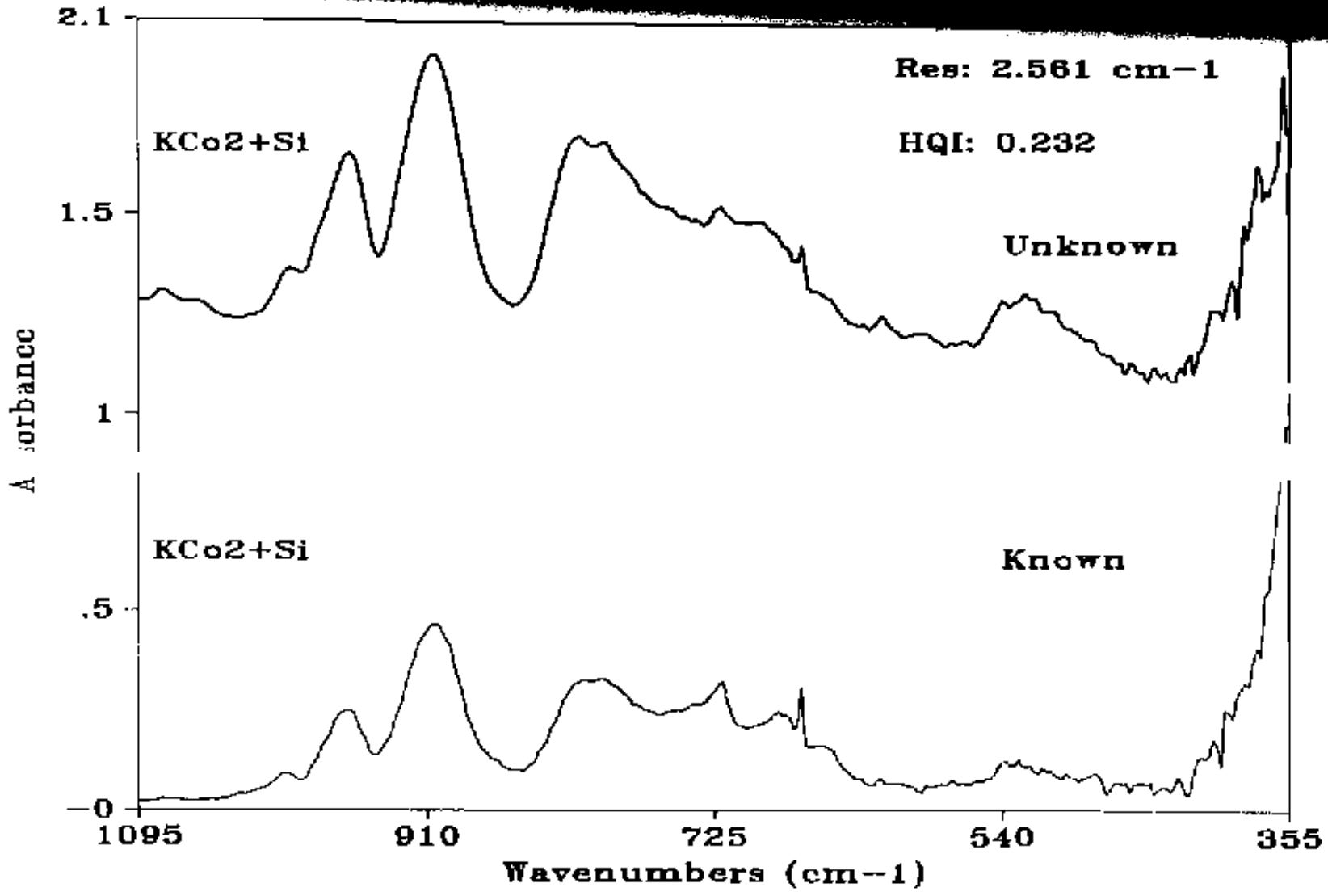
2.1
1.5
1
A orbance
KCo2+Si
Res: 2.561 cm-1
HQI: 0.232
Unknown
KCo2+Si
Known
.5
0
1095
910
725
540
355
Wavenumbers (cm-1)

FIGURE 15.

Two Spectra

of

Known KCo3+Bi and Unknown KCo2+Bi

Matched Using

Nujol Search Library

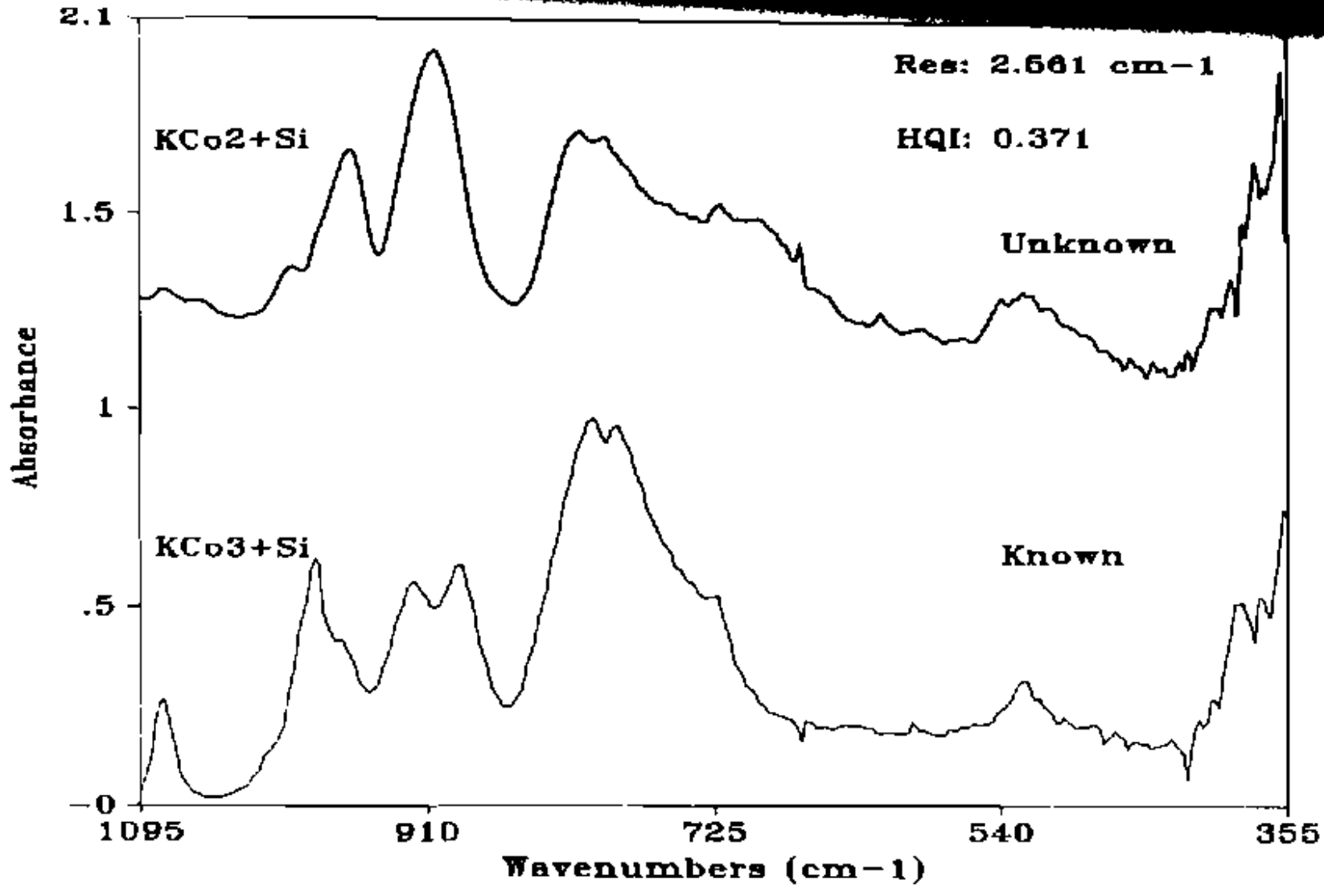
2.1
1.5
1
.5
0
Absorbance
Res: 2.661 cm-1
HQI: 0.371
KCo2+Si
Unknown
KCo3+Si
Known
1095
910
725
540
355
Wavenumbers (cm-1)

FIGURE 16.

Absorbance vs Concentration Plots

for

$AmCo(NO_3)_3$ in CCl_4

at

949 cm^{-1} and 901 cm^{-1}

Empty box : Data at 901 cm^{-1}

Filled box: Data at 949 cm^{-1}

First segment : 8.223 - 28.37 g/L

Second segment: 31.71 - 39.34 g/L

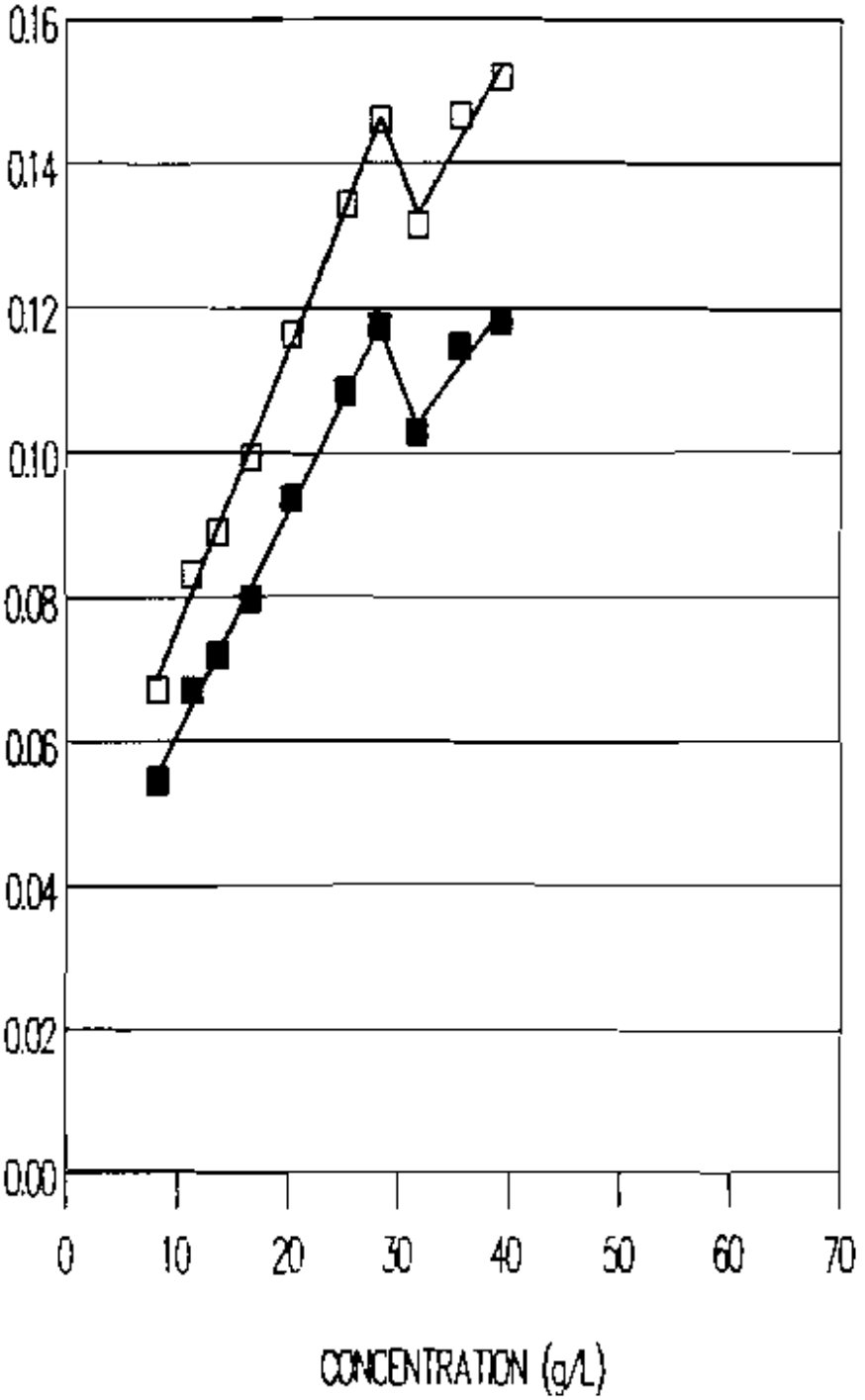
0.16
0.14
0.12
0.10
0.08
0.06
0.04
0.02
0.00
ABSORBANCE
0
10
20
30
40
50
60
70
CONCENTRATION (g/L)

FIGURE 17.

Absorbance vs Concentration Plots

for

$AmCo_2(SiO_4)_2$ in CCl_4

at

961 cm^{-1} and 909 cm^{-1}

Empty box : Data at 909 cm^{-1}

Filled box: Data at 961 cm^{-1}

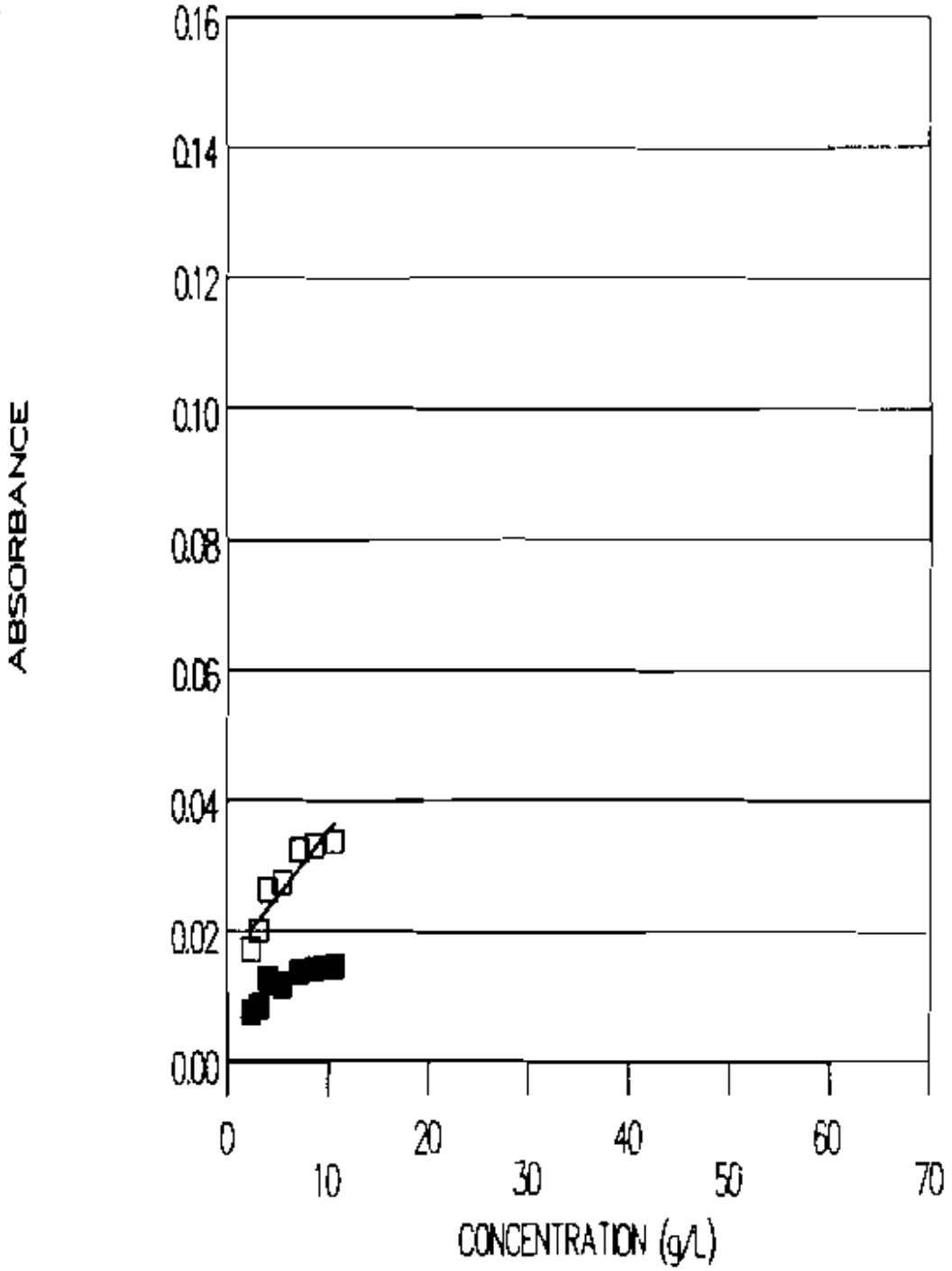
ABSORBANCE
0.16
0.14
0.12
0.10
0.08
0.06
0.04
0.02
0.00
0
10
20
30
40
50
60
70
CONCENTRATION (g/L)

FIGURE 18.

Absorbance vs Concentration Plots

for

$AmCo_3+Zn$ in CCl_4

at

939 cm^{-1} and 876 cm^{-1}

Empty box : Data at 876 cm^{-1}

Filled box: Data at 939 cm^{-1}

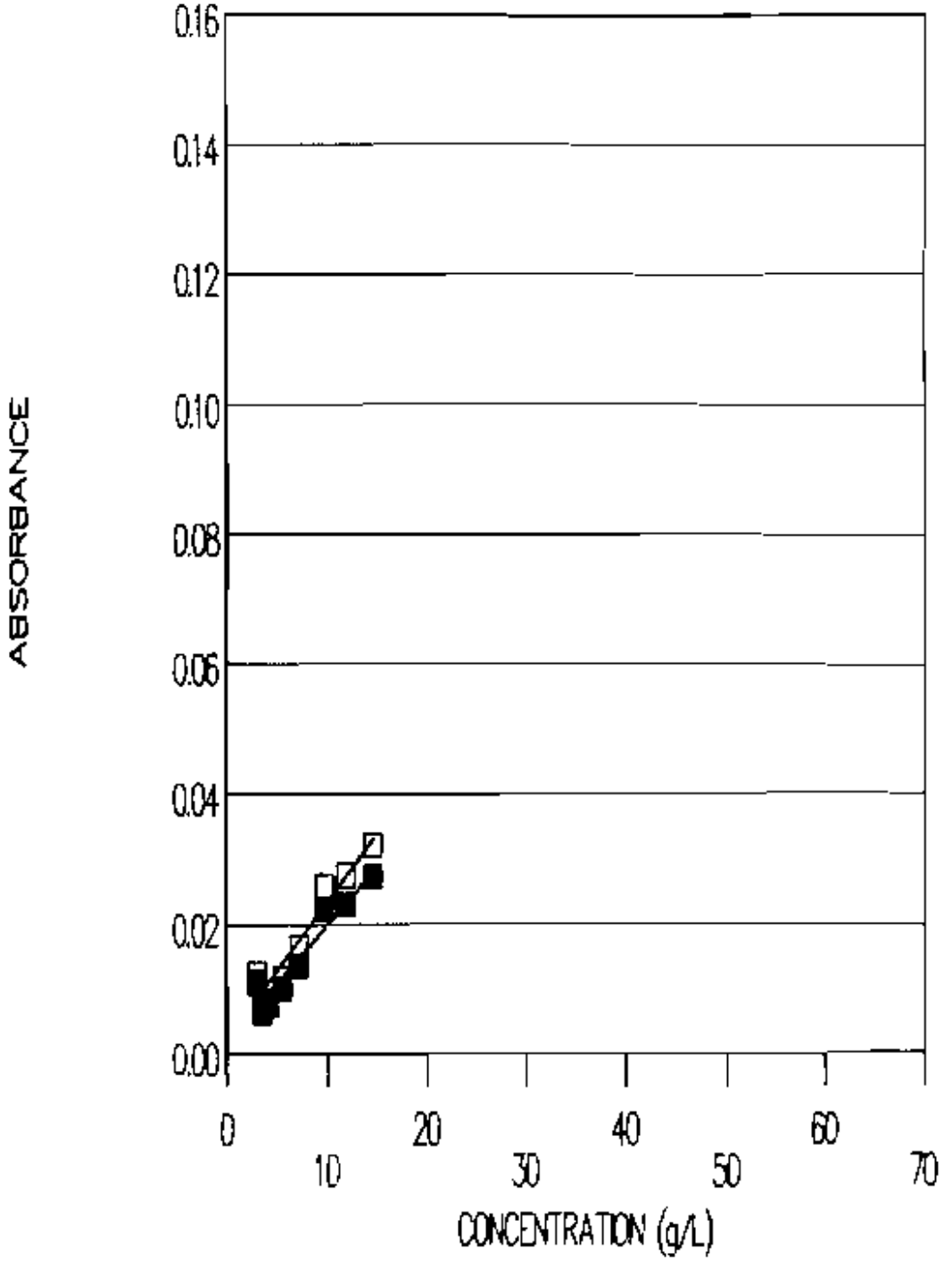
ABSORBANCE
0.16
0.14
0.12
0.10
0.08
0.06
0.04
0.02
0.00
0
10
20
30
40
50
60
70
CONCENTRATION (g/L)

FIGURE 19.

Absorbance vs Concentration Plots

for

$AmCo^{3+}Ga$ in CCl_4

at

947 cm^{-1} and 883 cm^{-1}

Empty box : Data at 883 cm^{-1}

Filled box: Data at 947 cm^{-1}

First segment : 7.449 - 29.86 g/L

Second segment: 29.86 - 45.62 g/L

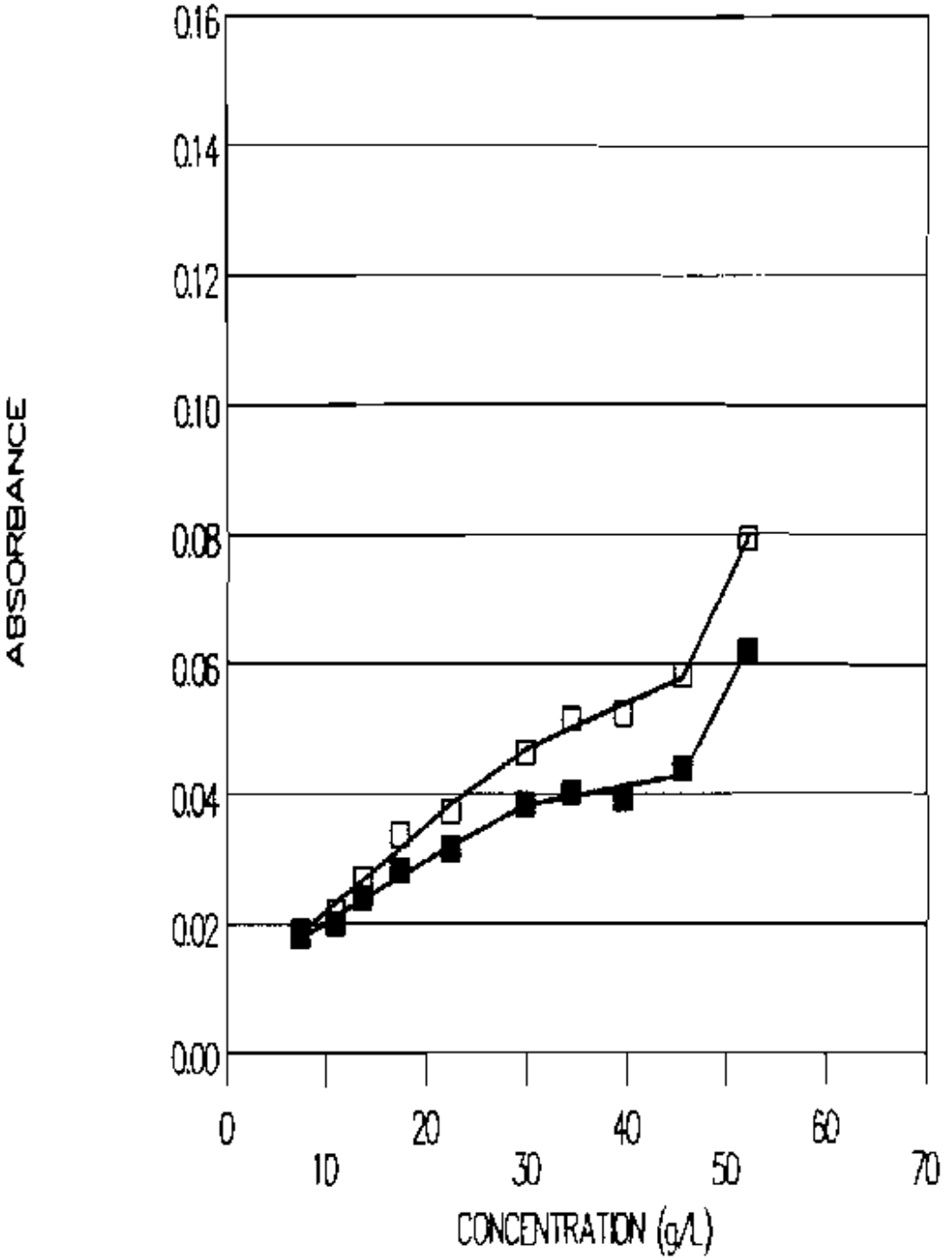
ABSORBANCE
0.16
0.14
0.12
0.10
0.08
0.06
0.04
0.02
0.00
0
10
20
30
40
50
60
70
CONCENTRATION (g/L)

FIGURE 20.

Absorbance vs Concentration Plots

for

$AmCo(CO_3)_3$+Ge in CS_2

at

949 cm^{-1} and 882 cm^{-1}

Empty box : Data at 882 cm^{-1}

Filled box: Data at 949 cm^{-1}

First segment : 1.665 - 16.59 g/L

Second segment: 16.59 - 42.40 g/L

Third segment : 42.40 - 54.77 g/L

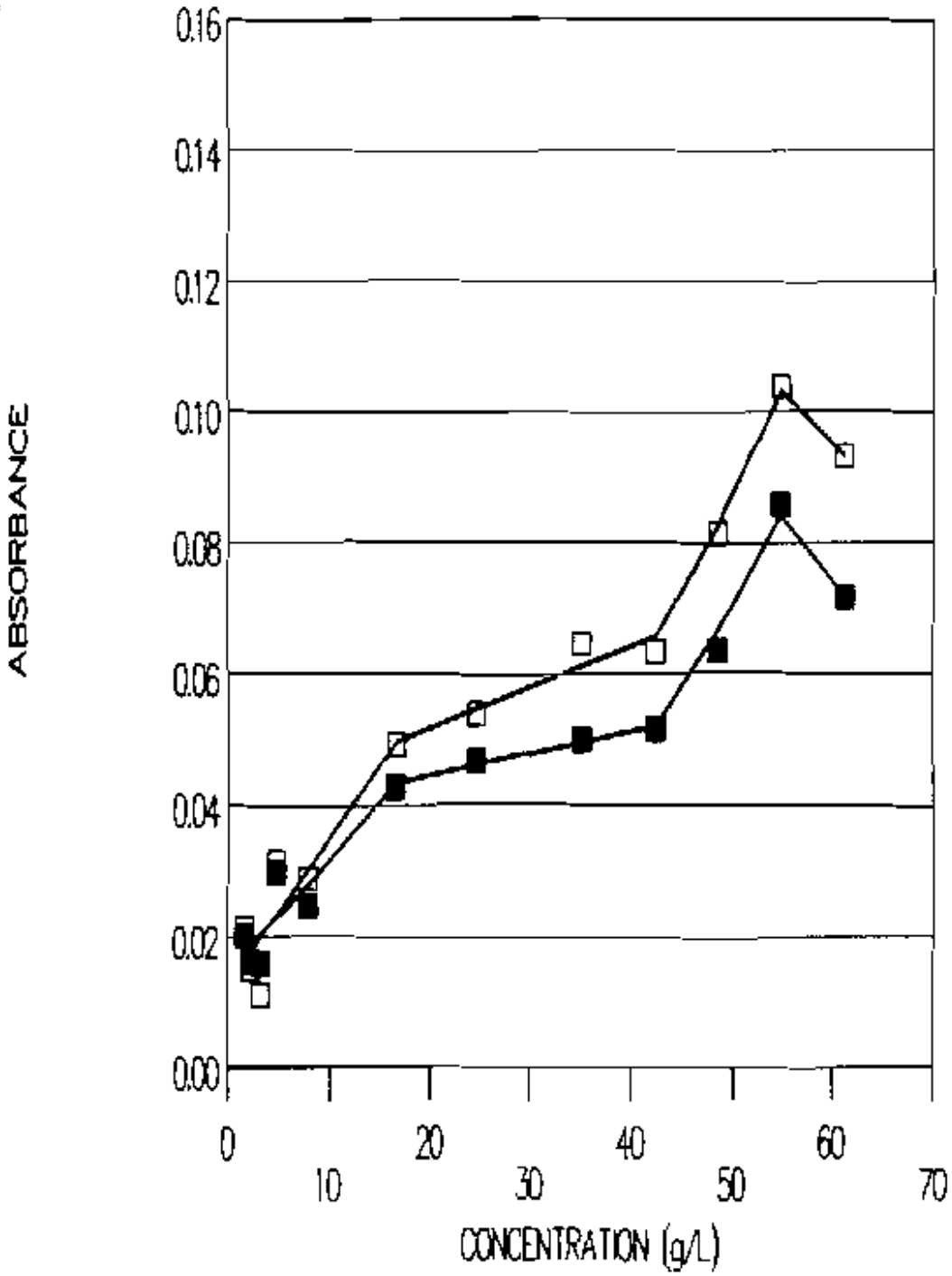
ABSORBANCE
0.16
0.14
0.12
0.10
0.08
0.06
0.04
0.02
0.00
0
10
20
30
40
50
60
70
CONCENTRATION (g/L)

FIGURE 21.

Absorbance vs Concentration Plots

for

$AmCo_2$+Ge in CCl_4

at

957 cm^{-1} and 885 cm^{-1}

Empty box : Data at 885 cm^{-1}

Filled box: Data at 957 cm^{-1}

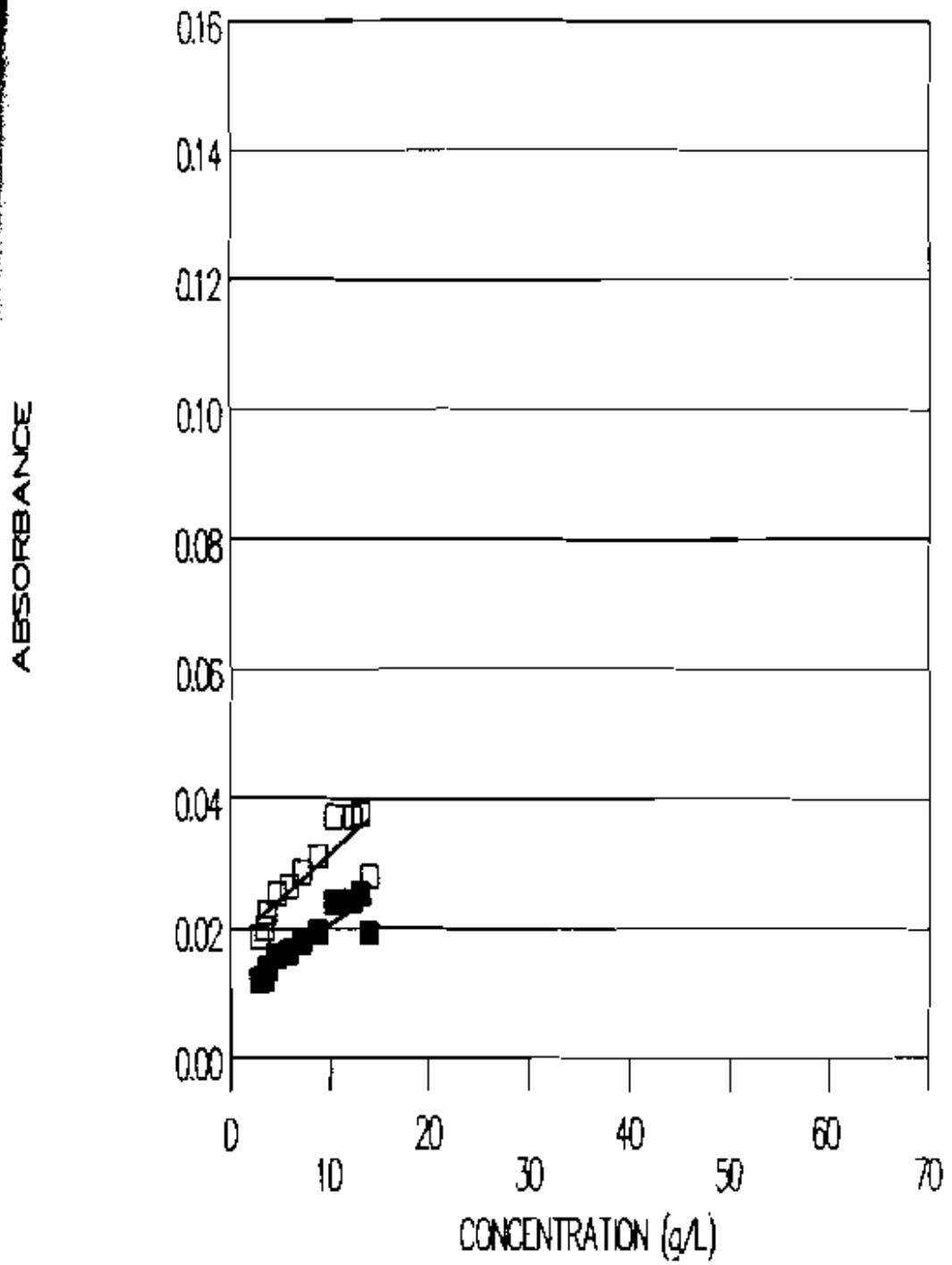
ABSORBANCE
0.16
0.14
0.12
0.10
0.08
0.06
0.04
0.02
0.00
0
10
20
30
40
50
60
70
CONCENTRATION (g/L)

FIGURE 22.

Absorbance vs Concentration Plots

for

Tripalmitin in CCl_4

at

1746 cm^{-1} for Technique Comparison

Empty box : Data for traditional weighing technique

Filled box: Data for new weighing technique

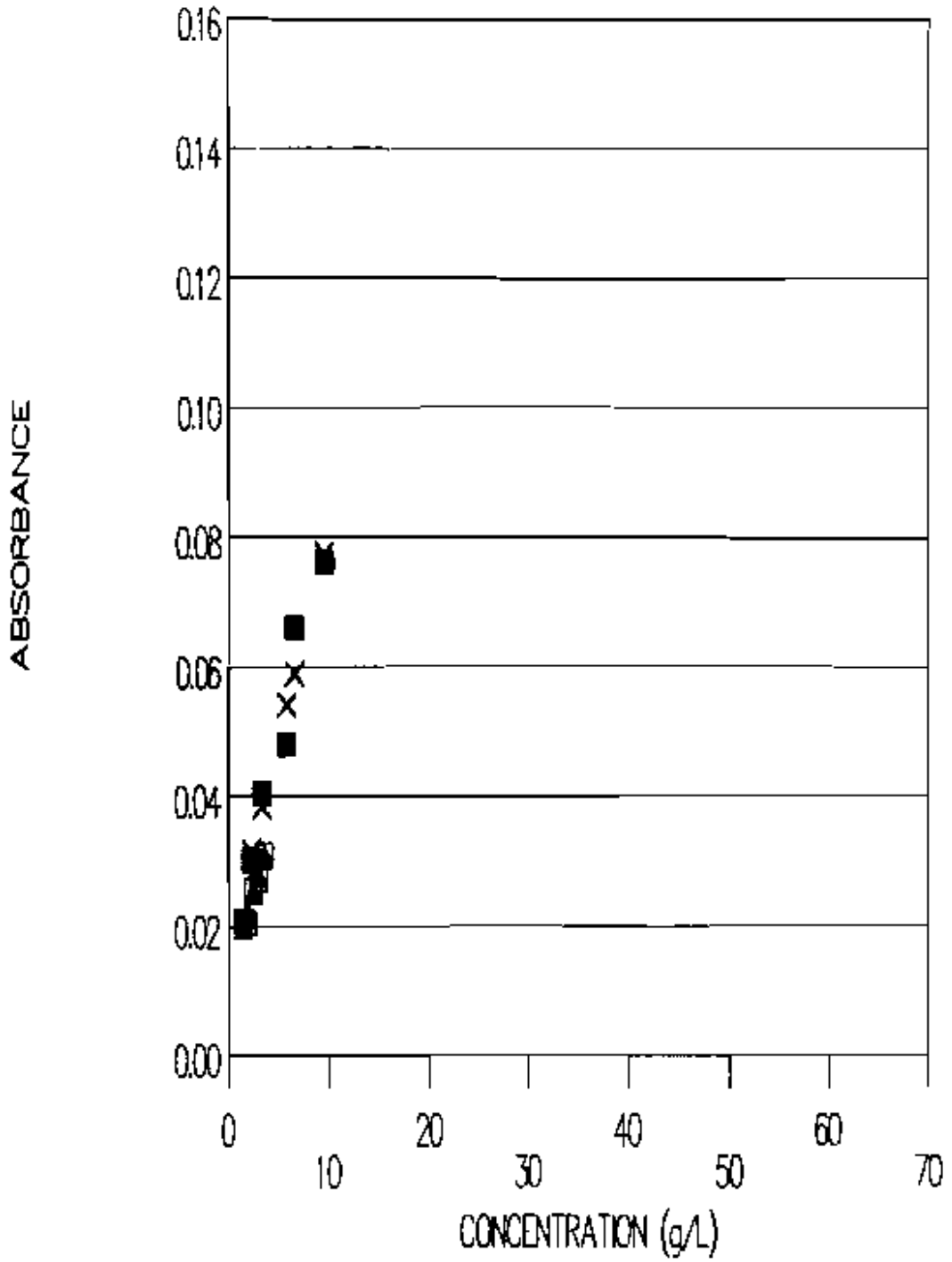
ABSORBANCE
0.16
0.14
0.12
0.10
0.08
0.06
0.04
0.02
0.00
0
10
20
30
40
50
60
70
CONCENTRATION (g/L)

FIGURE 23.

Two Plots

for

Second Highest Relative Absorbance Peak Position

vs

Concentration for

$AmCo3+B$ in CCl_4 and $AmCo3+Ga$ in CS_2

Triangle	: Peak positions for $AmCo3+Ga$
Filled boxes	: Peak positions for $AmCo3+Ga$
Empty boxes	: Peak positions for $AmCo3+Ga$
Empty boxes with cross	: Peak positions for $AmCo3+Ga$
Shaded crosses	: Peak positions for $AmCo3+B$

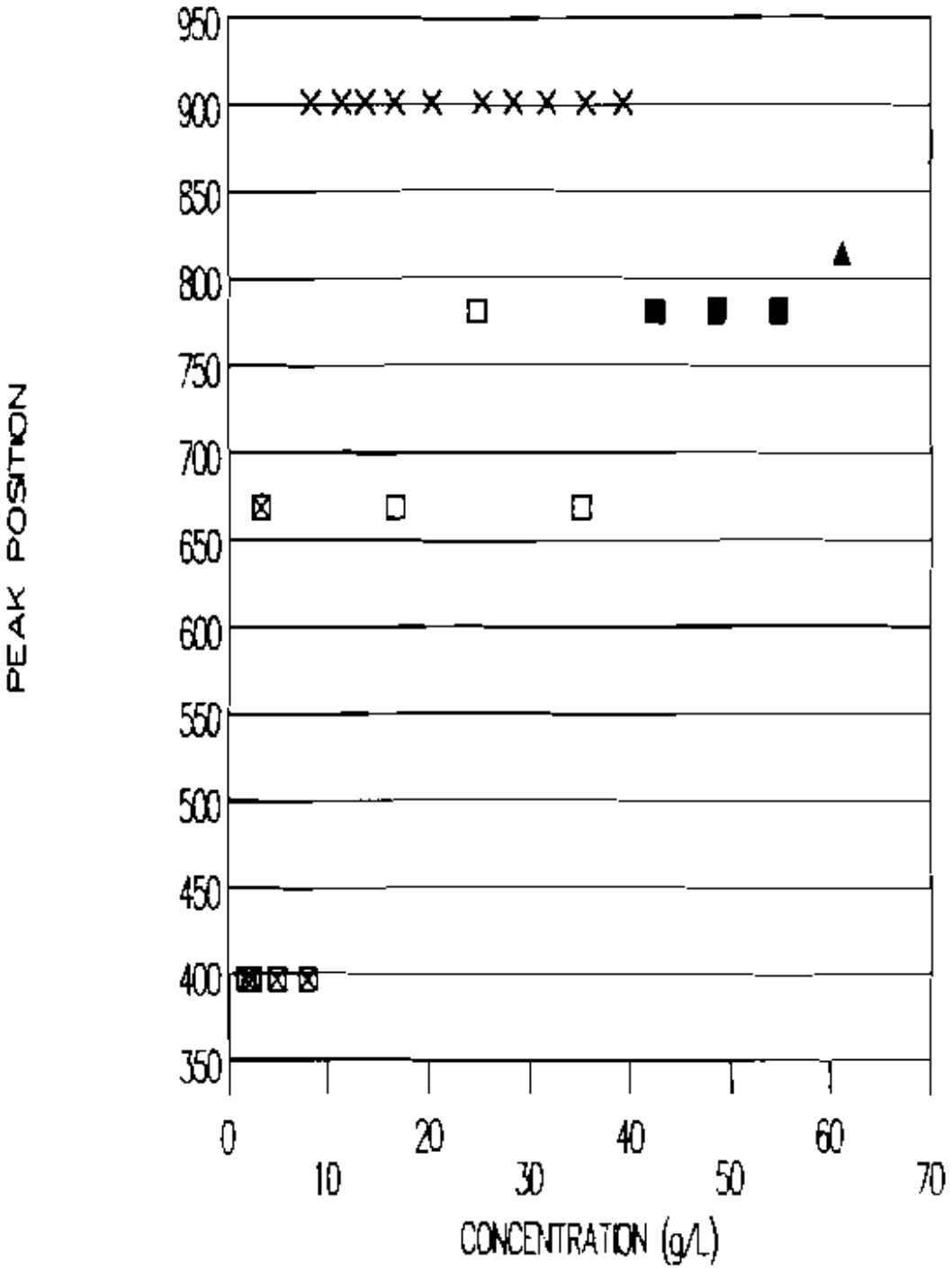
PEAK POSITION
950
900
850
800
750
700
650
600
550
500
450
400
350
0
10
20
30
40
50
60
70
CONCENTRATION (g/L)

FIGURE 24.

Three Spectra

of

$AmCo_2+Si$ in CCl_4

for

Nearly the Same Concentrations Collected

at

Three Different Times

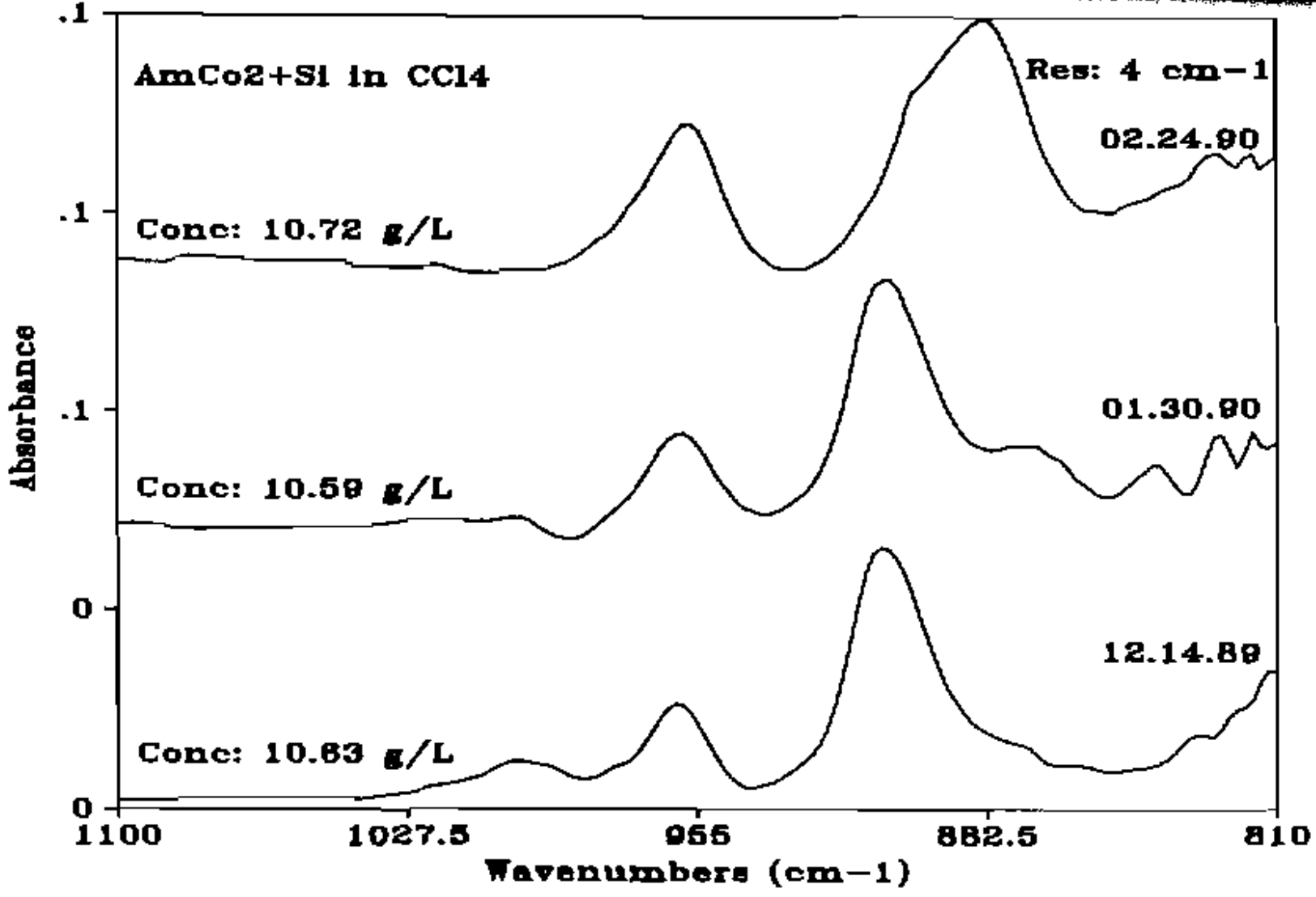
AmCo2+Si in CCl4
Res: 4 cm-1
02.24.90
Conc: 10.72 g/L
01.30.90
Conc: 10.59 g/L
12.14.89
Conc: 10.63 g/L
Absorbance
.1
.1
.1
0
0
1100
1027.5
955
882.5
810
Wavenumbers (cm-1)

APPENDIX B - TABLES

Table I

Peak Table
for
NaW6+H2 Spectrum
in
Nujol

Peak Sensitivity Factor: 20

Peak cm-1	Absorbance	Relative Absorbance
1055	0.027	0.240
941	0.086	0.764
880	0.102	0.843
775	0.121	0.998
770	0.122	1.000
721	0.095	0.786
683	0.084	0.693
669	0.096	0.792
658	0.070	0.580
473	0.062	0.513
457	0.068	0.563
419	0.090	0.742
399	0.082	0.672
384	0.074	0.611
374	0.099	0.812
370	0.090	0.736
361	0.090	0.742

Table 11

Peak Table
for
KCo3+H2 Spectrum
in
Nujol

Peak Sensitivity Factor: 20

Peak cm-1	Absorbance	Relative Absorbance
1044	0.002	0.033
1009	0.002	0.046
937	0.017	0.332
932	0.017	0.332
897	0.030	0.582
775	0.028	0.555
752	0.029	0.562
702	0.019	0.373
698	0.019	0.374
673	0.017	0.329
665	0.019	0.364
631	0.019	0.370
608	0.019	0.369
550	0.020	0.393
536	0.020	0.385
486	0.020	0.380
467	0.023	0.450
448	0.026	0.503
432	0.026	0.511
424	0.029	0.556
411	0.026	0.499
405	0.026	0.505
397	0.021	0.416
380	0.024	0.473
372	0.023	0.449
366	0.037	0.724
361	0.035	0.687
353	0.051	1.000

Table III

Peak Table
for
HW6+P Spectrum
in
Nujol

Peak Sensitivity Factor: 20

Peak cm-1	Absorbance	Relative Absorbance
1080	0.052	0.509
982	0.078	0.760
889	0.059	0.575
806	0.102	1.000
791	0.088	0.859
665	0.011	0.106
596	0.011	0.110
529	0.012	0.121
523	0.013	0.127
515	0.009	0.090
478	0.003	0.033
465	0.003	0.025
413	0.002	0.017
403	0.005	0.049
384	0.041	0.401
378	0.042	0.413
370	0.036	0.351
361	0.042	0.410
357	0.043	0.422

Table IV

Peak Table
for
KCo2+P Spectrum
in
Nujol

Peak Sensitivity Factor: 20

Peak cm⁻¹	Absorbance	Relative Absorbance
1078	0.047	0.590
1057	0.053	0.674
961	0.079	1.000
889	0.053	0.666
816	0.072	0.916
721	0.074	0.935
669	0.041	0.523
617	0.028	0.354
597	0.022	0.281
517	0.025	0.321
502	0.025	0.316
486	0.021	0.270
473	0.018	0.231
434	0.015	0.188
413	0.019	0.236
399	0.024	0.302
384	0.029	0.371
374	0.057	0.719
361	0.048	0.601
355	0.055	0.692

Table V

Peak Table
for
KCo3+B Spectrum
in
KBr

Peak Sensitivity Factor: 20

Peak cm-1	Absorbance	Relative Absorbance
991	0.366	0.422
949	0.588	0.677
889	0.647	0.746
808	0.868	1.000
689	0.464	0.535
669	0.454	0.524
617	0.361	0.416
509	0.453	0.522
432	0.321	0.369
388	0.535	0.617
378	0.595	0.686
368	0.634	0.730
361	0.588	0.678
353	0.559	0.644

Table VI

Peak Table
for
KCo3+B Spectrum
in
Nujol

Peak Sensitivity Factor: 20

Peak cm-1	Absorbance	Relative Absorbance
1076	0.030	0.260
951	0.080	0.698
916	0.078	0.678
895	0.080	0.692
810	0.079	0.687
768	0.079	0.685
723	0.115	1.000
687	0.042	0.364
665	0.038	0.330
529	0.030	0.261
500	0.031	0.265
484	0.025	0.216
438	0.015	0.128
413	0.020	0.171
403	0.029	0.255
386	0.043	0.373
376	0.045	0.389
353	0.104	0.899

Table VII

Peak Table
for
AmCo3+6 Spectrum
in
CCl4

Concentration: 39.34 g/L

Peak Sensitivity Factor: 20

Peak cm-1	Absorbance	Relative Absorbance
1055	0.013	0.050
991	0.030	0.119
949	0.127	0.508
901	0.161	0.642
831	0.250	1.000
725	0.026	0.102
692	0.012	0.050
667	0.007	0.029
642	0.002	0.007
569	0.003	0.011
532	0.019	0.076
511	0.010	0.041
476	0.003	0.012
471	0.005	0.021
459	0.004	0.017
451	0.005	0.021
444	0.007	0.028
422	0.020	0.081
390	0.071	0.285
376	0.044	0.177
368	0.025	0.101
361	0.017	0.066
353	0.004	0.018

Table VII1

Peak Table
for
KCo2+5i Spectrum
in
KBr

Peak Sensitivity Factor: 20

Peak cm-1	Absorbance	Relative Absorbance
999	0.302	0.285
955	0.566	0.534
901	1.058	1.000
802	0.824	0.778
795	0.828	0.785
787	0.836	0.790
754	0.733	0.693
702	0.677	0.640
602	0.298	0.282
588	0.294	0.278
538	0.418	0.395
529	0.429	0.406
424	0.247	0.233
401	0.355	0.336
366	0.681	0.643
363	0.681	0.643
359	0.656	0.620
351	0.525	0.496

Table IX

Peak Table
for
KCo2+Si Spectrum
in
KCl

Peak Sensitivity Factor: 20

Peak cm-1	Absorbance	Relative Absorbance
997	0.371	0.220
953	0.841	0.499
901	1.685	1.000
804	1.295	0.768
793	1.274	0.756
752	1.033	0.613
704	0.995	0.590
600	0.409	0.243
540	0.590	0.350
525	0.582	0.346
488	0.467	0.277
436	0.342	0.203
370	1.015	0.602
365	1.058	0.628
351	0.762	0.452

Table X

Peak Table
for
KCo2+Si Spectrum
in
Nujol

Peak Sensitivity Factor: 20

Peak cm 1	Absorbance	Relative Absorbance
1001	0.006	0.119
959	0.015	0.287
905	0.026	0.511
810	0.018	0.355
797	0.018	0.357
721	0.018	0.357
685	0.013	0 256
669	0.017	0.321
658	0.008	0.159
538	0.005	0.105
480	0.003	0.065
467	0.002	0.044
426	0.003	0.049
413	0.006	0.111
403	0.008	0.152
395	0.012	0.233
382	0.016	0.308
376	0.020	0.396
357	0.052	1.000
351	0.022	0.429

Table XI

Peak Table
for
KCo2+Zn Spectrum
in
Nujol

Peak Sensitivity Factor: 20

Peak cm-1	Absorbance	Relative Absorbance
939	0.094	0.701
880	0.103	0.771
799	0.106	0.796
787	0.115	0.861
721	0.120	0.901
669	0.099	0.741
658	0.078	0.583
617	0.055	0.408
473	0.063	0.473
457	0.071	0.533
419	0.074	0.553
399	0.061	0.458
384	0.056	0.420
374	0.094	0.702
370	0.088	0.662
359	0.103	0.774
353	0.134	1.000

Table XII

Peak Table
for
AmCo3+Zn Spectrum
in
CCl4

Concentration: 14.55 g/L

Peak Sensitivity Factor: 20

Peak cm-1	Absorbance	Relative Absorbance
1069	0.005	0.140
1051	0.004	0.132
939	0.027	0.826
876	0.032	0.971
831	0.012	0.373
822	0.013	0.394
725	0.018	0.554
691	0.007	0.209
667	0.007	0.201
654	0.006	0.182
635	0.004	0.132
613	0.004	0.135
577	0.005	0.151
548	0.005	0.139
532	0.006	0.174
527	0.005	0.158
517	0.005	0.143
488	0.005	0.140
478	0.006	0.186
473	0.007	0.198
451	0.013	0.398
438	0.009	0.272
419	0.004	0.119
413	0.005	0.152
399	0.004	0.133
392	0.008	0.244
384	0.009	0.258
376	0.012	0.351
368	0.016	0.481
363	0.011	0.341
357	0.033	1.000

Table XTTI

Peak Table
for
NaCo3+Ga Spectrum
in
Nujol

Peak Sensitivity Factor: 20

Peak cm-1	Absorbance	Relative Absorbance
1057	0.032	0.519
957	0.050	0.804
945	0.050	0.806
889	0.046	0.732
880	0.045	0.726
814	0.044	0.707
806	0.044	0.707
783	0.044	0.706
721	0.062	1.000
669	0.048	0.764
660	0.034	0.554
399	0.028	0.444
386	0.020	0.319
374	0.037	0.599
370	0.034	0.551
361	0.030	0.483
355	0.049	0.784

Table XIV

Peak Table
for
AmCo3+Ga Spectrum
in
CCl4

Concentration: 52.09 g/L

Peak Sensitivity Factor: 20

Peak cm-1	Absorbance	Relative Absorbance
1071	0.017	0.208
1059	0.017	0.218
1034	0.010	0.131
947	0.062	0.782
883	0.079	1.000
829	0.049	0.621
820	0.057	0.724
741	0.062	0.778
723	0.078	0.977
669	0.011	0.144
650	0.009	0.114
637	0.007	0.085
596	0.008	0.098
548	0.012	0.148
534	0.011	0.136
517	0.008	0.106
496	0.007	0.093
478	0.008	0.104
471	0.011	0.140
451	0.028	0.357
409	0.009	0.110
397	0.009	0.117
390	0.012	0.151
374	0.050	0.626
361	0.038	0.477
355	0.031	0.391

Table XV

Peak Table
for
AmCo3+Ga Spectrum
in
CS2

Concentration: 61.11 g/L

Peak Sensitivity Factor: 20

Peak cm-1	Absorbance	Relative Absorbance
1071	0.028	0.298
1055	0.028	0.302
949	0.072	0.771
882	0.093	1.000
814	0.087	0.936
781	0.087	0.934
725	0.068	0.734
669	0.035	0.374
652	0.034	0.369
473	0.022	0.232
457	0.031	0.331
448	0.032	0.348
419	0.025	0.274
399	0.041	0.443
380	0.028	0.297
374	0.052	0.556
370	0.046	0.496
366	0.041	0.442
355	0.030	0.319

Table XVI

Peak Table
for
KCo2+Ge Spectrum
in
KBr

Peak Sensitivity Factor: 20

Peak cm-1	Absorbance	Relative Absorbance
951	0.844	0.697
876	1.087	0.898
812	1.210	1.000
770	1.068	0.883
743	1.005	0.830
692	1.000	0.827
687	0.997	0.824
584	0.477	0.394
525	0.573	0.473
457	0.720	0.595
419	0.535	0.442
413	0.527	0.436
399	0.550	0.455
370	0.996	0.823
363	1.011	0.836

Table XVII

Peak Table
for
AmCo2+Ge Spectrum
in
Nujol

Concentration: 13.91 g/L

Peak Sensitivity Factor: 20

Peak cm-1	Absorbance	Relative Absorbance
957	0.019	0.244
885	0.028	0.355
824	0.019	0.245
814	0.019	0.236
719	0.015	0.193
679	0.022	0.284
669	0.041	0.519
656	0.018	0.227
650	0.018	0.228
617	0.009	0.113
557	0.005	0.060
548	0.005	0.061
527	0.006	0.076
503	0.005	0.059
473	0.006	0.079
457	0.010	0.126
428	0.005	0.068
419	0.008	0.099
397	0.012	0.156
384	0.016	0.209
374	0.025	0.322
357	0.024	0.303
351	0.079	1.000

Table XVIII

Search Result
For
Known KCo2+Si
in
Nujol Standard Library

From 356.44 - 1099 cm-1

Res: 2.561 cm-1 Points: 256

HIT	Name	HCI
1	KCo2+Si	
2	KCo3+B	0.443
3	KCo3+Si	0.476
4	KCo2+Ga	0.499
5	KCo2+P	0.521
6	KCo2+Ge	0.532
7	NaW6+H2	0.532
8	KCo2+B	0.537
9	KCo2+Zn	0.549
10	HW6+P	0.565
11	KCo3+Zn	0.576
12	KCo3+H2	0.593
13	Nujol	0.637
14	NaCo3+Ga	0.665

Table XIX

Search Result
for
Unknown KCo2+P
in
Nujol Standard Library

From 356.44 - 1095 cm-1

Res: 2.561 cm-1 Points: 256

HIT	Name	HQI
1	KCo2+P	0.138
2	HW6+F	0.393
3	KCo3+B	0.398
4	KCo3+Si	0.427
5	KCo2+B	0.443
6	KCo2+Ga	0.488
7	KCo2+Zn	0.504
8	KCo2+Ge	0.510
9	Nujol	0.515
10	NaCo3+Ga	0.515
11	NaW6+H2	0.537
12	KCo2+Si	0.571
13	KCo3+Zn	0.571
14	KCo3+H2	0.621

Table XX

Search Result
For
Unknown KCo2+Si
in
Nujol Standard Library

From 356.44 - 1095 cm-1

Res: 2.561 cm-1 Points: 256

HIT	Name	HQI
1	KCo2+Si	0.232
2	KCo3+Si	0.371
3	KCo3+B	0.388
4	KCo2+Ga	0.421
5	KCo2+B	0.438
6	KCo2+P	0.443
7	KCo2+Ge	0.454
8	NaW6+H2	0.476
9	HW6+P	0.482
10	KCo2+Zn	0.504
11	KCo3+H2	0.521
12	KCo3+Zn	0.543
13	Nujol	0.593
14	NaCo3+Ga	0.615

Table XXI

Absorbance vs Concentration
for
AmCo3+8 in CCl4
at
Wavelength = 949 cm-1.

Concentration g/L	Observed Absorbance	Calculated Absorbance	Difference (Cal - Obs)
8.22	0.055	0.055	0.001
11.31	0.067	0.065	-0.002
13.64	0.072	0.072	0.000
16.58	0.080	0.081	0.002
20.27	0.093	0.093	-0.001
25.25	0.109	0.108	-0.001
28.37	0.118	0.118	0.000
31.71	0.103	0.104	0.001
35.59	0.115	0.112	-0.003
39.34	0.118	0.120	0.001

__Regression Output_First_		__Regression Output_Second_	
Constant	0.0299	Constant	0.0382
Std Err of Y Est	0.0013	Std Err of Y Est	0.0032
R Squared	0.9971	R Squared	0.9225
No. of Points	7.0000	No. of Points	3.0000
Degree of Freedom	5.0000	Degree of Freedom	1.0000
X Coefficient(s)	0.0031	X Coefficient(s)	0.0021
Std Err of Coef.	0.0001	Std Err of Coef.	0.0006

Proportionality Constant, K, - First Segment : 0.0031 L/g
Intercept on Y- axis for First Segment : 0.0299

Proportionality Constant, K, - Second Segment: 0.0021 L/g
Intercept on Y- axis for Second Segment : 0.0382

Table XXII

Absorbance vs Concentration
for
$AmCo(C_3H_7)_3$ in CCl_4
at
Wavelength = 901 cm^{-1}.

Concentration g/L	Observed Absorbance	Calculated Absorbance	Difference (Cal - Obs)
8.22	0.067	0.069	0.001
11.31	0.083	0.081	-0.003
13.64	0.089	0.090	0.001
16.58	0.099	0.101	0.002
20.27	0.117	0.115	-0.001
25.25	0.134	0.134	0.000
28.37	0.146	0.146	0.000
31.71	0.132	0.133	0.002
35.59	0.147	0.144	-0.003
39.34	0.152	0.154	0.002

Regression output First		Regression output Second	
Constant	0.0368	Constant	0.0480
Std Err of Y Est	0.0017	Std Err of Y Est	0.0038
R Squared	0.9972	R Squared	0.9353
No. of Points	7.0000	No. of Points	3.0000
Degree of Freedom	5.0000	Degree of Freedom	1.0000
X Coefficient(s)	0.0039	X Coefficient(s)	0.0027
Std Err of Coef.	0.0001	Std Err of Coef.	0.0007

Proportionality Constant, K, - First Segment : 0.0039 L/g
Intercept on Y- axis for First Segment : 0.0368

Proportionality Constant, K, - Second Segment : 0.0027 L/g
Intercept on Y- axis for Second Segment : 0.0480

Table XXIII

Absorbance vs Concentration
for
AmCo2+Si in CCl4
at
Wavelength = 961 cm-1.

Concentration g/L	Observed Absorbance	Calculated Absorbance	Difference (Cal - Obs)
2.38	0.008	0.009	0.001
3.12	0.009	0.010	0.001
4.02	0.013	0.010	-0.002
5.43	0.012	0.012	-0.000
7.10	0.014	0.013	-0.001
8.60	0.014	0.014	-0.000
10.63	0.015	0.016	0.001

Regression output	
Constant	0.0073
Std Err of Y Est	0.0015
R Squared	0.7470
No. of Observation	7.0000
Degrees of Freedom	5.0000
X Coefficient(s)	0.0008
Std Err of Coef.	0.0002

Proportionality Constant, K: 0.0008 L/g
Intercept on Y- ais : 0.0073

Table XXIV

Absorbance vs Concentration
for
AmCo2+Si in CCl4
at
Wavelength = 909 cm-1.

Concentration g/L	Observed Absorbance	Calculated Absorbance	Difference (Cal - Obs)
2.38	0.017	0.020	0.003
3.12	0.020	0.022	0.002
4.02	0.026	0.024	-0.002
5.43	0.028	0.026	-0.001
7.10	0.032	0.030	-0.003
8.60	0.033	0.033	-0.000
10.63	0.034	0.037	0.003

Regressio output

Constant	0.0155
Std Err of Y Est	0.0028
R Squared	0.8501
No. of Observations	7.0000
Degrees of Freedom	5.0000
X Coefficient(s)	0.0020
Std Err of Coef.	0.0004

Proportionality Constant: 0.0020 L/g
Intercept on Y- axis : 0.0155

Table XXV

Absorbance vs Concentration
for
AmCo3+Zn in CCl4
at
Wavelength = 939 cm-1

CONCENTRATION g/L	Observed Absorbance	Calculated Absorbance	Difference (Cal - Obs)
3.03	0.011	0.007	-0.004
3.46	0.006	0.008	0.002
4.17	0.008	0.009	0.002
5.53	0.010	0.012	0.002
7.18	0.014	0.015	0.001
9.66	0.023	0.019	-0.003
11.82	0.023	0.023	0.000
14.55	0.027	0.028	0.001

Regression output	
Constant	0.0017
Std Err of Y Est	0.0024
R Squared	0.9195
No. of Observations	8.0000
Degrees of Freedom	6.0000
X Coefficient(s)	0.0018
Std Err of Coef.	0.0002

Proportionality Constant, K: 0.0018 L/g
Intercept on Y- axis : 0.0017

Table XXVI

Absorbance vs Concentration
for
AmCo3+Zn in CCl4
at
Wavelength = 876 cm-1.

CONCENTRATION g/L	Observed Absorbance	Calculated Absorbance	Difference (Cal - Obs)
3.03	0.012	0.009	-0.004
3.46	0.008	0.010	0.001
4.17	0.010	0.011	0.002
5.53	0.012	0.014	0.002
7.18	0.017	0.018	0.001
9.66	0.026	0.023	-0.003
11.82	0.028	0.027	-0.000
14.55	0.032	0.033	0.001

Regression output	
Constant	0.0023
Std Err of Y Est	0.0024
R Squared	0.9394
No. of Observations	8.0000
Degrees of Freedom	6.0000
X Coefficient(s)	0.0021
Std Err of Coef.	0.0002

Proportionality Constant, K: 0.0021 L/g
Intercept on Y- axis : 0.0023

Table XXVII

Absorbance vs Concentration
for
AmCo3+Ga in CCl4
at
Wavelength = 947 cm-1

Concentration g/L	Observed Absorbance	Calculatsd Absorbance	Difference (Cal - Obs)
7.45	0.018	0.018	-0.000
11.07	0.020	0.021	0.001
13.76	0.024	0.024	-0.000
17.40	0.028	0.027	-0.001
22.49	0.032	0.032	0.001
29.86	0.038	0.038	-0.000
34.51	0.040	0.040	-0.001
39.66	0.039	0.041	0.002
45.62	0.044	0.043	-0.001
52.09	0.062	0.062	

_Regression output_First__		_Regressioutput__Second___	
Constant	0.0107	Constant	0.0293
Std Err of Y Est	0.0010	Std Err of Y Est	0.0016
R Squared	0.9749	R Squared	0.7090
No. of Points	5.0000	No. of Points	4.0000
Degree of Freedom	3.0000	Degree of Freedom	2.0000
X Coefficient(s)	0.0010	X Coefficient(s)	0.0003
Std Err of Coef.	0.0001	Std Err of Coef.	0.0001

Proportionality Constant, K, - First Segment : 0.0010 L/g
Intercept on Y- axis for First Segment : 0.0107

Proportionality Constant, K, - Second Segment : 0.0003 L/g
Intercept on Y- axis for First Segment : 0.0293

Table XXVIII

Absorbance vs Concentration
for
AmCo3+Ga in CCl4
at
Wavelength = 883 cm-1

Concentration g/L	Observed Absorbance	Calculated Absorbance	Difference (Cal - Obs)
7.45	0.019	0.019	-0.000
11.07	0.022	0.023	0.001
13.76	0.027	0.027	-0.000
17.40	0.034	0.032	-0.002
22.49	0.037	0.038	0.001
29.86	0.046	0.047	0.000
34.51	0.052	0.050	-0.001
39.66	0.052	0.054	0.001
45.62	0.058	0.058	-0.000
52.09	0.079	0.079	

__Regression output_First_		__Regression output_Second_	
Constant	0.0261	Constant	0.0088
Std Err of Y Est	0.0015	Std Err of Y Est	0.0016
R Squared	0.9349	R Squared	0.9675
No. of Observatio	4.0000	No. of Observatio	5.0000
Degrees of Freedo	2.0000	Degrees of Freedo	3.0000
X Coefficient(s)	0.0007	X Coefficient(s)	0.0013
Std Err of Coef.	0.0001	Std Err of Coef.	0.0001

Proportionality Constant, K, - First Segment : 0.0007 L/g
Intercept on Y-axis for First Segment : 0.0261

Proportionality Constant, K, - Second Segment : 0.0013 L/g
Intercept on Y-axis for Second Segment : 0.0080

Table XXIX

Absorbance vs Concentration
for
AmCo3+Ga in CS2
at
Wavelength = 949 cm-1.

Concentration g/L	Observed Absorbance	Calculated Absorbance	Difference (Cal - Obs)
1.66	0.020	0.056	0.036
2.27	0.016	0.048	0.032
3.21	0.016	0.042	0.026
4.87	0.030	0.042	0.012
7.97	0.025	0.037	0.013
16.59	0.043	0.042	0.001
24.71	0.047	0.040	-0.006
35.18	0.050	0.040	-0.010
42.40	0.052	0.039	-0.012
48.45	0.063	-0.059	-0.122
54.77	0.086	-0.061	-0.147
61.11	0.072	0.072	

Regression output First		Regression output Second	
Constant	0.0148	Constant	0.0377
Std Err of Y Est	0.0048	Std Err of Y Est	0.0008
R Squared	0.[illegible]72	R Squared	0.9748
No. of Points	6.0000	No. of Points	4.0000
Degree of Freedom	4.0000	Degree of Freedom	2.0000
X Coefficient(s)	0.0017	X Coefficient(s)	0.0003
Std Err of Coef.	0.0004	Std Err of Coef.	0.0000

Regression output Third	
Constant	-0.0674
Std Err of Y	0.0040
R Squared	0.9740
No. of Points	3.0000
Degree of Freedom	1.0000
X Coefficient	0.0028
Std Err of Coef.	0.0005

Proportionality Constant, K, - First Segment : 0.0017 L/g
Intercept on Y-axis for First Segment : 0.0148

Proportionality Constant, K, - Second Segment : 0.0003 L/g
Intercept on Y-axis for Second Segment : 0.0377

Proportionality Constant, K, - Third Segment : 0.0028 L/g
Intercept on Y-axis for Third Segment :-0.0674

Table XXX

Absorbance vs Concentration
for
AmCo3+Ga in C92
at
Wavelength = 882 cm-1.

Concentration g/L	Observed Absorbance	Calculated Absorbance	Difference (Cal - Obs)
1.66	0.021	0.016	-0.005
2.27	0.015	0.018	0.003
3.21	0.011	0.020	0.009
4.87	0.031	0.023	-0.008
7.97	0.029	0.030	0.001
16.59	0.049	0.049	0.000
24.71	0.054	0.055	0.001
35.18	0.065	0.061	-0.003
42.40	0.063	0.066	0.002
48.45	0.081	0.083	0.001
54.77	0.104	0.103	-0.001
61.11	0.093	0.093	

Regression Output First		Regression output Second	
Constant	0.0127	Constant	0.0391
Std Err of Y Est	0.0066	Std Err of Y Est	0.0030
R Squared	0.8152	R Squared	0.8951
No. of Points	6.0000	No. of Points	4.0000
Degree of Freedom	4.0000	Degree of Freedom	2.0000
X Coefficient(s)	0.0022	K Coefficient(s)	0.0006
Std Err of Coef.	0.0005	Std Err of Coef.	0.0002

Regression output Third	
Constant	-0.0760
Std Err of Y Est	0.0014
R Squared	0.9977
No. of Points	3.0000
Degree of Freedom	1.0000
X Coefficient(s)	0.0033
Std Err of Coef.	0.0002

Proportionality Constant, K, - First Segment : 0.0022 L/g
Intercept on Y-axis for First Segment : 0.0127

Proportionality Constant, K, - Second Segment : 0.0006 L/g
Intercept on Y-axis for Second Segment : 0.0391

Proportionality Constant, K, - Third Segment : 0.0033 L/g
Intercept on Y-axis for Third Segment :-0.0760

Table XXXI

Absorbance vs Concentration
for
$AmCo_2(CO)_8Ge$ in CCl_4
at
Wavelength = 957 cm^{-1}.

Concentration g/L	Observed Absorbance	Calculated Absorbance	Difference (Cal - Obs)
2.88	0.012	0.013	0.001
3.35	0.012	0.014	0.001
3.65	0.014	0.014	0.000
4.54	0.016	0.015	-0.001
5.79	0.016	0.016	-0.000
7.07	0.018	0.018	-0.000
8.76	0.019	0.019	-0.000
10.31	0.024	0.021	-0.003
12.16	0.024	0.023	-0.001
13.08	0.025	0.024	-0.002
13.91	0.019	0.025	0.005

Regression Output	
Constant	0.010
Std Err of Y Est	0.002
Correlation Squared	0.787
No. of Observations	11.000
Degrees of Freedom	9.000
X Coefficient	0.001
Std Err of Coef.	0.000

Proportionality Constant, K: 0.001 L/g
Intercept on Y- axis : 0.010

Table XXXII

Absorbance vs Concentration
for
$AmCo_2(CO)_8$ in CCl_4
at
Wavelength = 885 cm^{-1}.

CONCENTRATION g/L	Observed Absorbance	Calculated Absorbance	Difference (Cal - Obs)
2.88	0.019	0.022	0.003
3.35	0.020	0.022	0.002
3.65	0.023	0.023	0.000
4.54	0.025	0.024	-0.001
5.79	0.027	0.026	-0.001
7.07	0.029	0.028	-0.001
8.76	0.031	0.030	-0.001
10.31	0.037	0.032	-0.005
12.16	0.037	0.035	-0.003
13.08	0.038	0.036	-0.002
13.91	0.028	0.037	0.009

Regression output	
Constant	0.018
Std Err of Y Est	0.004
R Squared	0.699
No. of Observations	11.000
Degrees of Freedom	9.000
X Coefficient(s)	0.001
Std Err of Coef.	0.000

Proportionality Constant, K: 0.001 L/g
Intercept on Y- axis : 0.018

Table XXXIII

Traditional Weighing Technique

Absorbance vs Concentration
for
Tripalmitin in CCL4
at
Wavelength = 1746 cm-1

Concentration g/L	Observed Absorbance	Calculated Absorbance	Difference (Cal - Obs)
2.29	0.030	0.032	0.001
3.34	0.040	0.038	-0.002
5.82	0.048	0.054	0.006
6.56	0.066	0.059	-0.007
9.48	0.076	0.078	0.001

Regression Output

Constant	0.0170
Std Err of Y Est	0.0057
R Squared	0.9310
No. of Observations	5.0000
Degrees of Freedom	3.0000
X Coefficient(s)	0.0064
Std Err of Coef.	0.0010

Proportionality Constant, K: 0.0064 L/g
Intercept on Y-axis : 0.0170

Table XXXIV

New Weighing Technique

Absorbance vs Concentration
for
Tripalmitin in CCL4
at
Wavelength = 1746 cm-1

Concentration g/L	Observed Absorbance	Calculated Absorbance	Difference (Cal - Obs)
1.49	0.021	0.020	-0.001
1.89	0.021	0.022	0.001
2.51	0.026	0.025	-0.001
3.02	0.027	0.028	0.001
3.55	0.031	0.031	-0.000

Regression Output	
Constant	0.0121
Std Err of Y Est	0.0011
R Squared	0.9520
No. of Observations	5.0000
Degrees of Freedom	3.0000
X Coefficient(s)	0.0053
Std Err of Coef.	0.0007

Proportionality Constant, K: 0.0053 L/g
Intercept on Y-axis : 0.0121

Table XXXV

Concentration vs Peak Position
of
Second Highest Absorbance
with
Respect to the Absorbance 882 cm-1
for
AmCo3+Ga in CS2

Overall Concentration g/L	First Segment cm-1	Second Segment cm-1	Third Segment cm-1	Fourth Segment cm-1
1.66	397			
2.27	397			
3.21	669			
4.87	397			
7.97	397			
16.59		669		
24.71		781		
35.18		669		
42.45			781	
48.45			781	
54.77			781	
61.11				814

Table XXXVI

Concentration vs Peak Position
of
Second Highest Absorbance
with
Respect to the Absorbance at 831 cm-1
for
AmCo3+8 in CCl4

Concentration g/L	Peak Position cm-1
8.22	901
11.31	901
13.64	901
16.58	901
20.27	901
25.29	901
28.37	901
31.71	901
35.59	901
39.34	901

Table XXXVII

Peak Shifting Table for AmCo3+Ga

A Particular Peak Position
at
Different Concentrations

for

AmCo3+Ga in CS2

Concentration g/L	Peak Position cm-1
1.66	947
2.27	949
3.21	949
4.87	951
7.97	949
16.59	949
24.71	949
35.18	949
42.20	949
48.45	949
54.77	949
61.11	949

Table XXXVIII

Peak Shifting Table for AmCo3+B

A Particular Peak Position
at
Different Concentrations

for

AmCo3+B in CCl4

Concentration g/L	Peak Position cm-1
8.22	949
11.31	949
13.64	949
16.58	949
20.27	949
25.25	949
28.37	949
31.71	949
35.59	949
39.34	949

APPENDIX C - GLOSSARY

a	Number of central hetero atom
A	Absorbance
A_1	Number of atoms in the HPA which are bonded to only one atom.
b	Number of peripheral hetero atom
B	Angle between infrared light source and optical axis of collimator.
$B(F_2)$	Total number of bands for F_2 mode of vibration.
c	(12-b)
cm	A unit for measuring path length.
cm-1	A unit for wavenumber
C	Concentration (Absorbance and Concentration are related by the formula, A = K * C).
C_2	a symmetry operation i.e. the rotation by 180°.
C_3	a symmetry operation i.e. the rotation by 120°.
C_s	a point group
d	Spatial displacement between fixed and movable mirrors of interferometer.
d.f.	Degree of freedoms.
D	Total number of data points on the spectrum
e	Net charge on the heteropoly anion.
E	Identity operation i.e. the rotation by 360°.
E_D	Optical throughput of dispersive instrument.
E_I	Optical throughput of Michelson interferometer.
$F(v)$	Modulated frequency
F_2	Vibrationally active mode of T_d point group.
FT-IR	Fourier Transform Infrared Spectroscopy.

FWHH Full width at half height

g A unit for weight

G(dm) Reducible representation for dipole moment of T_d point group.

G(F_2) Reducible representation for F_2 mode of vibration.

G(int) Reducible representation for internal coordinates of the HPA.

G(m) Reducible representation for all types of motion of atoms in the anion.

G(red) Reducible representation for redundancies present in internal coordinates.

G(t) Reducible representation for translatory motion of each atoms in the HPA.

G(v) Reducible representation for vibratory motion of each atom in the HPA.

h Point group order

Hit Order given to spectra stored in the library in matching a unknown spectrum.

HPA Heteropoly anion

HPC Heteropoly compound

HQI Hit quality index of the unknown spectrum matched against the spectra stored in the library.

Hz Hertz, a unit of frequency.

I(L) Intensity of light radiation of wavelength, L.

I(x) Intensity of interferogram, a modulated part of I'(x).

I'(x) Intensity of transmitted beam as a function of x.

I(v') Cosine Fourier inverse of I(x)

ILS Instrument line shape function.

IR Infra-red

K	Absorbance proportionality constant
K'	A modified absorbance proportionality constant.
l	Ligand attached to the peripheral hetero atom, Y
L	Wavelength
L	A symbol for liter, a unit of volume.
m	A unit for measuring the thickness of the spacer.
m	Band angle deformation
mg	A unit for measuring the mass
M	A unit for concentration in moles L^{-1}
M	Number of resolution elements of Fourier spectrometer.
M_l	Multiplicity of the coplannar bond meeting at the same atom.
n	Refractive index of solution at a given wavelength.
n	Out of plane bending
N	Number of atoms remain unshifted under each symmetry operation.
N_a	Number of atoms in the HPA
N_b	Number of bonds in the HPA
N_{dp}	Total number of data points used to match a unknown spectrum against a spectrum stored in the library
N_θ	Total number of internal coordinates corresponding to band angle deformations in the HPA during vibratory motion.
N_π	Total number of internal coordinates corresponding to out of plane bendings in the HPA during vibratory motion.
N_p	Total number of internal coordinates corresponding to torsions produced in the HPA during vibratory motion.
N_s	Total number of internal coordinates corresponding

to stretchings in the HPA during vibratory motion.

p — Torsion produced during the vibration

pi — Phase corrections due to optical, electronic and sampling effects.

Q — Angle of rotation due to each symmetry operation.

r — Repetitive number of each symmetry operation.

R — Resolution of the spectrometer.

Res — Resolution parameter same as that of R, but used for annotating the spectra.

Res — Resolution for matching a unknown spectrum with the spectra stored in the library.

s — Stretching in bond

S_d — Symmetry operation corresponding to reflection through a dihedral mirror plane.

S_h — Symmetry operation corresponding to reflection through a horizontal mirror plane.

S_4 — a symmetry operation i.e. first rotation by 90° and then reflection.

SincA — Sin(A)/A, a instrument line shape function.

SNR — Signal to noise ratio.

T_d — Tetrahedral symmetry point group.

v — Frequency of the source radiation.

v' — Wavenumber

v'_{max} — Maximum wavenumber on the spectrum.

v'_{min} — Minimum wavenumber on the spectrum.

V — Velocity of moving mirror in the interferometer.

w_1 — Weight of the solvent added each time after collecting a spectrum.

x — Optical path difference.

x_i Weight of the solute in grams before taking a spectrum.

X Central hetero atom

y_i Weight of the solvent in grams before taking a spectrum.

Y Peripheral hetero atom

z_i Weight of solution taken for collecting a spectrum.

Z Addendum atom

I, Mohan Lal Gupta, hereby submit this thesis to Emporia State University as partial fulfillment of the requirements for an advanced degree. I agree that the Library of the University may make it available for use in accordance with its regulations governing materials of this type. I further agree that quoting, photocopying, or other reproduction of this document is allowed for private study, scholarship (including teaching) and research purposes of a nonprofit nature. No copying which involves potential financial gain will be allowed without written permission of the author.

Mohanlal Gupta 5/9/90
Signature of Author

Date

Fourier Transform Infrared Studies of 1:12 and 1:11 Heteropoly Tungstates
Title of Thesis

Signature of Graduate Office Staff Member

Date Received